

Tunable Filter Design for the RF Section of a Smartphone

By:

Jonathon Michel

Michael Morales

Long Pham

Natasa Trkulja

Date: March 5th, 2014

Major Qualifying Project submitted to the Faculty of



WORCESTER POLYTECHNIC INSTITUTE

In partial fulfillment of the requirements for the degree of

Bachelor of Science

Approved:

Professor Reinhold Ludwig

Professor John McNeill

Dr. David Whitefield

Table of Contents

Table of Contents.....	2
Table of Figures.....	4
Table of Tables.....	6
CHAPTER 1: INTRODUCTION.....	7
CHAPTER 2: BACKGROUND.....	8
2.1 Current State-of-the-Art Handset Architecture	8
2.2 3GPP LTE Standard	10
2.3 RF Filter Classifications and Design Parameters	10
2.4 Tunable Filter Solutions	12
2.4.1 Yttrium Iron Garnet (YIG) Tunable Filters	12
2.4.2 Barium Strontium Titanate Tunable Filters.....	13
2.4.3 Varactor diodes.....	14
2.4.4 MEMS tunable capacitors.....	15
2.4.5 Digitally Tunable Capacitors.....	15
2.4.6 Comparison of Several Component Technologies	18
2.4.7 Prior Art Patents	18
2.5 Acoustic Filter Technology	20
2.5.1 SAW filter.....	20
2.5.2 BAW filter	20
2.5.3 Performance.....	21
CHAPTER 3: OBJECTIVES	22
CHAPTER 4: APPROACH.....	23
4.1 Fundamental Filter Theory	23
4.2 Ideal Fixed Filter Simulation.....	25
4.2.1 Butterworth	25
4.2.2 Butterworth (Linear phase).....	26
4.2.3 Chebyshev 3dB.....	27
4.2.4 Chebyshev 0.5dB	28
4.3 Potential Tunable Design Approaches.....	29
4.3.1 Third order tunable C-coupled shunt resonators	29
4.3.2 Fourth order tunable C-coupled shunt resonators.....	31
4.4 Mathematical Derivation of C-coupled Filters	32
4.4.1 Impedance and Admittance Inverters	32

4.4.2 Normalized Lowpass Filter Prototype Using Impedance/Admittance Inverters	33
4.4.3 Capacitive Coupled Filters	34
4.4.4 Simulation of mathematically derived C-coupled topologies	37
4.5 Non-ideality investigation	40
4.5.1 Inductors and Capacitors	41
4.5.2 Adding a Real Tunable Element.....	41
4.6 Summary	43
CHAPTER 5: RESULTS.....	45
5.1 Series Resonator Simulations	45
5.1.1 Butterworth 4 th Order, 25 MHz Bandwidth, Serial Resonator	45
5.1.2 Chebyshev 4 th Order, 25 MHz Bandwidth, Serial Resonator	46
5.1.3 Modified Chebyshev 4 th Order, 20 MHz, Serial Resonator.....	47
5.2 Filter Augmentation.....	49
5.2.1 Adding an Ideal LNA	49
5.2.2 Adding a Real LNA Model.....	51
CHAPTER 6: DISCUSSION	53
6.1 General Observations.....	53
6.2 Performance comparison	54
6.3 Cost and Board Size Analysis.....	55
CHAPTER 7: CONCLUSION	57
CHAPTER 8: DELIVERABLES	58
APPENDIX A: Derivation of the inverter networks at two ends of C-coupled filters.....	59
APPENDIX B: MATLAB Code	61
C-coupled Shunt Resonator	61
C-coupled Serial Resonator	62
APPENDIX C: NXP BB208 Varactor Diode Datasheet.....	64
APPENDIX D: Using realistic currently available high-quality lumped element models.....	72
APPENDIX E: Butterworth Filter Bandwidth/Roll-off	79
Non-ideal Butterworth Order Investigation.....	79
Non-ideal Butterworth Bandwidth Investigation.....	79
APPENDIX F: Coefficients of different filter configurations.....	80
References.....	82

Table of Figures

Figure 1. Ideal bandpass filter response compared with a more realistic response	7
Figure 2. Typical RF front end showing transmitters, receivers, fixed filters, RF switches, and antennas [27].....	8
Figure 3. Showing the potential for tunable filters in the typical cellular RF front end. The RF switches and fixed filters are replaced with the tunable filter only [27].	9
Figure 4. Magnitude responses of different filter configurations, Butterworth, Chebyshev I, Chebyshev II, and Elliptic [32]	11
Figure 5. Magnetic resonance filter	12
Figure 6. Ferroelectric material change of state at T_c [11].....	13
Figure 7. Varactor diode symbol	14
Figure 8. Cross section of an RF MEMS capacitor in the un-actuated (a) and actuated (b) position [16]..	15
Figure 9. Block diagram of DTC [13]	16
Figure 10. Equivalent circuit for DTC [13]	16
Figure 11. Capacitance in series and shunt configurations [13]	17
Figure 12. Quality factor of the DTC in shunt configuration [13]	17
Figure 13. Circuit diagram from Rice and Wortell's patent showing elements required to be tunable and elements required to be fixed for the filter to be tuned [6]	19
Figure 14. Circuit diagram showing the bandwidth and frequency controlled filter patented by Koechlin [7].....	19
Figure 15. SAW filter consists of two transducers and a piezoelectric crystal substrate [5]	20
Figure 16. In a BAW filter, acoustic wave bouncing from the top to bottom of the electrodes rather than on the surface of the substrate [4]	21
Figure 17. Two equivalent realizations of a normalized low pass filter [3]	23
Figure 18. General bandpass filter topologies [3]	24
Figure 19. Third order bandpass filter schematic	25
Figure 20. Amplitude (in dB) and phase (in degree) responses of a third order maximally flat Butterworth filter.....	26
Figure 21. Amplitude (in dB) and phase (in degree) responses of a third order linear phase Butterworth filter.....	27
Figure 22. Amplitude (in dB) and phase (in degree) response of a third order 0.3dB Chebyshev filter....	28
Figure 23. Amplitude (in dB) and phase (in degree) response of a third 0.5 dB Chebyshev filter	28
Figure 24. Structure of a third order capacitive coupled shunt resonators	29
Figure 25. ADS Simulation of a third order capacitive coupled tunable bandpass filter	30
Figure 26. Frequency response (in dB) of the third order C-coupled tunable bandpass filter, showing the circuit can be tuned to the 4 sections of the cellular handset receive band	30
Figure 27. ADS Simulation of a fourth order capacitive coupled shunt resonator filter	31
Figure 28. Frequency response (in dB) of the circuit shown in Figure 27, showing the circuit is able to be tuned to the 4 sections of the cellular handset receive band required with additional isolation at the transmitting frequency	31
Figure 29. Impedance Inverter (a) and Admittance Inverter (b)	32
Figure 30. Admittance Inverters (a, b), and Impedance Inverters (c,d) using lumped components [34]....	33
Figure 31. A series inductor with K-inverters on both sides looks like a shunt capacitor	33
Figure 32. (a) Lowpass filter prototype using shunt capacitors and admittance inverters [36].....	34
Figure 33. High order bandpass filters using serial resonators and impedance inverters [33, 34, 35, 36]..	35

Figure 34. The J inverters in serial resonator filters (a) and K inverters in shunt resonator filters (b) are replaced by equivalent capacitor networks	36
Figure 35. Final structure of a C-coupled serial resonator (a) and C-coupled shunt resonator (b) tunable filter [33]	37
Figure 36. Third Order Shunt Resonator C-Coupled Filter Schematic (based on topology of Figure 35a)	38
Figure 37. Frequency response (in dB) of an ideal tunable C-coupled shunt resonator	39
Figure 38. Third Order Serial Resonator C-Coupled Filter Schematic (based on topology of Figure 35b)	40
Figure 39. Frequency response (in dB) of a tunable C-coupled serial resonator filter	40
Figure 40. Third order C-coupled serial resonators with Q-values	41
Figure 41. Jeganathan's tunable filter design using varactor diodes as tunable elements [14]	42
Figure 42. Replacement of varactor diodes with capacitors of varying value	42
Figure 43. Frequency response (in dB) of filter schematic shown in Figure 42.	43
Figure 44. 25 MHz Butterworth Serial Resonator Schematic	45
Figure 45. Frequency response (in dB) of 25 MHz Butterworth Serial Resonator	46
Figure 46. 25MHz Chebyshev Serial Resonator Schematic	47
Figure 47. Frequency response (in dB) of 25 MHz Chebyshev Serial Resonator	47
Figure 48. Typical response of a weakly coupled resonator has a concave up passband which can compensate for the undesired downward concavity of the passband due to non-ideal components [34]. ..	48
Figure 49. 25MHz Modified Chebyshev Serial Resonator Schematic	48
Figure 50. Frequency response (in dB) of 25 MHz Chebyshev Serial Resonator	49
Figure 51. Schematic of the modified Chebyshev C-coupled serial resonator with an ideal LNA	50
Figure 52. Frequency response (in dB) of the modified Chebyshev with ideal LNA	50
Figure 53. Phase response (in degrees) of the modified Chebyshev filter with ideal LNA at center frequencies of 1.935GHz (a) and 1.98GHz (b). The filter experiences linear phase behavior at the passband	51
Figure 54. Frequency response (in dB) of design from Figure 51 with real LNA model (HMC548LP3) ..	52
Figure 55. Phase response (in degrees) of the modified Chebyshev filter with ideal LNA at center frequencies of 1.935GHz (a) and 1.98GHz (b). The filter experiences linear phase behavior at the passband	52
Figure 56. Frequency response (in dB) of the SAW filter (current technology)	54
Figure 57. Frequency response (in dB) of proposed filter design	54
Figure 58. Realization of admittance inverters at the ends of C-coupled filters	59
Figure 59. Realization of impedance inverters at the ends of C-coupled filters	60
Figure 60. Sample executions of the two MATLAB functions and results	61
Figure 61. Using real currently available high quality lumped element models	72
Figure 62. Frequency response (in dB) of the 3rd order C-coupled serial resonator	72
Figure 63. Murata High Frequency HiQ ceramic capacitors	73
Figure 64. Implementing Murata component models in the serial resonator design	77
Figure 65. Murata RF Inductors	77
Figure 66. LGQ15HN Murata Inductor behavior	78
Figure 67. Frequency response (in dB) of the 3rd order C-coupled serial resonator (ideal vs. model)	78

Table of Tables

Table 1. Comparison of Filter Classifications	10
Table 2. Comparison of competing technologies with BST [9, 11, 13, 28, 29, 30]	18
Table 3. Bandpass filter transformation and de-normalization	24
Table 4. Calculating component values for a third order maximally flat Butterworth filters	26
Table 5. Calculating component values for a third order linear phase Butterworth filters	26
Table 6. Calculating component values for the 3 rd order C-coupled shunt topology	38
Table 7. Calculating component values for the 3rd order C-coupled serial topology	39
Table 8. Calculated Component Values for 25MHz Butterworth Filter	45
Table 9. Calculated Component Values for 25MHz Chebyshev Filter	46
Table 10. Modified Component Values for 20MHz Chebyshev Filter	48
Table 11. Cost and Board Size Analysis	55
Table 12. Coefficients for maximally flat Butterworth low-pass filter (N=1 to 10) [9].....	80
Table 13: Coefficients for linear phase Butterworth low-pass filter (N=1 to 10) [9].....	80
Table 14: Coefficients for 3dB Chebyshev low-pass filter (N=1 to 10) [9].....	81
Table 15: Coefficients for 0.5dB Chebyshev low-pass filter (N=1 to 10) [9].....	81

CHAPTER 1: INTRODUCTION

Skyworks Inc. has sponsored a WPI Major Qualifying Project involving the design of a tunable filter for the radio-frequency (RF) section of a smartphone. In the RF section of a smartphone, there are several radios that are selected in order for the proper data to be transmitted and received by the RF front end. Each radio operates in a different frequency range and rejects any undesired data transfer. For example, 3G cellular data uses 850 MHz, 1700 MHz, 1900 MHz, and 2100 MHz bands, depending on the cellular carrier, while GPS uses 1.2 GHz, and 1.5 GHz, and 4G cellular Long Term Evolution (LTE) operates at 700 MHz. Bandpass filters with a center frequency and a bandwidth selection consistent with the particular cellular standard are used for this purpose. In general, the operation of bandpass filters is such that they ideally provide no attenuation in the pass band and total attenuation in the stop band. Figure 1 shows the ideal and realistic magnitude response of a bandpass filter.

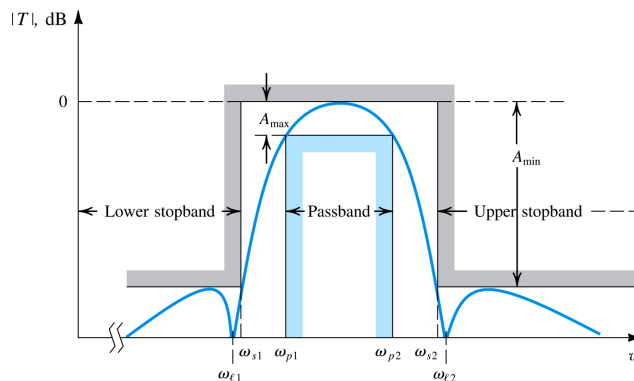


Figure 1. Ideal bandpass filter response compared with a more realistic response

Our project involves designing and analyzing a single bandpass filter that can be tuned to various center frequencies. This approach is in contrast to using one bandpass filter for each application and frequency range. A significant amount of research has been conducted on tunable components that can potentially be employed for our approach, such as capacitors. We first researched ways of tuning the bandpass filter's center frequency by investigating the diverse technologies for the implementation of tunable capacitors, discussed in Chapter 2. In addition, we researched a plethora of filter configurations that could provide us with the filter response set by the project requirements. By changing the capacitance values of the components in the design, we will be able to choose the operating center frequency for our filter. The band of frequencies that will be considered for this project include frequencies in cellular band 25 (1850 MHz – 1955 MHz). However, our challenge is not only to be able to tune the designed bandpass filter to the specified frequencies, but also to provide proper bandwidth and isolation from other frequency bands.

CHAPTER 2: BACKGROUND

In this section, we discuss the theoretical research conducted to provide a basis of knowledge for this project. First, we introduce the current state-of-the-art handset architecture of a smartphone including the current interface between RF switches and bandpass filters. Then, we discuss filter classifications and design parameters of several different types of bandpass filters. Finally, we present several different types of tunable components that could be used in our ultimate design.

2.1 Current State-of-the-Art Handset Architecture

The current “state of the art” in the cellular phone industry is a “smartphone”. These phones are not only able to make phone calls, but also provide data links to the Internet using both cellular service and Wi-Fi, determine the phone’s exact location using GPS, and interface to other devices using Bluetooth. Each of these functions uses RF frequency bands to communicate with base stations and other devices. However, one single radio cannot operate all the bands and functions required. Therefore, multiple radios are implemented for each cellular function. Figure 2 shows the cellular RF section of a phone, depicting multiple radios, fixed filters, and RF switches. A received signal from the base station is picked up from the antenna, switched to the proper path in block A, filtered through a duplex filter where the desired signal is isolated from interference, and routed to the receiver module of the RF transceiver chip. A transmitted signal from the handset originates from the transmit module of the RF transceiver chip and can take one of two paths depending on the standard that it is being transmitted in. The first is through a power amplifier, connected to a bandpass filter to isolate the signal from interference, then directly to the switch in block A to be connected to the antenna. The second is through a power amplifier, then into a switch in block B to select the filtering frequency range, then through a duplex filter to isolate from interference, and then to the switch in block A to be connected to the antenna.

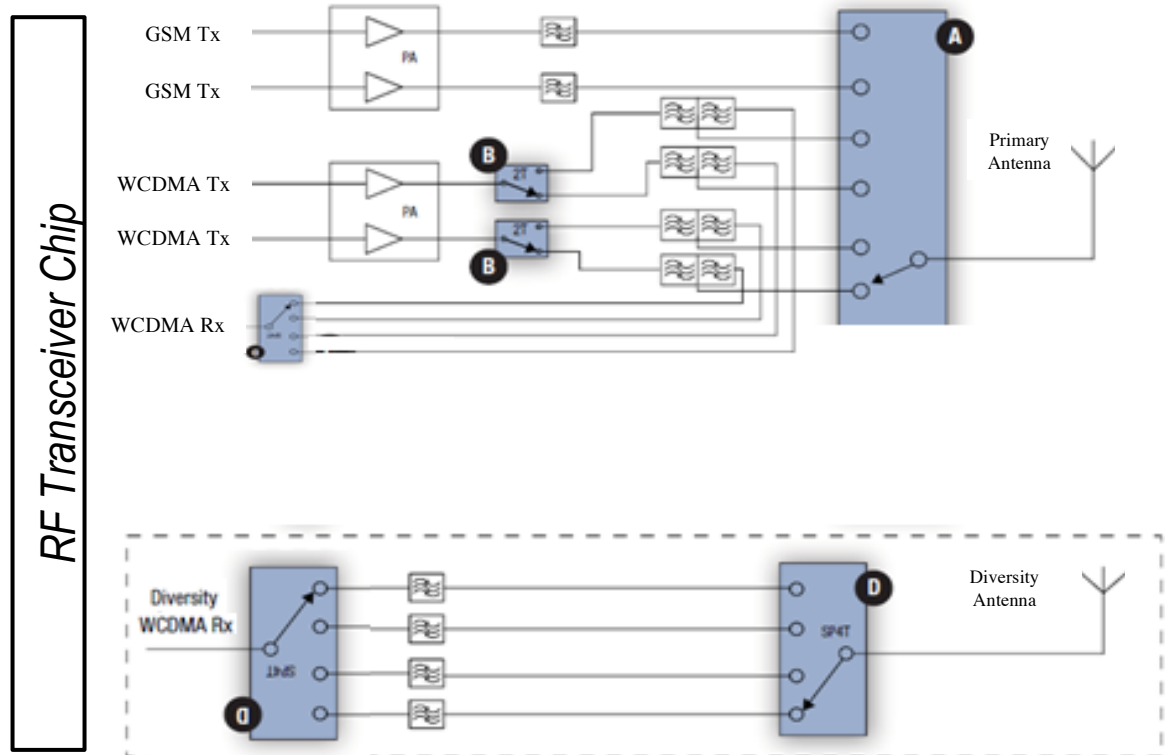


Figure 2. Typical RF front end showing transmitters, receivers, fixed filters, RF switches, and antennas [27]

Most cellular transmissions and receptions use frequency division duplexing (FDD), where the transmitter and receiver portion of the radio are active at the same time. This requires significant isolation between the transmitter and receiver so that the handset transmitter does not desensitize the handset receiver causing the signal from the base station to be degraded. The simplest method of isolating transmit and receive signals is to move the transmitter antenna far away from the receiver antenna. However, in smartphone handsets, where space is minimal, filters can be implemented to achieve the required isolation. Currently, each receiver and transmitter pair is connected to a fixed bandpass filter that provides at least 50 dB of isolation to the receiver from the transmitter frequency range. The filter used, called a duplexer, combines the filtered signals into a single transmission line, so that the transmitter and receiver can share the same antenna.

The filtered signals from the each duplexer are switched through an RF switch with the switching capacity to accommodate each radio pair in the phone, generally SP7T-SP10T in smartphones [27]. The RF switch is identified as “A” and “D” in Figure 2. A multi-band antenna, matched at all frequencies used through the RF switch, is connected to the output of the switch.

Cellular “Band 25” encompasses frequencies from 1850 MHz – 1955 MHz, and is commonly used for both voice and data applications in the United States cellular system. The band of 1850 MHz – 1915 MHz is used for base station transmission to handset receivers, and 1930 MHz – 1995 MHz is used for handset transmission to base station receivers. The specification for this band defines a 20 MHz or less carrier bandwidth and 80 MHz offset between transmit and receive frequencies [1]. The transmitter and receiver frequencies are assigned in pairs, so the offset between the two will always be the same within this band.

The potential implementation of tunable filters in a cellular handset is highly attractive as it could replace both the fixed bandpass filters and the RF switches, resulting in a reduction of components, saving space and cost, but at the disadvantage of reduced performance. Figure 3 highlights components that could be replaced with tunable filters.

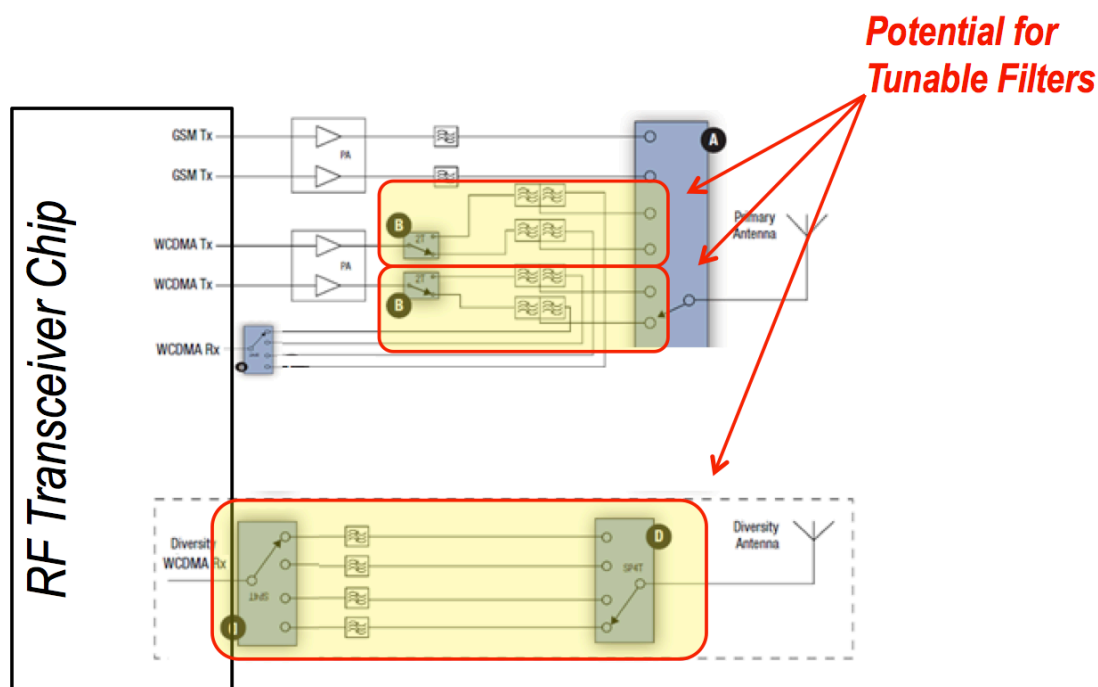


Figure 3. Showing the potential for tunable filters in the typical cellular RF front end. The RF switches and fixed filters are replaced with the tunable filter only [27].

2.2 3GPP LTE Standard

The Third Generation Partnership Project (3GPP) is a collaboration of telecommunications associations responsible for developing global standards for cellular communication. The latest standard developed for cellular telecommunication is called Long Term Evolution (LTE), and is mainly geared toward data communication. The infrastructure is fully IP based and designed to support voice communication over IP [26]. One physical requirement of the LTE standard is that the bandwidth of the carrier signal can be selectable to 1.4 MHz, 3 MHz, 5 MHz, 10 MHz, 15 MHz, and 20 MHz based on available frequency resources. Additionally, the supported antenna configuration is up to 4 transmitter antennas and 4 receiver antennas, using Multiple Input Multiple Output (MIMO) technology. According to the LTE technical standard, these different bandwidth and antenna configurations can be dynamically assigned by the base station sending a signal to the handset, selecting the appropriate configuration [25]. The peak data rate of the LTE standard with 20MHz bandwidth and the best antenna configuration is 300 Mb/s downlink (base station to handset), and 170 Mb/s uplink (handset to base station). LTE uses Orthogonal Frequency Division Multiple Access (OFDMA). This is in contrast to previous data transmission standards that used Time Division Multiple Access (TDMA), and Code Division Multiple Access (CDMA) such as GSM/EDGE (Global Standard for Mobile Communication/Enhanced Data for GSM Evolution), and UMTS/HSPA (Universal Standard Telecommunications System/High Speed Packet Access) [23, 24]. LTE has been implemented alongside these standards in handset devices, so that they can continue to use legacy infrastructure as LTE is rolled out.

OFDMA is a method of multiplexing signals where a high speed data signal is modulated on multiple low speed carriers, the many signals are recollect and combined at the receiver to reform the high speed signal. This method of transmission minimizes multipath distortion [26]. TDMA is a method of multiplexing where multiple users share the same frequency, but transmit and receive at different times. The time is very short and is not noticeable to the end user. CDMA allows multiple users to share the same frequency and time, but are distinguished by codes encoded in the signal [31]. Newer cellular devices are capable of operating in all three of these transmission modes, and they should be kept in mind for the design relating to this project.

2.3 RF Filter Classifications and Design Parameters

There are many design parameters that must be taken into account when analyzing the performance of an RF filter. Not only do the values of the inductors and capacitors influence the filter characteristic, but the configuration of these components can also lead to different design parameters [2]. Bandpass filters are unique because they pass a specific range of frequencies centered about a center frequency. The frequencies between the upper and lower limit, referred to as the pass band, have very low attenuation compared to other frequencies in the transition band and stop band. Ideally, there would be no attenuation in the pass band and complete attenuation in the stop band; however, this is not a realistic expectation since no component is perfect [2]. Filters can be designed to comply with several requirements. In order for the filter to meet the different criteria, basic circuit configurations and values may differ. Four different filter topologies we considered are the Butterworth bandpass filter, Chebyshev I bandpass filter, Chebyshev II bandpass filter, and the Elliptic bandpass filter. Table 1 compares the typical behavior of each of these filters.

Table 1. Comparison of Filter Classifications

	Butterworth	Chebyshev I	Chebyshev II	Elliptic
Ripple	No ripple in either band	Ripple in pass band	Ripple in stop band	Ripple in both pass band and stop band
Roll-off	Low	High	Moderate	Very high

The key design parameters in Table 1 review the band of frequencies where ripples occur as well as the roll-off, which is defined by the transition from pass band to stop band. Other design parameters that should be explored when designing a filter include insertion loss, quality factor, phase, and the filter order [3]. The filter order increases for each capacitor or inductor used in the design. Additionally, the roll-off from pass band to stop band increases with each additional energy storage component. Figure 4 shows the magnitude response of the considered filter topologies superimposed on the same plot. Each filter was designed to have the same center frequency, low cutoff frequency, and high cutoff frequency.

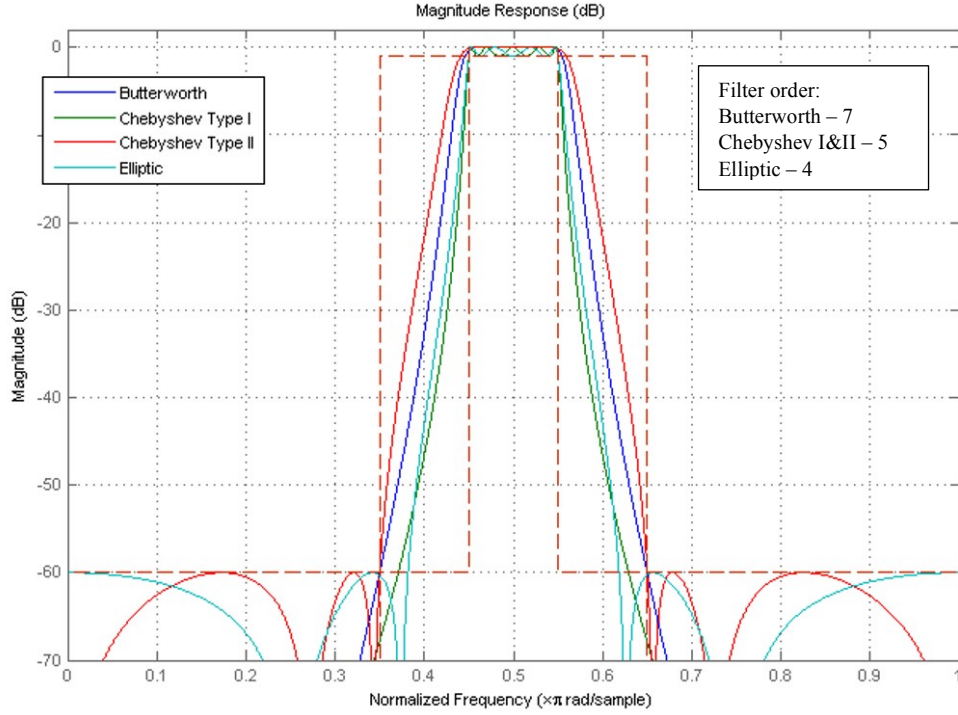


Figure 4. Magnitude responses of different filter configurations, Butterworth, Chebyshev I, Chebyshev II, and Elliptic [32]

As previously mentioned, a perfect filter would introduce no power loss in the pass band. This is another way of specifying that there would be no insertion loss; however, realistically, a power loss is expected. The insertion loss quantifies how much below the 0 dB line the power amplitude response drops [3]. The insertion loss (IL) is quantified by:

$$IL [dB] = 10 \log \left(\frac{P_A}{P_L} \right) = -20 \log |S_{21}| \quad (1)$$

In Equation (1), P_L is the power delivered to the load, P_A is the available power from the source, and S_{21} is the scattering parameter expressing the forward voltage gain. Even ideal filters with ideal inductors and capacitors suffer from insertion losses [3]. The quality factor at the filter's resonant frequency is quantified by:

$$Q = \omega \frac{W_{stored}}{P_{loss}} \quad (2)$$

In Equation (2), P_{loss} is the power loss of the filter and W_{stored} is the energy stored in the filter. The quality factor is also the inverse of the loss tangent ($\tan \Delta$). Typically, capacitors have higher quality factors than

inductors due to the equivalent series resistance (ESR) being much greater in inductors than capacitors [3].

2.4 Tunable Filter Solutions

In this section, we examine a set of various technologies that have been utilized to design tunable filters throughout the history of engineering. The devices that we have researched include: Yttrium Iron Garnet ferrimagnet, Barium Strontium Titanate ferroelectric material, varactor diodes, MEMS capacitors and digitally tunable capacitors. For each implementation, there are many parameters regarding these technologies that can affect the performance of the circuit. Therefore, it is important to consider all these before making a choice on which technology to use for a specific application. We conclude the chapter with a review of some implementation of these technologies that have been patented.

2.4.1 Yttrium Iron Garnet (YIG) Tunable Filters

One of the oldest technologies for implementing filter tuning is the Yttrium Iron Garnet technology. Yttrium Iron Garnet is a ferrimagnetic material whose magnetic dipoles precess at a frequency of the external magnetic field applied to the material. Additionally, this technology exhibits extremely low losses, which attributes to YIG being a good candidate for tunable filter technology [8]. Phillip S. Carter began exploring this technology in the 1960s and was one of the first researchers to investigate and explain its concept of operation. In his article from 1961, "Magnetically-Tunable Microwave Filters Using Single-Crystal Yttrium-Iron-Garnet Resonators" he provides the illustration of concept shown in Figure 5.

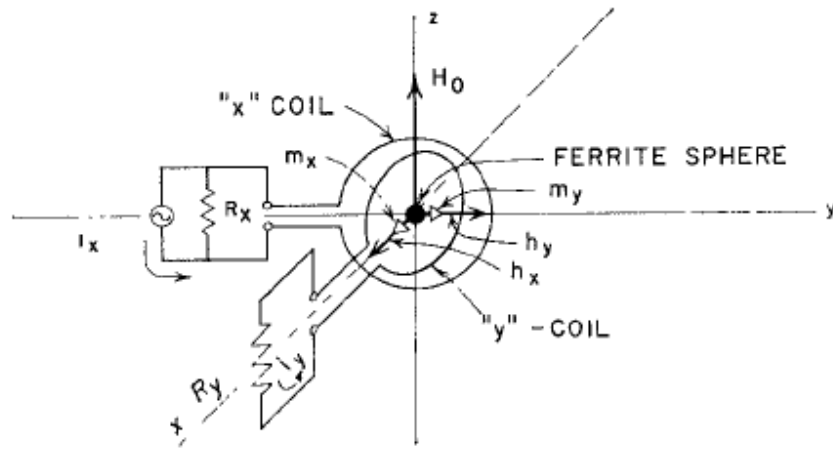


Figure 5. Magnetic resonance filter

The two coils are perpendicular to each other and a small sample of YIG ferrite is placed at the center of their cross section, as shown in Figure 5. Once the DC magnetic field is applied along the z-axis and a RF driven current $I_x e^{j\omega t}$ (note the frequency dependency) is provided at the terminals of the x coil, magnetic dipoles in the YIG ferrite precess around the x-axis. This induces an RF magnetic moment along the y-axis and voltage in the y circuit. Therefore, the resonant frequency of the YIG filter is tuned by changing the magnetic field and the current that are externally applied to the ferrite [9].

However, there is a requirement that the unloaded Q value of the resonator be high in a low-insertion and narrow bandpass filter implementation. The unloaded Q value refers to the properties of the ferrite that includes the damping time and the gyromagnetic ratio. The second requirement for low insertion loss is that the narrow passband requires the external Q value to be significantly lower than the unloaded Q

value. External Q value relates to the loops, strip-transmission lines and TE₁₀ mode rectangular waveguide that are operating in conjunction with the YIG ferrite material. One of the disadvantages of the YIG ferromagnetic tunable filters is the low tuning speed, which is generally in range from tens of microseconds to a few milliseconds [10].

2.4.2 Barium Strontium Titanate Tunable Filters

Barium Strontium Titanate (BST) is a ferroelectric material that is a promising candidate for the applications of tunable filters. A few ideal characteristics include its dependence on the dielectric permittivity of an applied electric field, high dielectric constant and low production costs.

Ferroelectric materials are dielectric materials known for their ability to achieve spontaneous polarization that can be reversed in the presence of an external electric field. When an external field is applied to a regular dielectric material, the electric dipole moments within the material will align themselves in accordance with the direction of the applied electric field. On the other hand, in materials such as ferroelectrics, this polarization can happen even without the external electric field. Once the electric field that does not exceed the breakdown limit of the crystal is applied to the ferroelectric, its dipole moments will reverse to align with the field.

Another unique aspect of the ferroelectric materials is that they become paraelectric past the transition temperature, known as the Curie temperature [11]. At the Curie temperature they undergo a structural change while achieving the highest dielectric constant that decreases with further temperature increase, as shown in Figure 6.

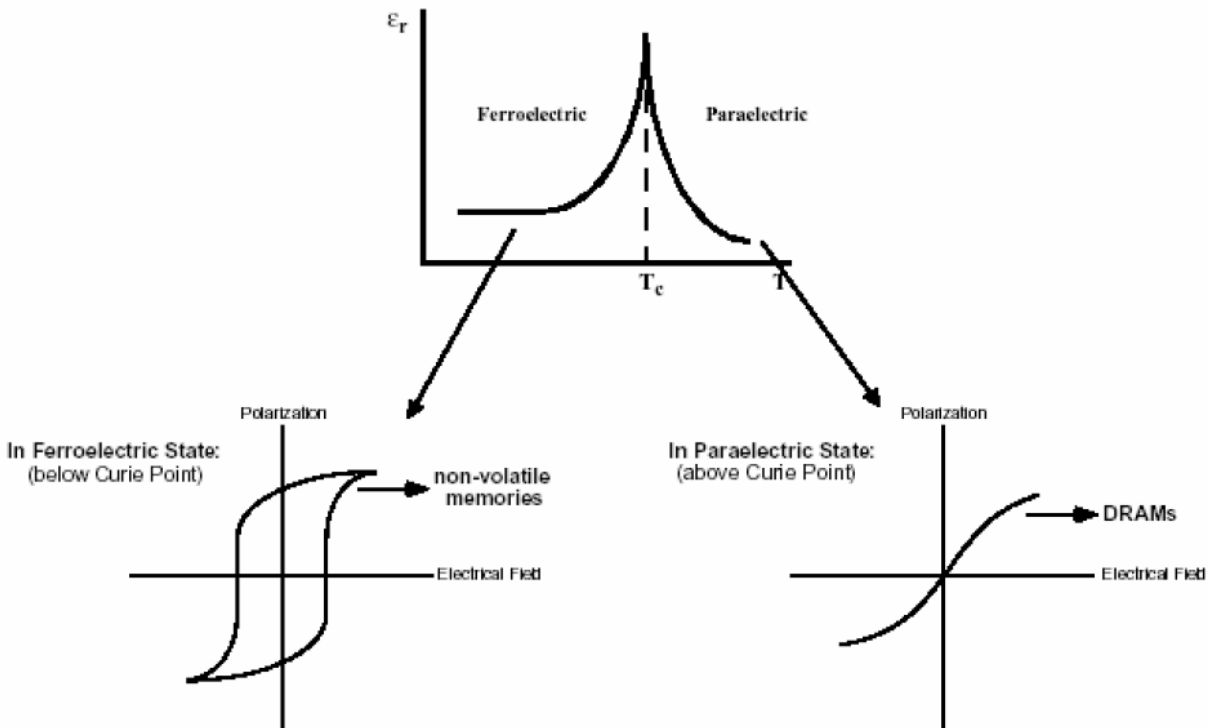


Figure 6. Ferroelectric material change of state at Tc [11]

Above the Curie temperature, the material no longer has spontaneous polarization and it obtains paraelectric properties. Paraelectric materials become polarized in the presence of an external electric field just like the ferroelectric materials, but unlike ferroelectrics, polarization in paraelectrics can occur

even when there is no permanent electric dipole in the material. Additionally, polarization of paraelectric materials returns to zero in the absence of the external field.

BST has been found as one of the most suitable ferroelectrics for the tunable filter application as it has a higher dielectric constant, lower losses and higher tunability. Moreover, its high capacitance density allows for construction of higher capacitor values within a smaller area [11]. Unlike conventional varactor diodes, BST varactors have no forward conduction region and perform well in applications involving high RF voltage swings over the full range of the DC tuning voltage [12].

2.4.3 Varactor diodes

Varactor diodes, or varicap diodes, are semiconductor devices whose capacitance varies as a function of the voltage applied across its terminals. They are widely used in applications where voltage controlled variable capacitance is required [18]. Thus, a varactor diode is one of the candidates that can be integrated as part of a tunable filter design approach.

Varactor diode is in essence a p-n junction exhibiting the characteristics of a variable capacitor. Under reverse bias condition, no current can flow and the diode's reverse resistance is almost infinity. The depletion region at the p-n junction acts like an insulating dielectric sandwiched between conductive plates of a capacitor. The symbol for the varactor diode can be seen in Figure 7.



Figure 7. Varactor diode symbol

Generally, capacitance is a function of the plate surface area, the dielectric constant of the insulator and the distance between the two plates. In the case of a varactor diode, the distance between two plates depends on the width of the depletion region that also varies with the applied voltage. Therefore, the capacitance of the diode can be controlled by an applied voltage between the p-n junctions. The capacitance of the varactor diode is described by:

$$C = \frac{C_0}{\left(\frac{V}{V_{bi}} + 1\right)^n} \quad (3)$$

In Equation (3), C is the varactor diode capacitance, C_0 is the zero bias capacitance, V is the reverse bias voltage, V_{bi} is the built-in voltage potential, and n represents the slope of the $\log C$ vs. $\log V$ curve.

As Equation (3) illustrates, when the magnitude of the reverse bias voltage increases, the capacitance decreases and vice versa. In addition, the varactor diode capacitance is also a function of the doping structure introduced within the semiconductor during the wafer fabrication process. In particular, the exponent n is 0.33 if the diode has a graded junction (linear variation), 0.5 for an abrupt junction (constant doping density). If the density jumps abruptly at the junction and then decreases (called hyper-abrupt), n can be as high as 2 [19, 20].

A varactor diode tends to be physically small, inexpensive and has a very high tuning speed, which makes its use advantageous in tunable filters. However, its disadvantages include low Q value, poor power handling capabilities and highly nonlinear characteristics at high frequencies [15].

2.4.4 MEMS tunable capacitors

Another important type of tunable components that can be used to implement a tunable filter is the MEMS or micro-electro-mechanical systems capacitor that is made through micro fabrication. Due to the unique capabilities enabled by micromechanical tuning and the low loss materials used in the construction, RF-MEMS has become a key technology in many RF applications [15].

Although there are many types of tunable MEMS capacitors, their operation is basically the same. MEMS technology operates using a DC voltage to control the mechanical structure of the capacitor such as the area of the two plates, or the distance between the two plates. An example of a MEMS capacitor is the metal membrane variable capacitor. It consists of two parallel plate electrodes, one of which is metallic [16]. The capacitance is tuned by varying the gap between the two plates by electrostatic actuation as shown in Figure 8.

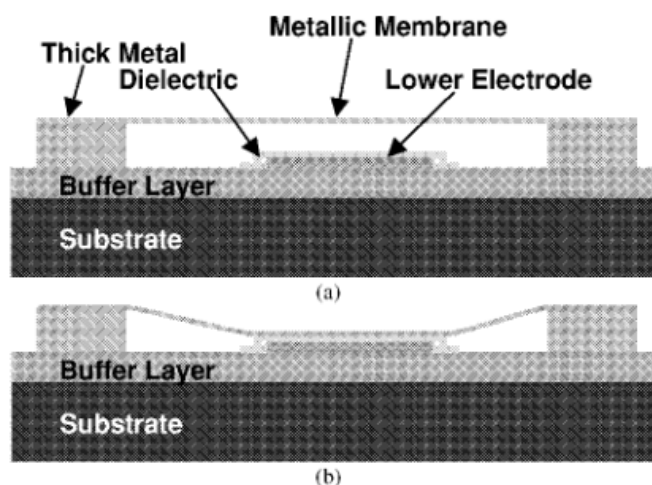


Figure 8. Cross section of an RF MEMS capacitor in the un-actuated (a) and actuated (b) position [16]

In general, RF tunable MEMS capacitors are easily integrated, have excellent functionality, and perform well for RF applications. They have good linearity, low power consumption, small size and high Q value at high frequencies. However, a disadvantage of MEMS technology is its challenging fabrication and packaging process that requires the ability to deposit very thin films of material on the substrate [15].

2.4.5 Digitally Tunable Capacitors

Digitally Tunable Capacitors (DTCs) are variable circuit components whose capacitance is controlled by a set of FET switches in a combination with a digital SPI interface. The DTCs are made up of several high Q-factor metal-insulator-metal (MIM) capacitors and an array of digitally controlled FET switches that determine the total value of the capacitor bank available at a certain control setting as can be seen in Figure 9. This control setting is a digital input that feeds in a binary value corresponding to a certain number of switches to be turned on and hence determining how many capacitors will contribute to the total capacitance value. All this is contained within a single die and there is no need for additional control components [13].

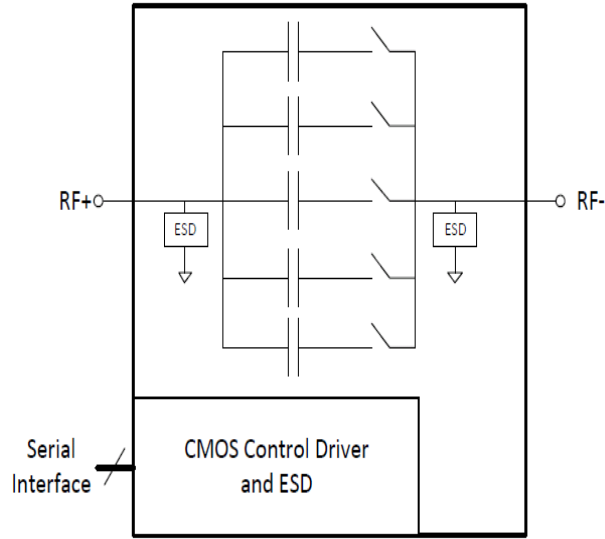


Figure 9. Block diagram of DTC [13]

MIM capacitors are generally connected in parallel to each other and each capacitor is connected to a FET switch in series. The maximum capacitance is achieved when all the switches are ON since the total capacitance of individually connected capacitors in parallel is additive. The minimum capacitance is achieved when all the switches are off.

Shown in Figure 10 is the equivalent circuit for the DTC. It consists of three main parts: The tuning core (R_S and C_S), the parasitic package inductance (L_S) and the shunt parasitic network (C_P , R_{P1} , R_{P2}).

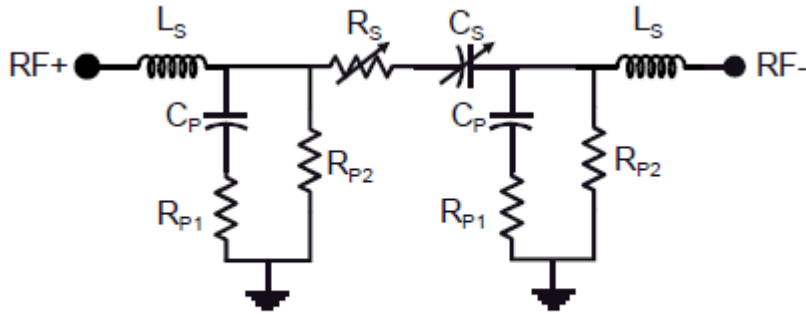


Figure 10. Equivalent circuit for DTC [13]

One advantage of the DTC is that it has a very linear response. Its capacitance is proportional to input from the digital control circuit in a discrete fashion. The resolution is dependent on the number of discrete steps between the minimum and maximum capacitance value. Additionally, there will be a difference in capacitance values between series and parallel configurations. More specifically, the capacitance values will be higher should the DTC be configured in parallel with the rest of the circuitry. This is due to the fact that when in parallel DTC's RF- end is usually connected to ground which results in C_S and C_P essentially being in a parallel connection as well. Parallel connection between the tuning core capacitance C_S and the parasitic capacitance C_P results in addition of the two and hence creating capacitance values that are greater than those of the series connection. Figure 11 portrays the capacitance difference between

these two configurations. However and most importantly, both configurations still exhibit the desired linear behavior.

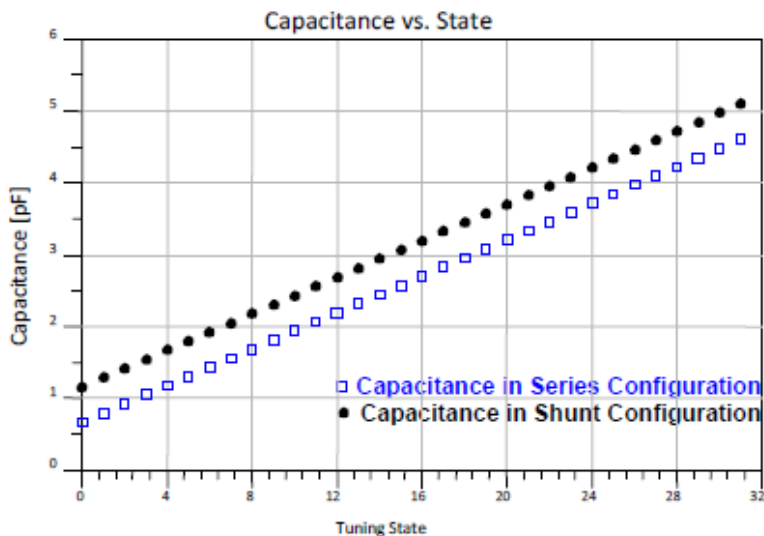


Figure 11. Capacitance in series and shunt configurations [13]

The Q value is dependent on the configuration the DTC is in. It is significantly more difficult to determine the dissipative losses in series connection as they depend on the source and load impedances. [13] The Q value behavior for the shunt configuration is dependent on the Q value of the tuning core and the parasitic network capacitance. The Q value of the DTC in shunt configuration decreases with frequency and the state it is in as can be observed in Figure 12. In State 31, which represents 31 capacitors on, and at 300MHz, the quality factor is in its 40s, whereas at 2GHz it drops to approximately 12. This is one of the downsides and potential design challenges of implementing the DTC for our project.

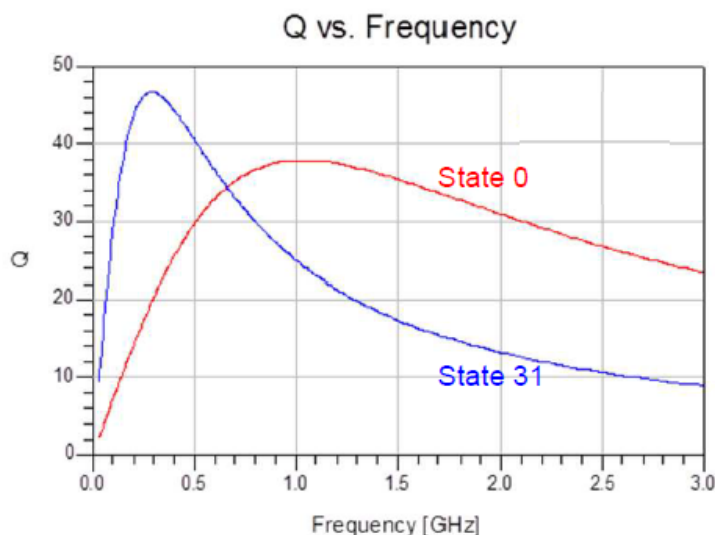


Figure 12. Quality factor of the DTC in shunt configuration [13]

2.4.6 Comparison of Several Component Technologies

Several of the aforementioned technologies available for tunable microwave applications are compared in Table 3.

Table 2. Comparison of competing technologies with BST [9, 11, 13, 28, 29, 30]

Properties	Varactor Diode	MEMS	BST	DTC	YIG
Tunability (High Q)	Good	Low	Good	High	High
RF loss	Moderate (Q < 60 typically)	Very Good (Q < 200)	Moderate (Q < 100 typically)	Moderate (Q < 50 typically)	Very good (Q < 200)
Control Voltage	< 10V	< 60V	< 5-30V	< 30V	< 28V
Tuning Speed	Fast 1-5 nanoseconds	Slow > 5 microseconds	Fast < 30 nanoseconds	Fast < 12 nanoseconds	Slow > 1 milliseconds
Power Handling Capability	Poor	Excellent	Trades with Control Voltage	Excellent	Excellent

According to Table 2, varactor diodes have good tunability, fast tuning speed and small size. However, these components have junction noise, poor power handling capability and require a reverse bias condition to sustain a capacitive effect. MEMS based devices are linear in response as well as maintain very low RF loss high tunability properties. Nevertheless, these devices are relatively slow, can be unreliable and have high packaging cost. BST technology is advantageous over both semiconductor and MEMS devices due to low cost, higher break down voltages, higher power handling capability and low packaging cost. YIG materials excel in all factors except in the tuning speed as they exhibits speeds in the range of milliseconds. Finally, the DTCs have high tunability, moderate RF loss, operate at high speeds and have excellent power handling capability.

2.4.7 Prior Art Patents

Christopher Rice and Harry Worstell of Lucent Technologies Inc. hold a patent entitled “Filter having tunable center frequency and/or tunable bandwidth” [6]. They detail in their patent a basic bandpass filter topology and identify the elements needed to be tunable in order to change the center frequency as well as the passband of the filter response. As shown in the circuit diagram in Figure 13, they show that the shunt capacitances and inductances should be tunable, while the coupling capacitors remain of constant value. According to the schematic, both the shunt inductance and capacitance need to be variable to adjust the frequency and bandwidth of the filter response. The capacitance must change a ratio less than 1:9:1 and the inductance must change over 7:0:1. The inventors recommend the use of microstrip lines, and FET switches to vary the capacitances and inductances, but recognize that other tunable elements can be used [6]. This approach may not be practical for the application of tunable filters within a smartphone handset, because a tunable inductor is very difficult to implement. The method previously discussed of switching microstrip lines of appropriate length to provide different inductances could not be realized in the small space available in phone handsets.

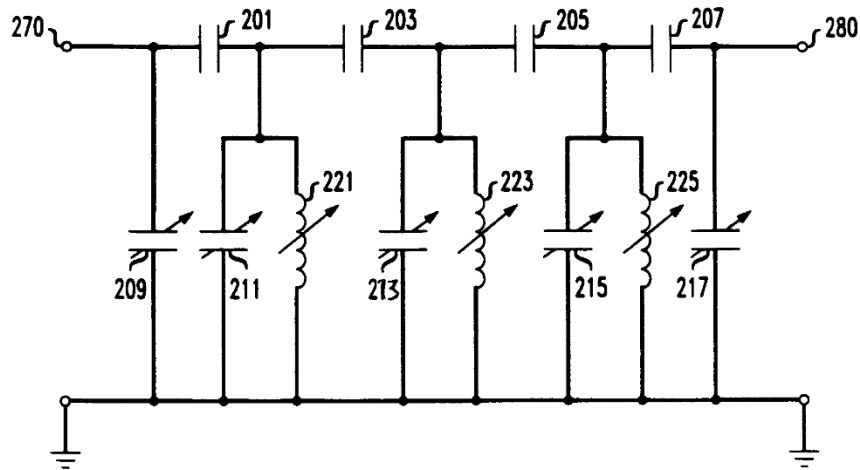


Figure 13. Circuit diagram from Rice and Wortell's patent showing elements required to be tunable and elements required to be fixed for the filter to be tuned [6]

Michael Koechlin of Hittite Microwave Corporation holds a patent “Wideband analog bandpass filter.” The inventor provides a schematic of a bandpass filter that is tunable in both frequency and bandwidth using varactor diodes, but acknowledges the potential use of MEMS capacitors or discretely tunable elements. In his design he couples the varactor diodes anode to anode in shunt with an inductor, with the control voltage connected between the two diodes, changing the capacitance and tuning the response of the filter. He also asserts that it is important to use the resistor, R1, as shown in Figure 14, to improve rejection of harmonics in the stopband [7]. This implementation could be realized for the purposes of this project, however as discussed earlier in this section, varactor diodes have drawbacks that can be overcome using other components.

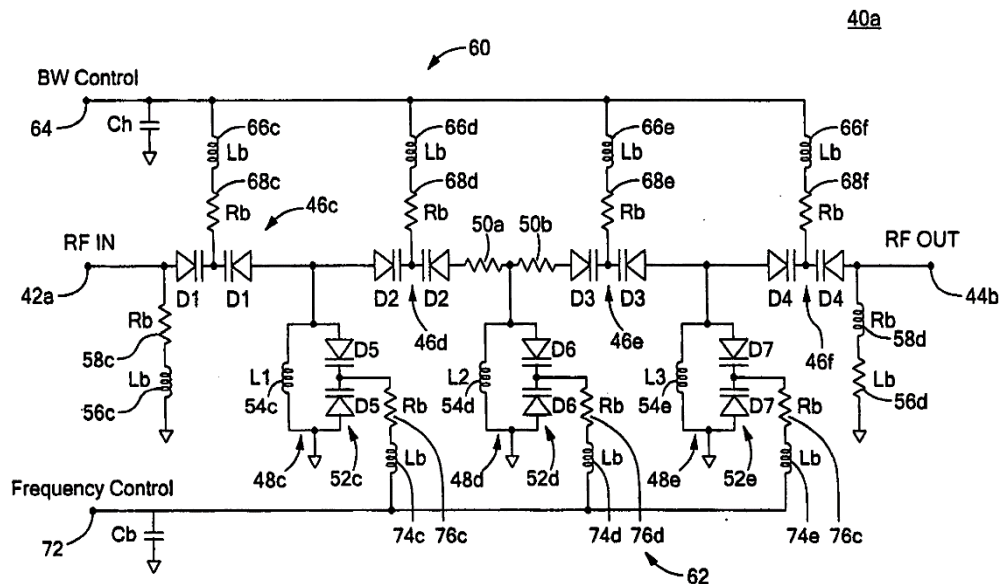


Figure 14. Circuit diagram showing the bandwidth and frequency controlled filter patented by Koechlin [7]

2.5 Acoustic Filter Technology

Another filter technology that currently dominates in wireless communications is acoustic filtering. Surface-Acoustic-Wave (SAW) filters and Bulk-Acoustic-Wave (BAW) filters are two different types of acoustic filters that are available on the market [4]. Both of them are mechanical filters that exploit the piezoelectric properties of the substrate. While SAW filters have been used in many applications since the early days of mobile phones, BAW filters were first introduced in 2001. This section concentrates on providing background information of these two filters including the operation, performances, as well as their strengths and weaknesses.

2.5.1 SAW filter

A SAW filter consists of three main elements that are two interdigital transducers and a piezoelectric substrate. The structure of a SAW filter is shown in Figure 15.

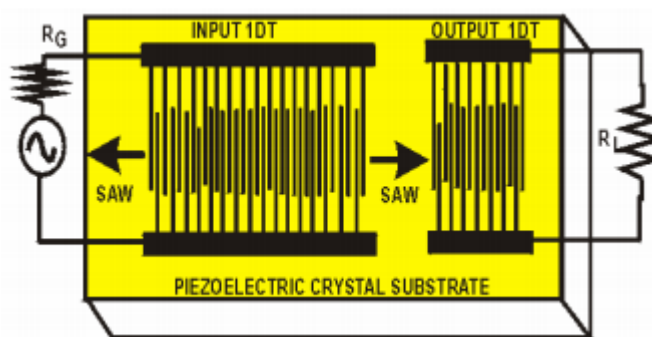


Figure 15. SAW filter consists of two transducers and a piezoelectric crystal substrate [5]

When an electromagnetic signal is transmitted to the input interdigital transducer, it is then converted to an acoustic wave. This acoustic wave propagates through a piezoelectric substrate before being detected and converted back to an electric signal by the output transducer. However, certain frequencies transmitted through the filter generate standing waves across the substrate. Other frequency components are diminished because of destructive interference. Thus, the system behaves exactly like a bandpass filter. The choice and cut of piezoelectric substrate material and the shape and spacing of the transducer electrodes play a crucial role in determining every signal characteristic of the filter including the resonant frequency, bandwidth and roll-off factor [5].

2.5.2 BAW filter

Unlike SAW filters, the acoustic wave in a Bulk-Acoustic-Wave Filter (BAW) propagates vertically inside rather than on the surface of the substrate, as shown in Figure 16. Therefore, their structures are different. BAW resonators consist of a thin layer of a piezoelectric material and two metal transducers parched on the opposite faces of the substrate [21]. These electrodes then generate and detect acoustics waves bouncing from the top to bottom electrodes. Similar to the SAW filter, standing waves are formed between the two electrodes and the resonance frequencies are strictly controlled by the mechanical structure of the filter such as layer thickness, distance between the two electrodes [22].

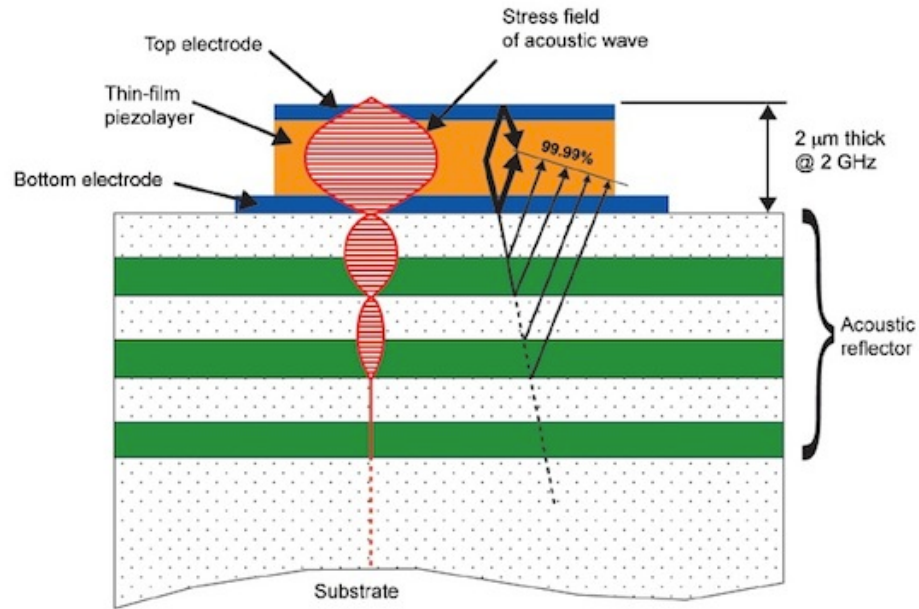


Figure 16. In a BAW filter, acoustic wave bouncing from the top to bottom of the electrodes rather than on the surface of the substrate [4]

2.5.3 Performance

The conversion between electrical and acoustic waves at the two transducers induces extremely low insertion loss. Not only are SAW and BAW filters highly selective for the pass band, but they also have high quality factors and fast roll-off. Additionally, they are small in size and have low power consumption, which could conserve battery life in a mobile phone application. Although the BAW filter is more complicated to produce compared to the SAW filter, it performs better at microwave frequencies. Although these filter technologies are highly superior, they are also nonlinear and have a high process complexity [4, 5]. Due to their mechanical nature, these types of filters are unable to be tunable and will not be investigated for the purposes of design in this project.

CHAPTER 3: OBJECTIVES

The objective of this project is to design and simulate a tunable filter that is suitable for cellular band 25 (1850 - 2100 MHz) and which meets the requirements for the cellular 3GPP LTE standard. Band 25 specification requires transmit and receive bandwidth of up to 20MHz. In addition, there is an 80 MHz offset between transmit and receive frequencies. The filter will be first designed using lumped element inductors and capacitors. In order to demonstrate the characteristics of the filter, the industry standard Advanced Design System (ADS) was used to simulate the filter and show its response. Specifically, the requirements are:

1. Design a tunable bandpass filter constrained by the specifications of cellular band 25
 - a. Filter bandwidth of 20 MHz
 - b. Isolation of -50 dB needs to be provided at an offset of 80 MHz between transmit and receive frequency
2. Choose components within the constraints of available technology
 - a. Use lumped elements
 - b. Limit inductor and capacitor values to what is available to Skyworks
 - c. Limit the tuning range of the components to what is available
 - d. Limit Q values of components to those that are commonly available in production
3. Use Agilent's Advanced Design System to simulate this filter
 - a. Provide frequency and phase response plots for all frequency bands that the filter will operate in

CHAPTER 4: APPROACH

We have researched the current state-of-the-art of the RF section of cellular devices, filter types and topologies, and tunable elements that can be used to adjust the center frequency of the filter while keeping the bandwidth constant. The potential filter topologies were simulated in ADS using ideal lumped element components.

The next step was to investigate the performance of different types of filters including Butterworth and Chebyshev. The amplitude and phase response of the filters were observed by plotting the magnitude and phase of the S21 parameter in ADS. The responses and the complexity of these filters were compared in order to determine the best solution that satisfies the desired specification.

Once fully realized, the filter would not perform according to the ideal behavior of the virtual components. Therefore, we decided in our research to simulate the lumped elements with appropriate Q values. To determine the Q values of each component, we researched several available components on the market. It was expected that design modifications would become necessary in order for the filter to perform to specification with the lessened quality factor of the components.

Determining component values that provided the desired response was a key consideration in designing our filter configuration. In this section, we used the ADS simulator as well as a mathematical model to determine values for the filter components. It was expected that the mathematical model would be more useful in the initial design phase.

Once filter topologies were realized that meet the objectives of the project, we prepared and presented the design options and our recommendations for the design with the best performance.

4.1 Fundamental Filter Theory

The approach to RF filter design that is commonly used is based on a normalized low pass filter configuration, which can then be synthesized into a unique filter performance [2]. A normalized filter has a cut-off frequency of 1 radian per second, or 0.159 Hz, and is terminated with a $1\ \Omega$ resistance. Two equivalent realizations of the normalized lowpass filter are shown in Figure 17.

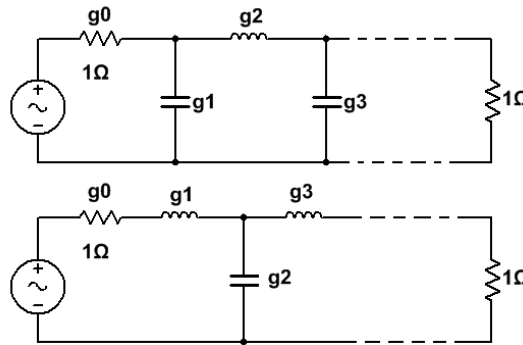
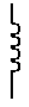


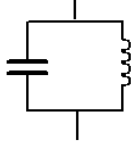


Figure 17. Two equivalent realizations of a normalized low pass filter [3]

In Figure 17, the values for the g 's involve inductors and capacitors in Henries and Farads, respectively, and can be found in many pre-calculated tables for different types of filters. In order to arrive at the realizable filters, these coefficients are de-normalized to meet realistic frequency and impedance requirements [3]. The transformation between normalized lowpass filter and actual bandpass filter is captured in Table 3.

Table 3. Bandpass filter transformation and de-normalization

Lowpass filter prototype	Bandpass filter realization
 $L = g_k$	 $\frac{LR_G}{2\pi(f_2 - f_1)}$ $\frac{(f_2 - f_1)}{2\pi f_1 f_2 L R_G}$
 $C = g_k$	$\frac{C}{2\pi(f_2 - f_1)R_G}$  $\frac{R_G(f_2 - f_1)}{2\pi f_1 f_2 C}$

In Table 3, f_1 and f_2 refer to the low and high cutoff frequencies, respectively, and R_G denotes the serial impedance of the source which is usually mapped to the characteristic impedance of the transmission line. The final standard bandpass filter schematics are shown in Figure 18. The choice of inductors and capacitors is crucial to the performance characteristic of the filter. It is important to note that high quality components should be used when constructing these filters to ensure that the required performance is obtained [2].

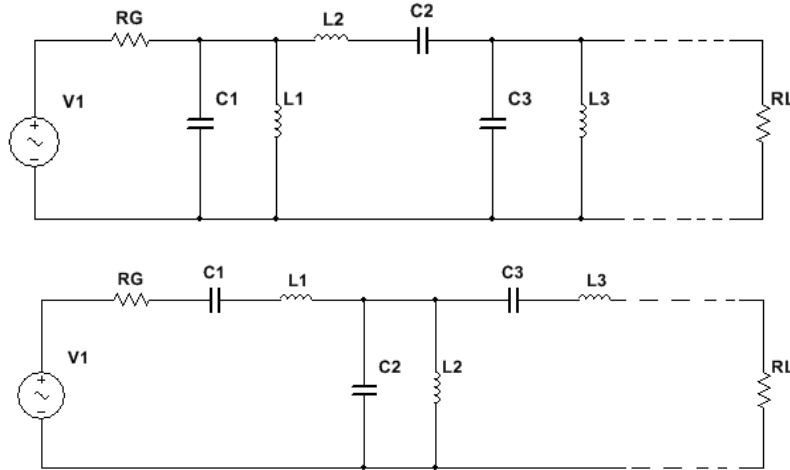


Figure 18. General bandpass filter topologies [3]

Applying the processes described above, we started our design with a third order bandpass filter. The center frequency is around 1.95 GHz and the filter has to meet a bandwidth of 20MHz. and match to a 50Ω characteristic line impedance. The values for the g coefficients were determined using the existing literature. For example, we found that the coefficients for a third order maximally flat Butterworth lowpass filter prototype are $g_1 = g_3 = 1$ and $g_2 = 2$ [2]. In this filter prototype the cutoff frequency is 1 rad/s and both generator and load impedances are equal to unity. In our specifications, we have the low and high cut off frequencies of 1.94 GHz and 1.96 GHz, respectively. Therefore, we must apply transformations described by Table 3 and calculate the component values:

$$L_1 = L_3 = \frac{g_1 R_G}{2\pi(f_2 - f_1)} = 398 \text{ nH} \quad (1a)$$

$$L_2 = \frac{R_G(f_2 - f_1)}{2\pi f_1 f_2 C} = 20.9 \text{ pH} \quad (1b)$$

$$C_1 = C_3 = \frac{g_1 R_G}{2\pi(f_2 - f_1)} = 16.7 \text{ fF} \quad (1c)$$

$$C_2 = \frac{C}{2\pi(f_2 - f_1)R_G} = 31.8 \text{ pF} \quad (1d)$$

This example shows the general process of designing a fixed bandpass filter structure that meets our specifications. The resulting schematic is shown in Figure 19. As the calculation indicates, for a very high frequency and narrow bandpass filter, the component values are very small and very difficult to realize since they are on the order of femtofarads and picohenries. The next section provides the frequency responses created by ADS simulation of four different bandpass filter topologies using the same method as described above.

4.2 Ideal Fixed Filter Simulation

Using Agilent's Advance Design System (ADS) software, we investigated different ideal filter topologies including the maximally flat Butterworth, the linear phase Butterworth, and the Chebyshev 3dB and 0.5 dB filters. We chose the T-network topology as our normalized lowpass filter, then we derived the third order bandpass filter shown in Figure 19.

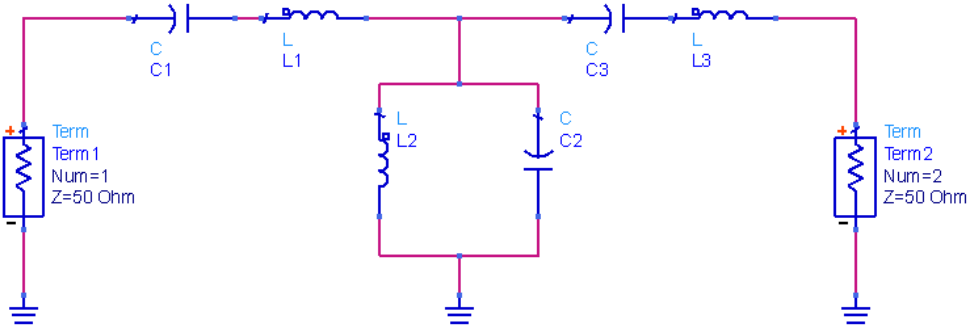


Figure 19. Third order bandpass filter schematic

To achieve a filter response that passes frequencies between 1940MHz and 1960MHz, inductor and capacitor values were calculated using Table 3 for each filter topology, as discussed in Section 4.1. Note that the source and load impedances are matched to the characteristic impedance Z_0 of 50Ω. Next, the response of each filter was investigated by plotting the S21 parameters in ADS. Among these filter types, we found that the maximally flat Butterworth filter provided the best response in the passband, while the 3dB Chebyshev filter had the highest isolation at the rejection band. The detailed component values as well as the performance of each filter are discussed in the following subsections.

4.2.1 Butterworth

In this section, we present the magnitude and phase versus frequency responses using the g coefficients for the maximally flat Butterworth filter design. Table 4 reports the appropriate coefficients as well as the corresponding inductor and capacitor values.

Table 4. Calculating component values for a third order maximally flat Butterworth filters

Coefficients	1	2	1
Inductors	398 nH	20.9 pH	398 nH
Capacitors	16.7 fF	318.4 pF	16.7 fF

After constructing the suitable filter topology with these inductor and capacitor values, we observed the following response shown in Figure 20.

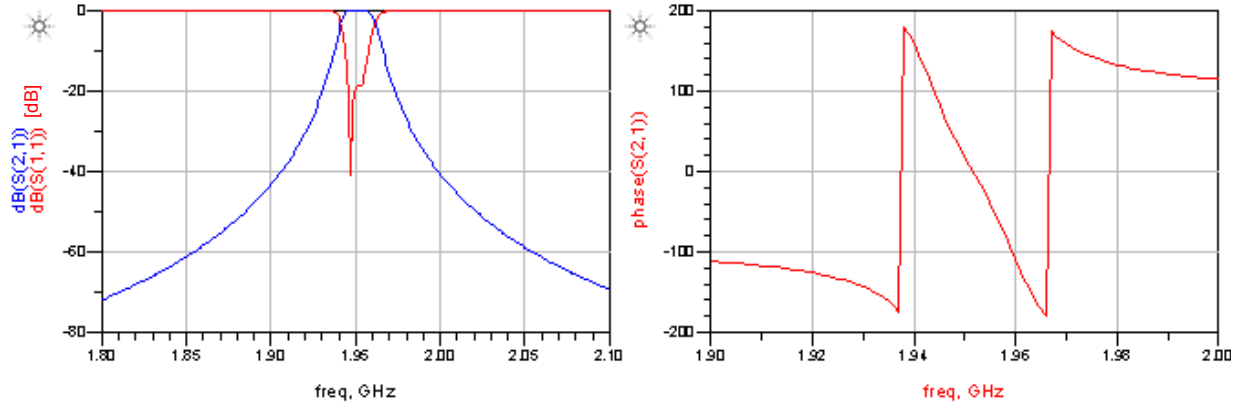


Figure 20. Amplitude (in dB) and phase (in degree) responses of a third order maximally flat Butterworth filter

The maximally flat Butterworth filter topology using ideal lumped element components provided a response adequate for what for the requirement of band 25. As can be seen in Figure 20, the passband of the filter is 20 MHz wide. Additionally, proper isolation was achieved at the offset of 80 MHz below the center frequency. We also observed that there is no ripple in the passband, and the phase response in the passband of the filter is as expected.

4.2.2 Butterworth (Linear phase)

In this section, we compare the magnitude and phase versus frequency responses of the linear phase Butterworth filter design and the maximally flat Butterworth filter design discussed in the previous section. Table 5 reports the coefficients as well as the inductor and capacitor values for this filter implementation, using the appropriate g coefficients.

Table 5. Calculating component values for a third order linear phase Butterworth filters

Coefficients	1.255	0.5528	0.1922
Inductors	499.4 nH	75.7 pH	76.5 nH
Capacitors	13.34 fF	88 pF	87.12 fF

Figure 21 shows the simulated magnitude and phase responses for this Butterworth filter using the appropriate coefficients.

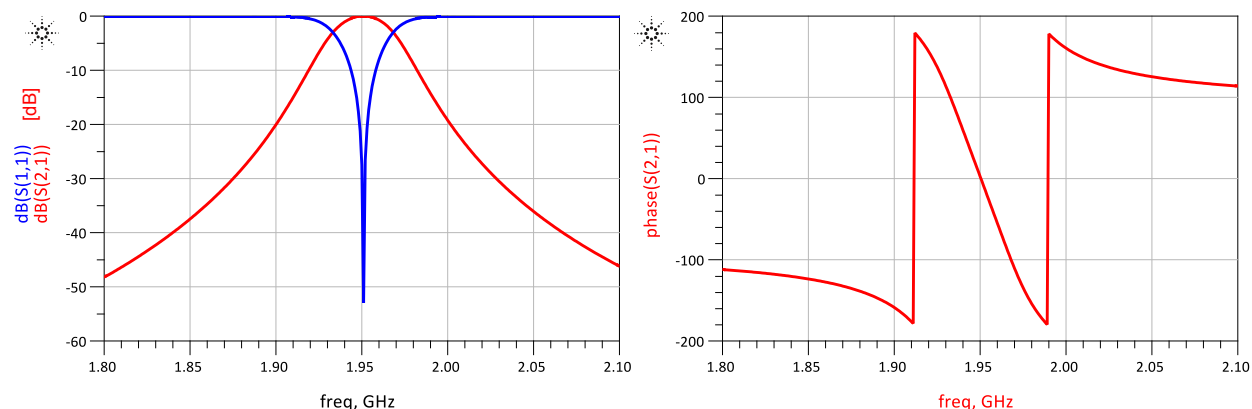


Figure 21. Amplitude (in dB) and phase (in degree) responses of a third order linear phase Butterworth filter

Compared to the maximally flat Butterworth type, the linear phase type filter has an amplitude response that does not provide the required -50dB rejection at the offset of 80 MHz below the center frequency. Additionally, there is also some attenuation in the passband, which prevents this design from being ideal. However, the phase response in the passband of the filter is significantly more linear than that of the maximally flat Butterworth filter, and spans a wider range of frequencies (80 MHz). It is possible to achieve a better roll-off by adding stages, and duplicating the circuitry shown in series.

4.2.3 Chebyshev 3dB

In this section, we present the magnitude and phase frequency responses using the g coefficients for the Chebyshev 3dB filter topology. Table 6 lists the coefficients as well as the inductor and capacitor values for this filter implementation.

Table 6. Calculating component values for a third order Chebyshev 3dB filter

Coefficients	3.3487	0.7117	3.3487
Inductors	1.334 uH	58.8 pH	1.334 uH
Capacitors	5 fF	113.3 pF	5 fF

After simulating this filter implementation with the appropriate inductor and capacitor values, we observed the following response shown in Figure 22.

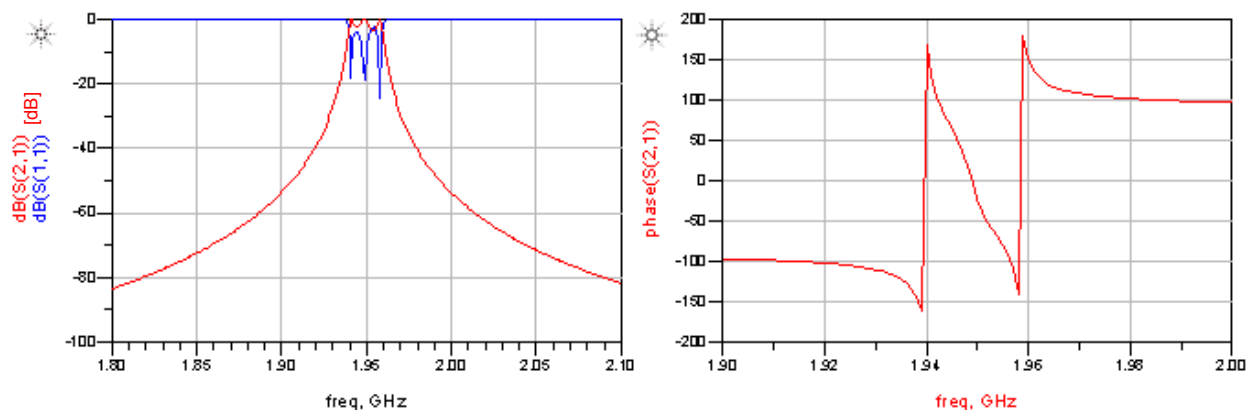


Figure 22. Amplitude (in dB) and phase (in degree) response of a third order 0.3dB Chebyshev filter

The 3dB Chebyshev filter using ideal lumped element components also provided the desired response for band 25. Although there are 3dB ripples in the passband, the roll-off factor of this filter is much higher than that of either Butterworth filter. At -67dB, this configuration surpassed the desired isolation at an offset of 80MHz below the center frequency, and it also maintained a relatively linear phase response.

4.2.4 Chebyshev 0.5dB

In this section, we compare the magnitude and phase frequency responses of the Chebyshev 0.5dB filter and the Chebyshev 3dB filter design discussed in the previous section. Table 7 shows the coefficients as well as the inductor and capacitor values for this filter implementation.

Table 7. Calculating component values for a third order Chebyshev 0.5dB filter

Coefficients	1.5963	1.0967	1.5963
Inductors	635 nH	38.2 pH	635 nH
Capacitors	10.5 fF	175 pF	10.5 fF

Figure 23 depicts the corresponding magnitude and phase response of this filter implementation.

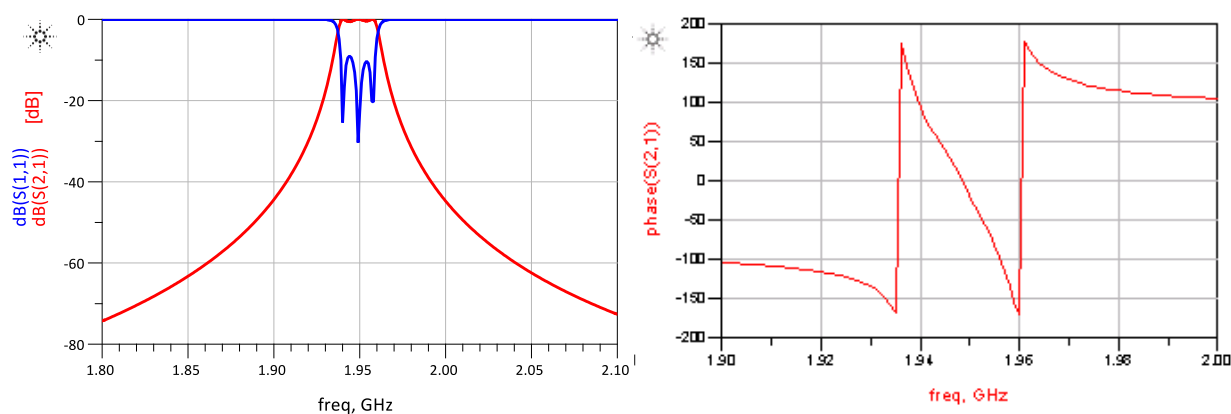


Figure 23. Amplitude (in dB) and phase (in degree) response of a third 0.5 dB Chebyshev filter

As discussed in Chapter 2, ripples in the passband of a Chebyshev filter are a tradeoff for a good roll-off factor. Therefore, a 0.5dB Chebyshev has fewer ripples in the passband but lower isolation in the stopband compared to the 3dB Chebyshev filter. The attenuation at the offset of 80MHz below the center frequency is -55dB which still meets the requirement of band 25.

4.3 Potential Tunable Design Approaches

Although three of the ideal lumped component bandpass filters above provided desired responses for band 25, they all have one common problem. Capacitors C_1 and C_3 require very low values and are therefore not practical with the available process technology. As a result, we decided to investigate another filter topology using capacitive coupled resonators. The structure of this filter type is depicted in Figure 24. This topology not only uses more reasonable component values, but also allows for easier control of the characteristic response by tuning the capacitor values.

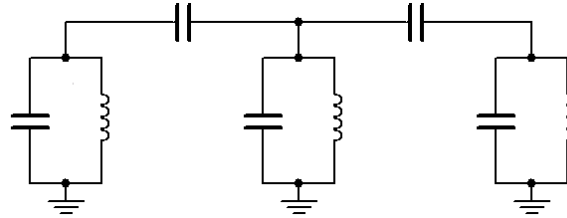


Figure 24. Structure of a third order capacitive coupled shunt resonators

All of the components values were calculated based on the maximally flat Butterworth filter model and then manually adjusted using ADS to achieve the desired characteristic. We investigated the performances of both a third order filter and a fourth order filter. The simulation results for each filter implementation are discussed in the following subsections.

4.3.1 Third order tunable C-coupled shunt resonators

In this section, we present the results of our simulations for the third order tunable C-coupled shunt resonators using two coupling capacitors. For this implementation, we needed to manually adjust the capacitor values to tune to several frequencies in band 25. Figure 25 captures the simulation setup and the schematic of the five stage (third order) tunable bandpass filter using C-coupled shunt resonators.

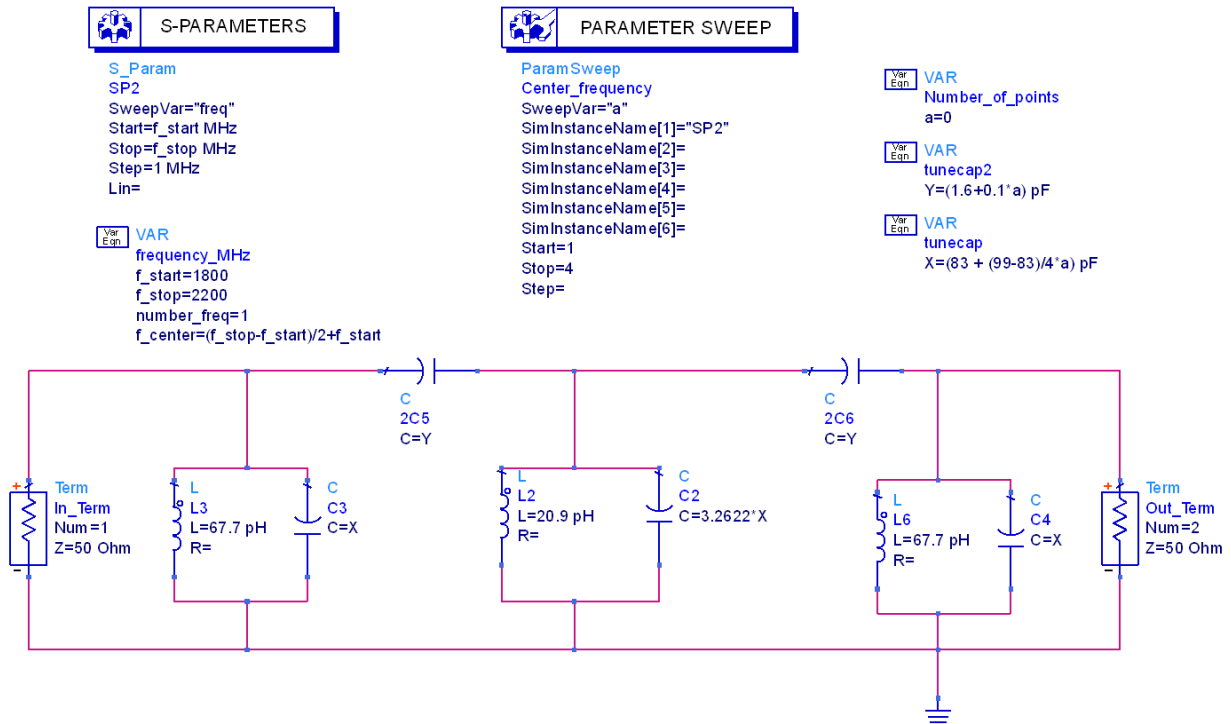


Figure 25. ADS Simulation of a third order capacitive coupled tunable bandpass filter

After appropriately setting up the software, we were able to attain the frequency response of the filter shown in Figure 26.

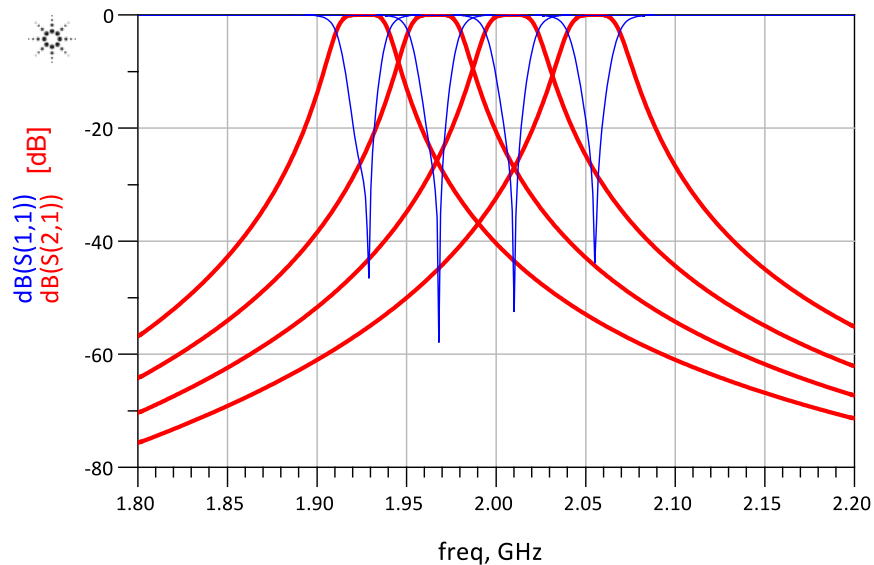


Figure 26. Frequency response (in dB) of the third order C-coupled tunable bandpass filter, showing the circuit can be tuned to the 4 sections of the cellular handset receive band

To achieve the desired center frequencies we found that the tuning range of capacitors C3 and C4 were required to be 83pF to 99pF for a ratio of 1:1.3 and the tuning range of capacitor C2 was required to be 270.8pF to 349.1pF for a ratio of 1:1.7. When tuning the center frequency of the filter by changing the

shunt capacitors of the resonators, the bandwidth also changes unintentionally. Therefore, in order to achieve a constant bandwidth of 20MHz, the coupling capacitors were required to change from 1.6pF to 2pF. When examining the response of the filter at the 80MHz offset frequency where the transmitter frequency is located, the isolation is only 30 dB, which is not acceptable for this application.

4.3.2 Fourth order tunable C-coupled shunt resonators

To increase the isolation, we heuristically attempted adding another stage to the filter, as shown in Figure 27. The frequency response of the filter, which exhibits greater isolation, is shown in Figure 28.

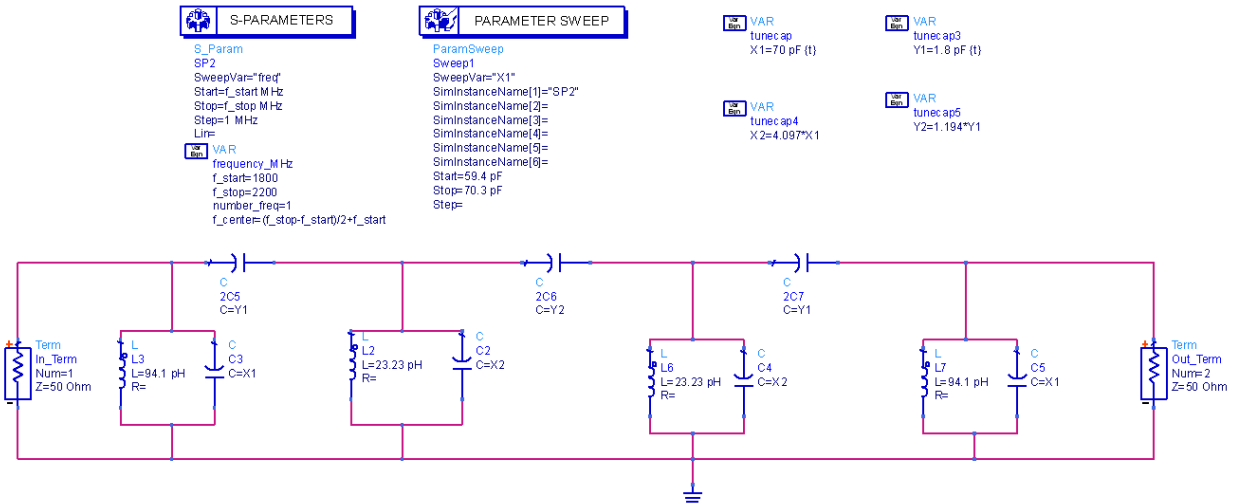


Figure 27. ADS Simulation of a fourth order capacitive coupled shunt resonator filter

Adding another stage to the filter required changing the tuning values to accommodate the additional stage. In this design, the tunable range of capacitors C3 and C5 is required to be 59.4 pF to 73 pF, and the tunable range of capacitor C2 and C4 is 243.4 pF to 299.1 pF. Without changing the coupling capacitors the bandwidth remains within acceptable limits between 20 MHz and 28 MHz. This filter design does provide the required -50 dB of isolation at the 80 MHz offset transmitter frequency.

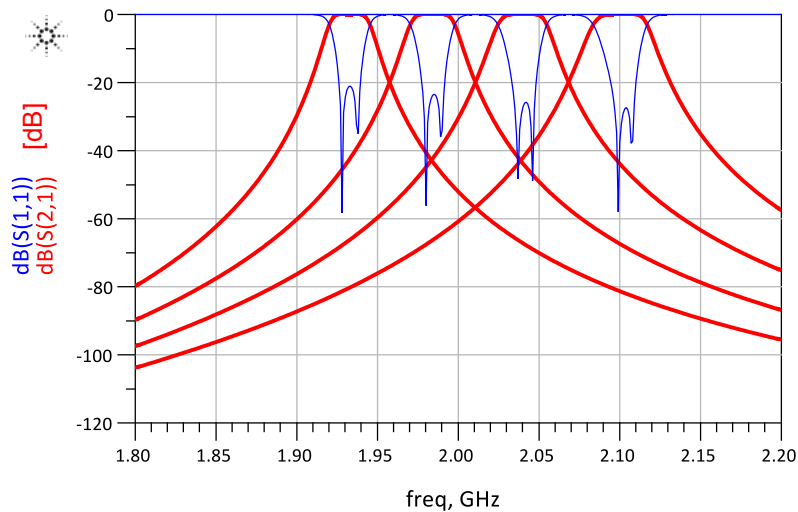


Figure 28. Frequency response (in dB) of the circuit shown in Figure 27, showing the circuit is able to be tuned to the 4 sections of the cellular handset receive band required with additional isolation at the transmitting frequency

The component values that were determined in these simulations have been realized using the ADS simulation-tuning tool and cannot be generalized to all filters. Therefore we continue in the next section to derive a mathematical model for generating filter component values.

4.4 Mathematical Derivation of C-coupled Filters

In this section, we introduce the concept of impedance/admittance inverters and their realizations using lumped components. Next, we describe the modifications of the standard lowpass filter prototype, which incorporates inverters. Finally, we investigate the derivation of the C-coupled bandpass filter topologies, and then simulate the results to verify the responses.

4.4.1 Impedance and Admittance Inverters

An idealized impedance inverter or admittance inverter is a circuit which provides an input impedance or input admittance inversely proportional to the load impedance or admittance and is scaled by a factor of K or J respectively [34, 36]. Considering the circuit in Figure 29 the impedance and admittance seen from the left end can be expressed by Equation (4) and Equation (5). As implied by the two equations, an inverter will have an image phase shift of ± 90 degrees if the load is complex.

$$Z_{in} = \frac{K^2}{Z_L} \quad (4)$$

$$Y_{in} = \frac{J^2}{Y_L} \quad (5)$$

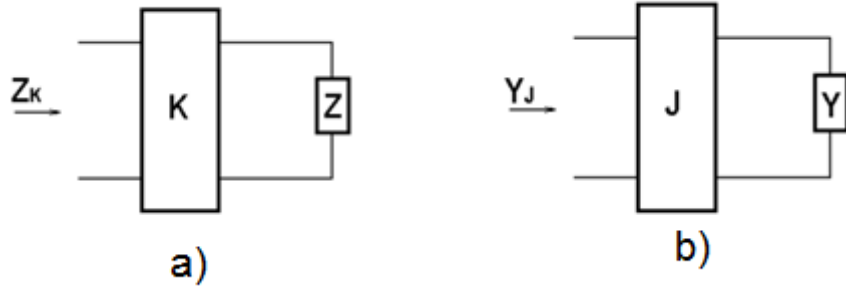


Figure 29. Impedance Inverter (a) and Admittance Inverter (b)

One representation of these inverters is a quarter wave transformer with a characteristic impedance of Z_0 or a characteristic admittance of Y_0 . The input impedance/admittance looking into the transmission line can be calculated by Equation (6) and Equation (7)

$$Z_{in} = \frac{Z_0^2}{Z_L} \quad (6)$$

$$Y_{in} = \frac{Y_0^2}{Y_L} \quad (7)$$

Since a quarter wave transformer is a transmission line that has length of $\lambda/4$ which is only true for a specific frequency, it would not be considered as an ideal inverter. In fact, an idealized impedance/admittance inverter operates like a quarter wave transformer with a characteristic impedance/admittance

of K/J at all frequencies [33,34,36]. Although most of the existing inverters are frequency dependent, they are still widely used in various applications including filter design, especially for narrow bandpass filters.

Besides a quarter wave transformer, there are other lumped element circuits that operate as inverters. Figure 30 shows two possible admittance inverter and two impedance inverter networks.

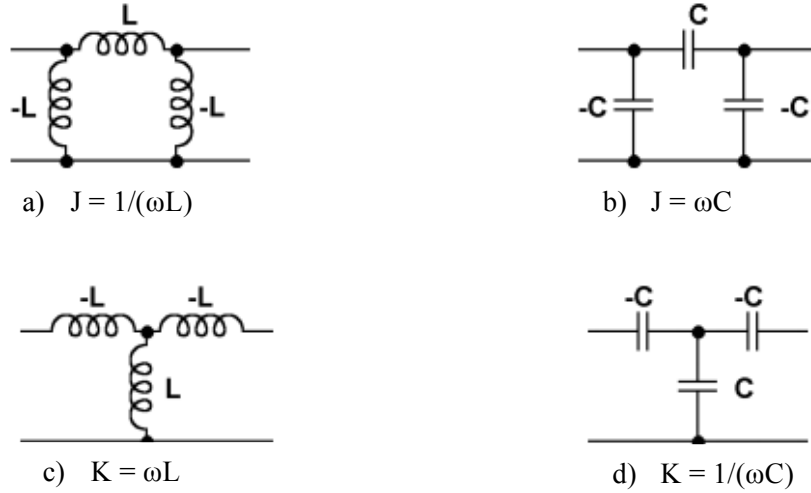


Figure 30. Admittance Inverters (a, b), and Impedance Inverters (c,d) using lumped components [34]

As demonstrated in the circuit diagram, all networks have components with negative values. Although it is not practical to realize such capacitors and inductors, they will be absorbed by adjunction of the components. In this project, we concentrate on developing capacitive coupling filters that incorporate the two Pi and T capacitor ladders in Figure 30 b and c.

4.4.2 Normalized Lowpass Filter Prototype Using Impedance/Admittance Inverters

Due to their inverting property, admittance and impedance inverters have the ability to convert a shunt inductor/capacitor to a serial capacitor/inductor and vice versa [36]. For example, a serial inductor that has an impedance of $j\omega L$ with two impedance inverters K on both sides can look like a shunt capacitance of $\frac{L}{K^2}$ as illustrated by Figure 31.

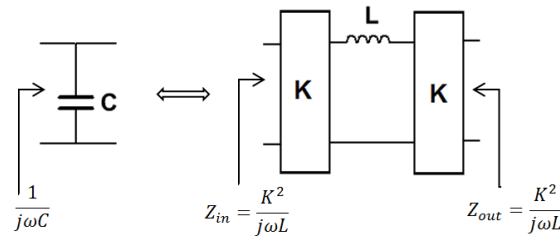


Figure 31. A series inductor with K -inverters on both sides looks like a shunt capacitor

Making use of this property, the conventional normalized lowpass filter prototype could be converted to equivalent prototypes, which either contains only serial inductors along with impedance inverters or shunt capacitors along with admittance inverters. Figure 32a shows a lowpass filter prototype circuit in which all of the serial inductors are replaced by shunt capacitors with appropriate admittance inverters in between. Similarly, Figure 32b is resulted by replacing all the shunt capacitors by serial inductors and impedance inverters.

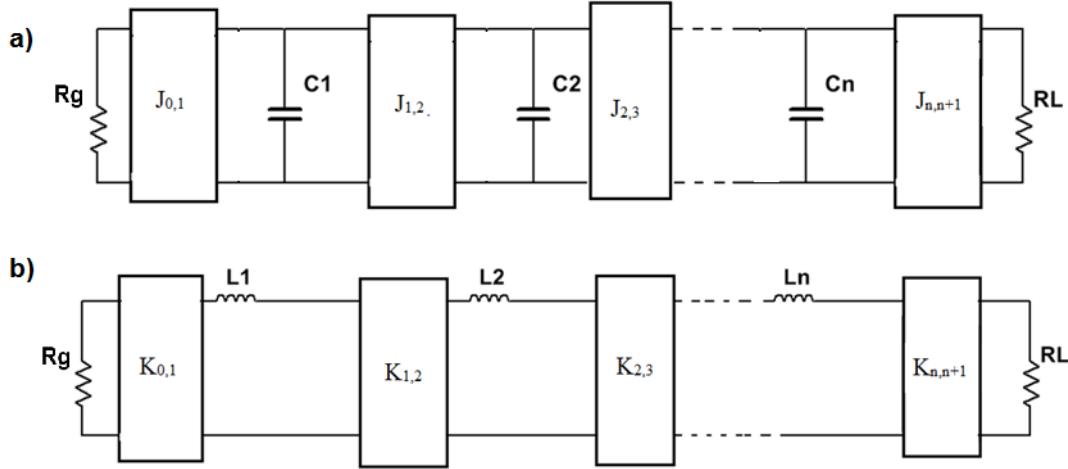


Figure 32. (a) Lowpass filter prototype using shunt capacitors and admittance inverters [36].
(b) Lowpass filter prototype using series inductor and impedance inverters [36].

As discussed in Section 4.1, the component values of the conventional lowpass filter are denoted by the g coefficients. Qualitatively, the inversion factors K and J are chosen such that the input impedance and output impedance at any stage of the circuits are the same as the corresponding impedance of the conventional prototype. Therefore, K and J parameters are strictly related to the g coefficients as well as the designed capacitor and inductor values of each stage. If the source and load are matched to an impedance of Z_0 and all the capacitors and inductors are configured as shown in Figure 32, then the J and K factors can be calculated using Equation (8) and Equation (9) [36].

Admittance inverters of the lowpass filter prototype shown in Figure 32a:

$$\text{a) } J_{0,1} = \sqrt{\frac{C_1}{Z_0 g_0 g_1}} \quad \text{b) } J_{i,i+1} = \sqrt{\frac{C_i C_{i+1}}{g_i g_{i+1}}} \quad \text{c) } J_{n,n+1} = \sqrt{\frac{C_n}{Z_0 g_n g_{n+1}}} \quad (8)$$

Impedance inverters of the lowpass filter prototype shown in Figure 32b:

$$\text{a) } K_{0,1} = \sqrt{\frac{Z_0 L_1}{g_0 g_1}} \quad \text{b) } K_{i,i+1} = \sqrt{\frac{L_i L_{i+1}}{g_i g_{i+1}}} \quad \text{c) } K_{n,n+1} = \sqrt{\frac{Z_0 L_n}{g_n g_{n+1}}} \quad (9)$$

In Equation (8a, 8b, 8c) and Equations (9a, 9b, 9c), g_i signifies the coefficient of the standard bandpass filter, and Z_0 represents the characteristic impedance of the source and the load. In Equation (8b), $J_{i,i+1}$ constitutes the admittance inverter between the i^{th} and $(i+1)^{\text{th}}$ resonators. In Equation (9b), $K_{i,i+1}$ characterizes the impedance inverter between the i^{th} and $(i+1)^{\text{th}}$ resonators.

4.4.3 Capacitive Coupled Filters

The conventional bandpass filter structure consists of series resonators alternating with shunt resonators in an arrangement that is difficult to achieve in practical implementation. In addition, the component values of the structure are fixed and often unrealizable for a very high frequency narrow bandpass filter. Therefore, this section will provide an alternative structure that resulted from the modified lowpass filter prototype discussed in Section 4.4.2. Applying the lowpass to bandpass transformation processed shown in Table 3 yields the bandpass circuits in Figure 33. It should be noted that, since the lowpass filter prototype only consists of either all shunt capacitors or all serial inductors, the two consequent bandpass topologies have either all shunt resonators or series resonators. In addition, by choosing appropriate inverter factors we can set the desired component values for the design.

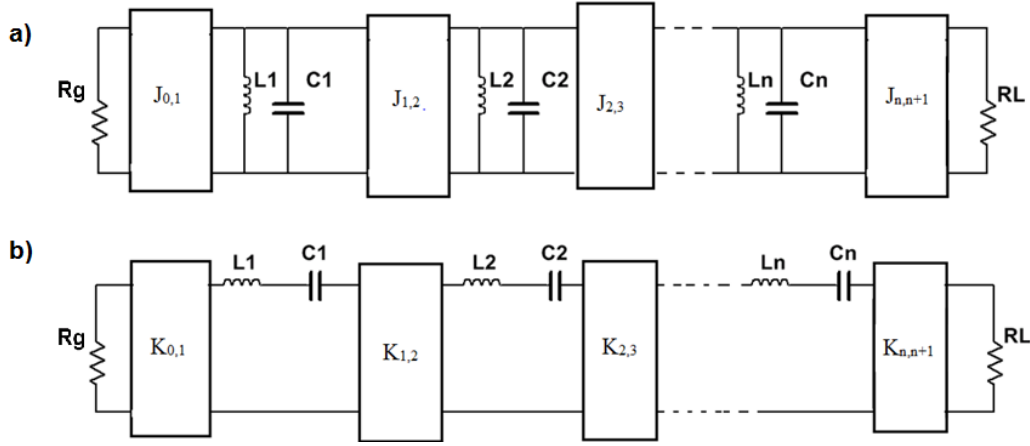


Figure 33. High order bandpass filters using serial resonators and impedance inverters [33, 34, 35, 36]

As Figure 33 shows, resonators are mutually coupled within the resonators using J and K inverters. In filter design, it is often desirable to use the same resonators in each section of the filter, and have the same characteristic impedance at the source and load, in this case, 50Ω . If all resonators are tuned to the same frequency with inductance of L_0 and capacitance of C_0 ; the load and source impedance of Z_0 is matched, the admittance and impedance parameters of the bandpass prototype can be transformed from Equation (8) and Equation (9) yielding Equation (10) and Equation (11) [34].

Admittance inverters:

$$\text{a) } J_{0,1} = \sqrt{\frac{C_0 BW}{Z_0 g_0 g_1}} \quad \text{b) } J_{i,i+1} = \frac{BWC_0}{\sqrt{g_i g_{i+1}}} \quad \text{c) } J_{n,n+1} = \sqrt{\frac{C_0 BW}{Z_0 g_n g_{n+1}}} \quad (10)$$

Impedance inverters:

$$\text{a) } K_{0,1} = \sqrt{\frac{Z_0 L_0 BW}{g_0 g_1}} \quad \text{b) } K_{i,i+1} = \frac{BWL_0}{\sqrt{g_i g_{i+1}}} \quad \text{c) } K_{N,N+1} = \sqrt{\frac{Z_0 L_0 BW}{g_N g_{N+1}}} \quad (11)$$

The coupling inverters between resonators can be realized by inductive coupling, capacitive coupling, or magnetic coupling. Using capacitive coupled resonators in filter design is beneficial because it occupies a smaller area and has a higher quality factor compared to inductors. Since the admittance and impedance inverters can be replaced by any of the equivalent circuits shown in Figure 30, it is possible to use the T and Pi capacitive networks as inverters to couple the resonators. It is important to note that the negative capacitances of the inverters should be absorbed into the positive capacitances in the resonators. However, the negative capacitances adjacent to the source and the load cannot be absorbed this way. Therefore, another equivalent circuit needs to be explored in order to deal with the J-inverter at the two ends. The details of these derivations can be found in Appendix A. These realized coupling networks result in the C-coupled filter structures shown in Figure 34. As the figure illustrates, the structure of the inverters at each end is different from that of the inverters in the middle.

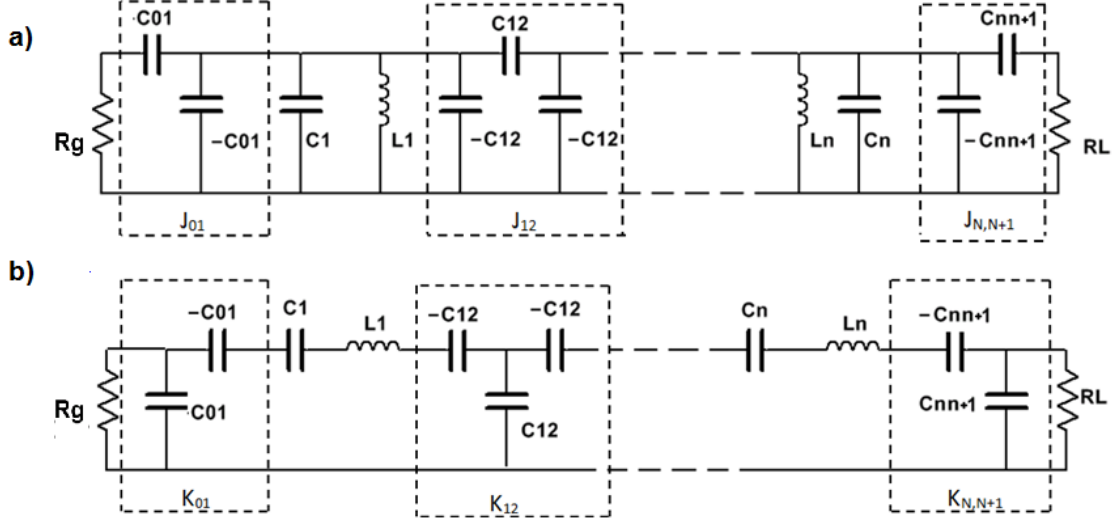


Figure 34. The J inverters in serial resonator filters (a) and K inverters in shunt resonator filters (b) are replaced by equivalent capacitor networks

By definition of the inverters depicted in Figure 30, we can derive the formula for the coupling capacitors in both the shunt and the serial configurations.

C-Coupled shunt topology:

$$C_{0,1} = \frac{J_{01}}{2\pi f_o \sqrt{1 - (J_{01}Z_0)^2}} \quad (12a)$$

$$C_{i,i+1} = \frac{J_{i,1+1}}{2\pi f_o} \quad (12b)$$

$$C_{N,N+1} = \frac{J_{N,N+1}}{2\pi f_o \sqrt{1 - (J_{01}Z_0)^2}} \quad (12c)$$

C-coupled serial topology

$$C_{0,1} = \frac{\sqrt{1 - (K_{01}/Z_0)^2}}{2\pi f_o K_{01}} \quad (13a)$$

$$C_{i,i+1} = \frac{1}{2\pi f_o K_{i,i+1}} \quad (13b)$$

$$C_{N,N+1} = \frac{\sqrt{1 - (K_{N,N+1}/Z_0)^2}}{2\pi f_o K_{N,N+1}} \quad (13c)$$

In Equations (12a, 12b, 12c) and Equations (13a, 13b, 13c), $C_{0,1}$ and $C_{N,N+1}$ represent the coupling capacitors at the two ends, f_o characterizes the center frequency and is calculated using $\frac{1}{2\pi\sqrt{L_0C_0}}$. The coupling capacitor between the i^{th} and $(i+1)^{\text{th}}$ resonators is represented by $C_{i,i+1}$. The admittance and impedance inverter parameters are represented by J and K, respectively.

After determining the coupling capacitor values for the desired filter characteristics as discussed above, the next step was to calculate the corresponding capacitance of the resonators, taking into account the absorbed negative coupling capacitances. If C_0 denotes the original resonator capacitance, the equivalent

effective capacitance can be calculated by Equation (14) and (15) for the shunt and serial topology, respectively. The final resulted design of the C-coupled bandpass filter topology is captured in Figure 35.

Resonator capacitance of the C-coupled shunt topology

$$C_i = C_0 - C_{i-1,i} - C_{i,i+1} \quad (14)$$

Resonator capacitance of the C-coupled serial topology

$$\frac{1}{C_i} = \frac{1}{C_0} - \frac{1}{C_{i-1,i}} - \frac{1}{C_{i,i+1}} \quad (15)$$

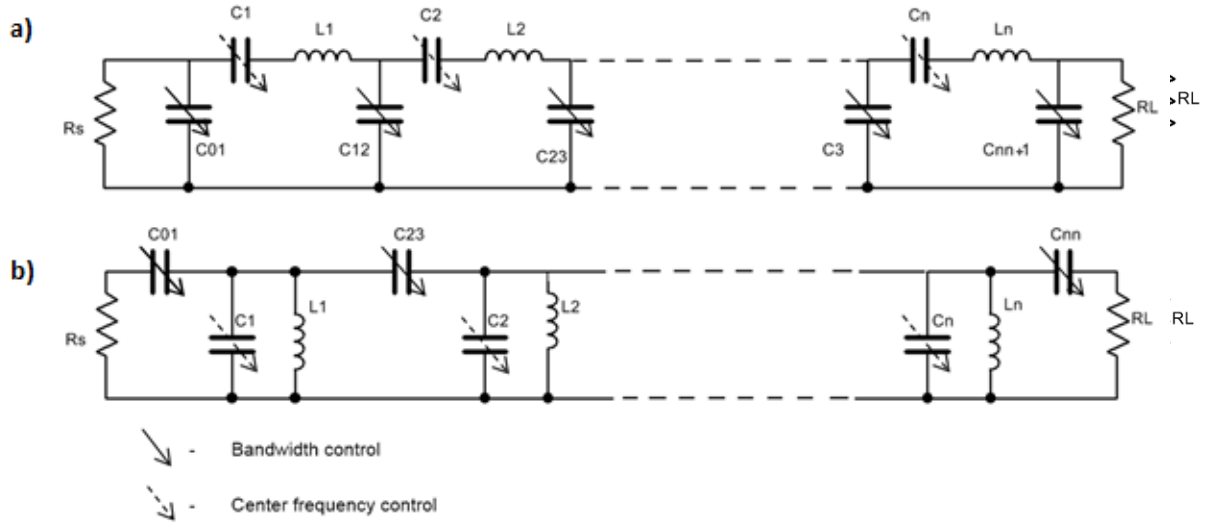


Figure 35. Final structure of a C-coupled serial resonator (a) and C-coupled shunt resonator (b) tunable filter [33]

There are three main advantages associating with C-coupled resonators. The first advantage is that the values of the inductors can be chosen in order to get reasonable capacitor values. Thus, this approach is much more flexible compared to the standard bandpass filter topology with fixed component values corresponding to filter specifications. In addition, all the inductors are the same for each resonator making the design more realizable. Finally, the center frequency of the filter is easily tunable by changing the value of the resonant capacitors while keeping the inductor unchanged; and the bandwidth of the response can be controlled by the coupling capacitors. Although those coupling lumped element inverters are frequency dependent, these C-coupled filter topologies still perform well within the specifications for this project since the desired bandwidth is narrow compared to the center frequency.

4.4.4 Simulation of mathematically derived C-coupled topologies

Using the mathematical processes described in the previous section, we developed two MATLAB functions that can calculate the component values corresponding to filter specifications and topologies. The inputs of those functions are the coefficients g 's of the normalized lowpass filter prototype, the bandwidth, center frequency and a desired inductor value. The functions output all the coupling capacitances and the resonator capacitances of the C-coupled shunt and serial topologies, respectively. The detailed code of those functions is found in Appendix B. Following the numerical computation of the component values, we entered the component values into a schematic in ADS for both serial and parallel resonator configurations. We then simulated the circuits using all ideal components and created plots of

the magnitude and phase responses. The circuit diagrams and response plots are presented in the following sections.

Third order tunable C-coupled shunt resonators

Using the appropriate g coefficients for a third order maximally flat Butterworth filter and a 4nH inductor, we calculated the capacitor values for the center frequency of 1.93GHz and bandwidth of 20MHz as presented in Table 6.

Table 6. Calculating component values for the 3rd order C-coupled shunt topology

Inductor	4nH
Coupling caps C_{01}, C_{34}	0.1714 pF
Coupling caps C_{12}, C_{23}	12.5 fF
Resonator caps C_1, C_3	1.516 pF
Resonator caps C_2	1.675 pF

Using these values, we simulated the capacitive coupled shunt resonator topology, the schematic for this filter can be seen in Figure 36.

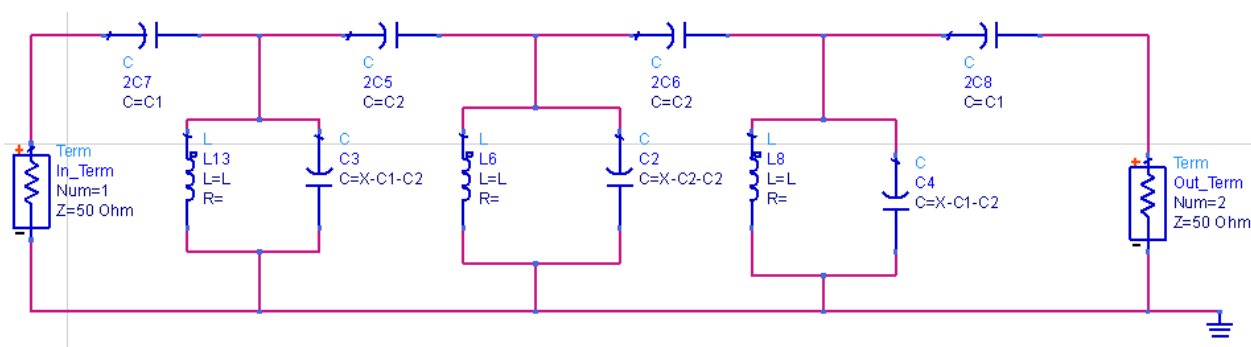


Figure 36. Third Order Shunt Resonator C-Coupled Filter Schematic (based on topology of Figure 35a)

It is clear from Figure 36 that the capacitors C_{12} and C_{23} have very low values, and are not realizable as a component due to existing process technology. In fact, for a narrow bandwidth of about 5% and below, the coupling capacitors are in order of femtofarads. To verify the design approach, we simulated the circuit using ADS and the frequency response is depicted in Figure 37.

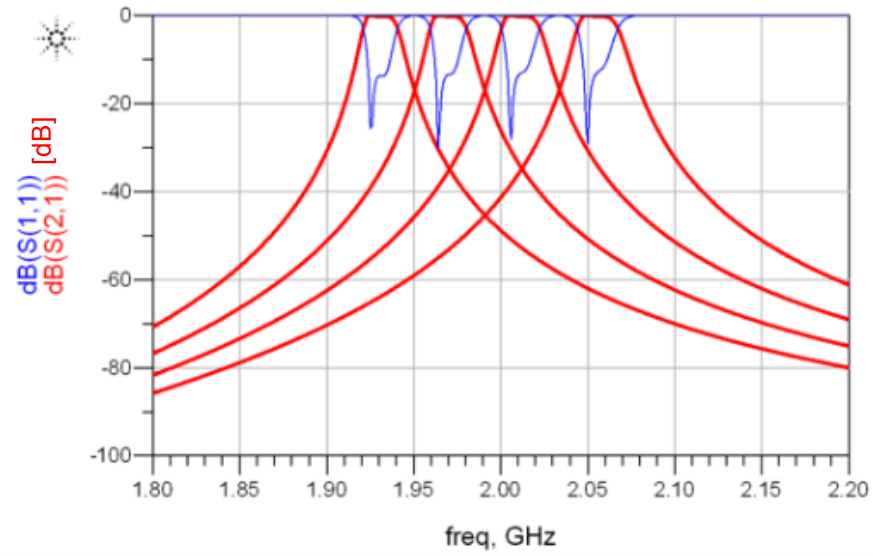


Figure 37. Frequency response (in dB) of an ideal tunable C-coupled shunt resonator

The ideal third order shunt maximally flat Butterworth produced a roll-off of about 55dB at 80 MHz offset from the center frequency. The capacitor's tuning ranges are within 1:1.2 which is acceptable in order to cover the entire band 25, while keeping the bandwidth reasonably constant. However, as previously mentioned, the main disadvantage of the C-coupled shunt resonator topology is that the coupling capacitances are too small for a narrow band filter. Therefore, the next simulation concentrates on exploring the serial resonator topology which uses more reasonable values of all capacitors.

Third order tunable C-coupled serial resonators

The second simulated filter structure is the C-coupled serial resonator. The same filter specifications are plugged in to the MATLAB function to calculate the components values. For a third order maximally flat Butterworth bandpass filter with the inductor value of 4nH, the calculated capacitances are reported in Table 7.

Table 7. Calculating component values for the 3rd order C-coupled serial topology

Inductor	4nH
Coupling caps C_{01}, C_{34}	16.37 pF
Coupling caps C_{12}, C_{23}	232 pF
Resonator caps C_1, C_3	1.913 pF
Resonator caps C_2	1.725 pF

We used the values from Table 7 to create an ADS schematic for simulation; this schematic is shown in Figure 38.

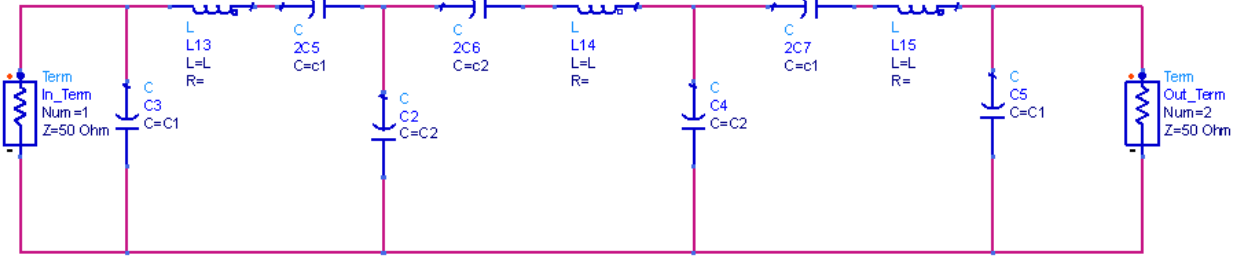


Figure 38. Third Order Serial Resonator C-Coupled Filter Schematic (based on topology of Figure 35b)

As shown in Table 7, the coupling capacitors of the “series-trap” filter are much larger than those of the shunt topology. In fact, they are on the order of hundreds picofarads, which is slightly larger than the range of a typical realizable capacitor values. However, if we use a larger inductor of about 10nH, the coupling capacitors decrease on the order of less than 100 pF.

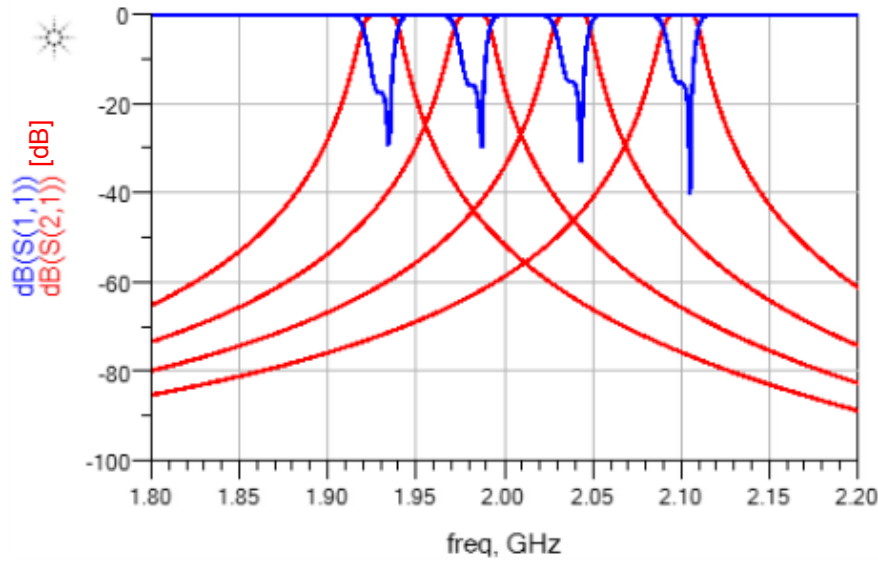


Figure 39. Frequency response (in dB) of a tunable C-coupled serial resonator filter

Figure 39 shows the simulated frequency response of the third order Butterworth serial resonator filter using the ADS software. We have again investigated tuning capabilities of both the center frequency and the bandwidth of the filter and they exhibit similar results compared to those of the shunt topology. The design provided desired roll off of about 55dB at 80MHz offset from center frequency and bandwidth of about 20MHz. Therefore, due to more reasonable component values, the serial topology is more applicable to our project. We decided to concentrate on exploring and optimizing this topology as the final approach of our project.

4.5 Non-ideality investigation

In this section, we explore the filter’s behavior when real components are added to the C-coupled serial resonator filter design. We expected that changing the quality factor of the components would introduce additional losses as well as potentially influence other aspects of the response. Additionally, we

investigate a prior-art design, where a real tunable element is used to adjust the center frequency of the filter. We also discuss and comment on adding this type of tunable element to our filter design.

4.5.1 Inductors and Capacitors

Using the filter design shown in Figure 38 above, we replaced the ideal components shown with models of real components, where we define a quality factor. We then simulated the circuit at different quality factors to demonstrate the loss factor introduced by adding non-ideal circuit components into our design. A plot showing the results can be seen in Figure 40.

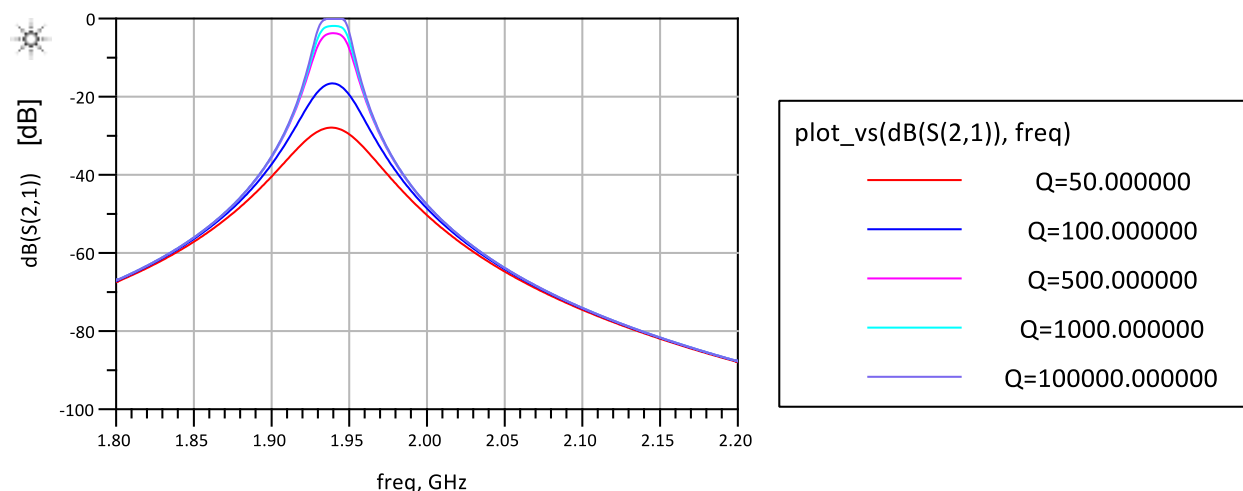


Figure 40. Third order C-coupled serial resonators with Q-values

As can be seen in Figure 40, as the quality factor increased, the amount of loss experienced by the filter decreased. With the quality factor set to 100,000 the response is very close to ideal, and when it is set to 50-100, the filter does not retain its shape or bandwidth and the loss is between 25dB and 20dB.

4.5.2 Adding a Real Tunable Element

K. Jeganathan from the University at Singapore presents a journal article suggesting a potential approach to tuning the center frequency of a bandpass filter [14]. Jeganathan used varactor diodes as tunable elements, and chose component values to tune the filter from 100 MHz to 230 MHz. The control circuitry changes the bias voltage of the varactor diode to adjust the capacitance that changes the frequency response of the filter [14]. The control circuitry consists of a variable DC source that is connected to a voltage divider built from three resistors. The DC voltage is connected between the cathode of the diode and a capacitor (C3 and C8). The capacitors C3 and C8 block the DC control voltage so that it does not interfere with the RF signal path. Jeganathan's circuit is shown in Figure 41.

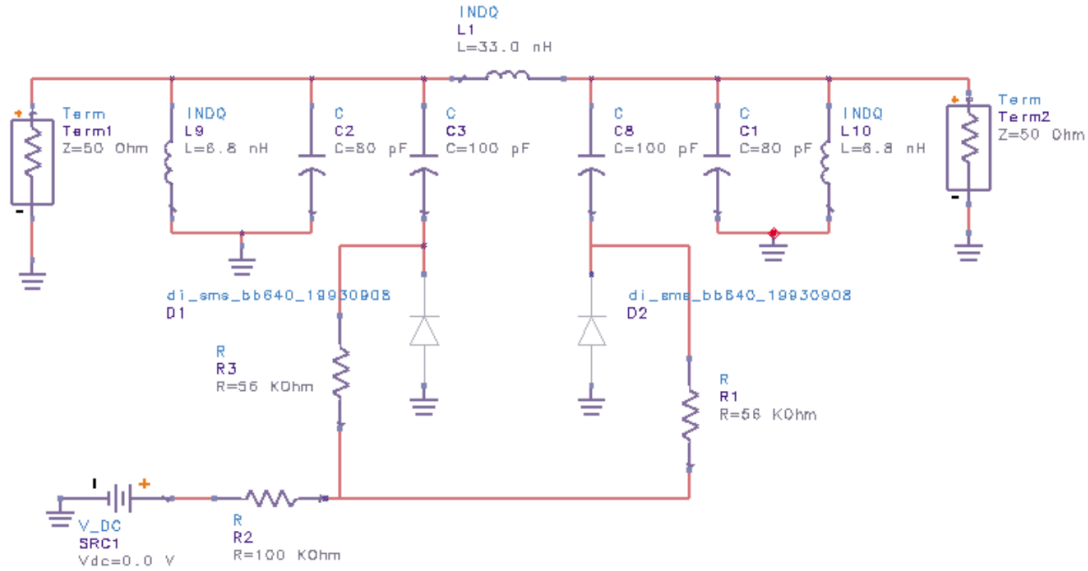


Figure 41. Jeganathan's tunable filter design using varactor diodes as tunable elements [14]

To experiment with this potential filter topology, we simulated the circuit in ADS. The varactor diodes used by Jeganathan were not simulated by ADS, and we replaced them with ideal capacitors. The values of these capacitors were varied using the tune function of the software. The equivalent circuit we developed and simulated is shown in Figure 42.

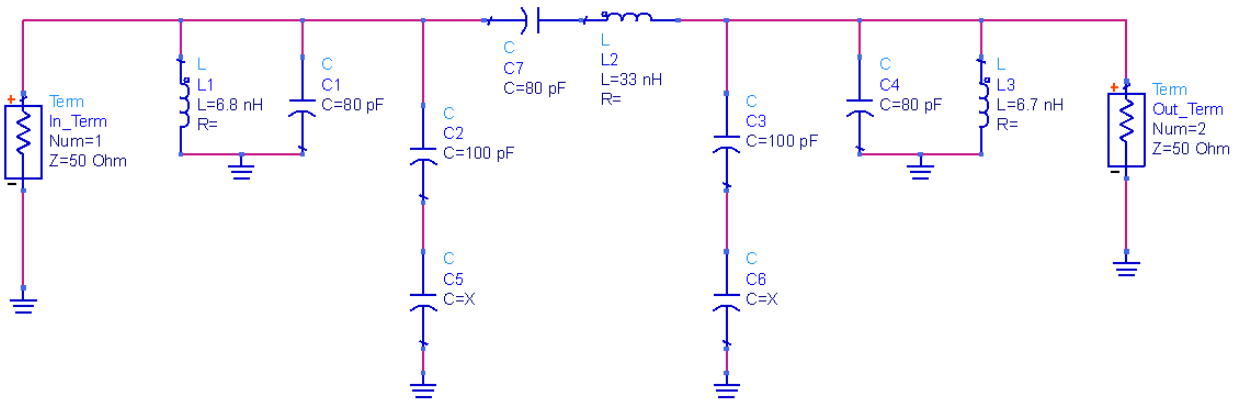


Figure 42. Replacement of varactor diodes with capacitors of varying value

In order to change the value of the capacitors replacing the varactor diodes, we defined their value to be a variable "X" and simulated the circuit behavior while changing the values. Changing the capacitance X from a value of 1 pF to 100 pF resulted in a change of the center frequency of the bandpass filter from 240 MHz to 170 MHz. This response is shown in Figure 43. Assuming a similar filter topology can be used at the higher frequencies required for the objective of this project, we should be able to adjust component values to achieve a similar response.

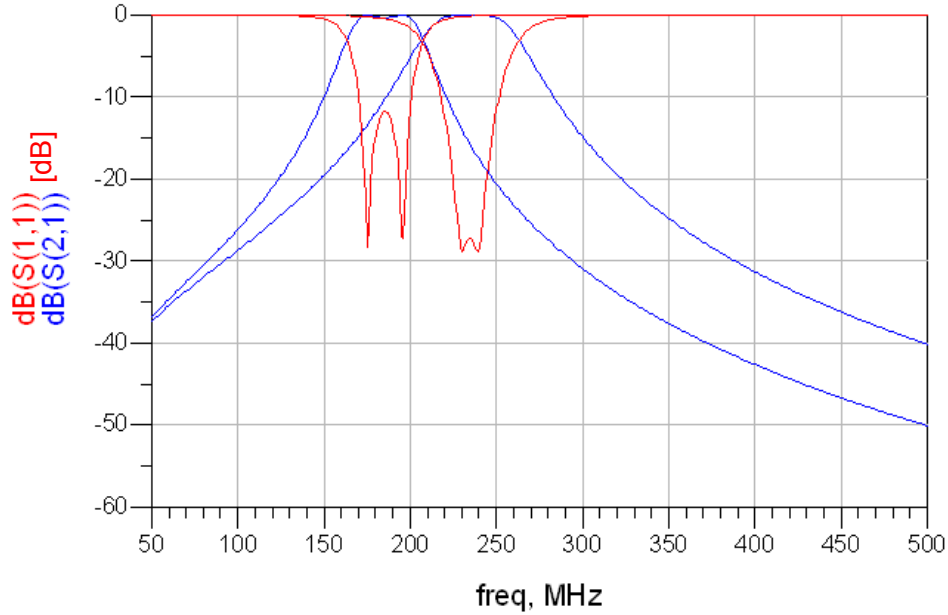


Figure 43. Frequency response (in dB) of filter schematic shown in Figure 42.

Seeing this as a feasible approach to tuning the center frequency of our filter design, we downloaded some libraries of “varicap” diodes from NXP semiconductor. After simulating various models, we selected the BB208-03 because of its characteristic low loss and high capacitance to voltage linearity. Varying the control voltage across the NXP BB208-03 diode produces the change in capacitance from 4.9pF at 7.5V to 21.5pF at 1V. This ratio is more than enough to provide the desired range of capacitance in a serial resonator configuration. More information about the NXP BB208-03, can be found in its data sheet included in the report in Appendix C. In the next section we implement this component into our filter circuit, and simulate at the frequencies required for band 25.

4.6 Summary

This section discusses the basic approach of designing a filter that meets the specifications of the project objectives. First, we reviewed the fundamental lowpass filter structure and demonstrated how to convert it into a bandpass filter. Four fixed filter topologies were simulated in ADS; those included the third order maximally flat Butterworth, the third order 3dB Chebyshev and the third order 0.5dB Chebyshev. Each of these topologies provide responses that satisfy a desired bandwidth of 20MHz and an isolation of at least -50dB between the transmit and receive frequencies. However, all of them experience a problem of unrealizable capacitor and inductor values. Therefore, in the next simulations, we replaced these serial resonators with coupling capacitors. This capacitive coupled LC resonator topology not only used reasonable component values, but also facilitated the ability to tune the filter by only changing the capacitance.

In previous simulations, the values used for the components in the filter were realized using the simulation-tuning tool in ADS. Subsequently, we investigated and derived a mathematical model to determine the capacitor values of both the C-coupled shunt and C-coupled serial resonator configurations with a defined inductance. For a very high frequency narrow bandpass filter, the coupling capacitors of the shunt topology are very small and difficult to realize. Contrarily, those of the serial topology have more reasonable values. We then simulated each of these filters using the mathematically calculated values and tested the range of the component values needed to tune the band required. As the simulation

of the fourth order C-coupled filter confirmed (Figure 39), the capacitive coupled serial resonator is the best solution to achieve the objectives of this project.

Finally, we investigated the non-ideal behavior of the C-coupled topology by firstly added quality factors to the capacitors and inductors. Once finite quality factors of the components were added into the circuit, the system experienced losses and mismatches. The simulation showed that if the components' quality factors decreased to less than 500, the loss exceeded -5dB. When the quality factor decreased to less than 100, which is the typical value of real components, the loss increased to more than -20dB and the shape of the pass-band was no longer preserved. Additionally, to explore the non-ideality of tunable components we introduced a potential tunable filter design approach using varactor diodes. We found that it would be feasible to incorporate a varactor diode into our C-coupled filter design. Therefore, we investigated component models from NXP semiconductor to apply to simulations in ADS. It is expected that the design approach including filter topology, filter order, and component values will need to be adjusted in order to optimize the frequency response of the non-ideal filter.

CHAPTER 5: RESULTS

This chapter discusses the results that we obtained by optimizing the approach defined in Chapter 4. As determined, the series resonator topology is the best solution to achieve the objectives of this project. Therefore, this is the topology further investigated in this Chapter.

5.1 Series Resonator Simulations

We incorporated the NXP BB208 varactor diode into the simulations of the serial topology to show the non-idealities of using a real tunable element in the filter. In this section, we investigate and compare Butterworth and Chebyshev topologies using the values calculated using the model detailed in section 4.4. Finally, we use the ADS simulation tool to optimize the circuit for a maximally flat frequency response.

5.1.1 Butterworth 4th Order, 25 MHz Bandwidth, Serial Resonator

We first calculated values for a Butterworth, 4th order, 25MHz bandwidth filter. Using the coefficients defined Table 12 in Appendix F [9], we calculated the capacitor values using a fixed inductance of 10nH, a source/load impedance of 50Ω, a bandwidth of 25MHz, and a center frequency of 1930MHz. The values were calculated using the procedure defined in Section 4.3 and are tabulated in Table 8 below:

Table 8. Calculated Component Values for 25MHz Butterworth Filter

Coupling Capacitor 1/5	7.97 pF
Resonator Capacitor 1/4	0.761 pF
Coupling Capacitor 2/4	62.4 pF
Resonator Capacitor 2/3	0.701 pF
Coupling Capacitor 3	97 pF

The schematic shown in Figure 44 demonstrates a Butterworth filter with serial resonators.

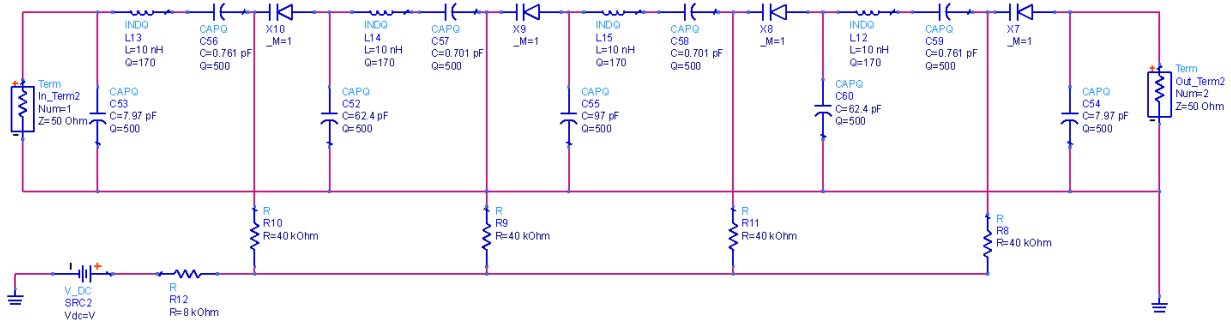


Figure 44. 25 MHz Butterworth Serial Resonator Schematic

The varactor diode is added in series with the resonator capacitor in order to tune the center frequency of the filter. The control voltage is adjusted from 0V to 4.2V to achieve the desired response. In reference to Table 8 above the coupling capacitors are pictured vertically, and the resonator capacitors are pictured horizontally. The numbers refer to the schematic from left to right. Figure 45 captures the response of the filter shown in the schematic shown in Figure 44.

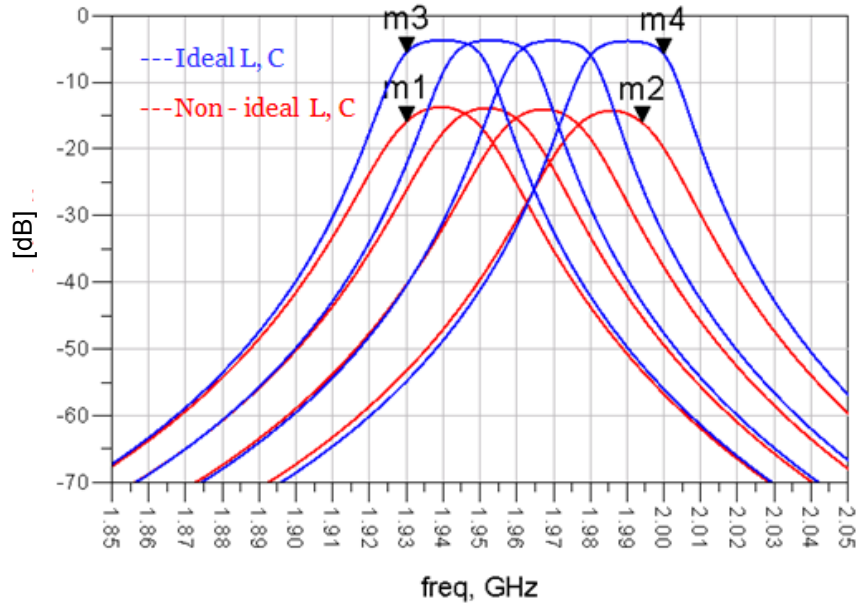


Figure 45. Frequency response (in dB) of 25 MHz Butterworth Serial Resonator

Figure 45 demonstrates that with ideal components the filter is able to tune across the desired range of frequencies with the desired isolation using the varactor diode. However, when adding non-ideal inductors and capacitors, the isolation is no longer acceptable (40dB). Therefore, we look to a Chebyshev filter topology in the next section.

5.1.2 Chebyshev 4th Order, 25 MHz Bandwidth, Serial Resonator

Similar to the procedure outlined in the previous section, we used coefficients from Table 14 in Appendix F [9] to calculate the capacitor values for a Chebyshev 25MHz filter. Using the procedure outlined in Section 4.3, we came to realize the following capacitor values for this circuit with a fixed inductor value of 10nH, a source/load impedance of 50Ω, a bandwidth of 25MHz, and a center frequency of 1930 MHz. The values are tabulated in Table 9.

Table 9. Calculated Component Values for 25MHz Chebyshev Filter

Coupling Capacitor 1/5	17.16 pF
Resonator Capacitor 1/4	0.722 pF
Coupling Capacitor 2/4	84.2 pF
Resonator Capacitor 2/3	0.699 pF
Coupling Capacitor 3	94.7 pF

The schematic shown in Figure 46 demonstrates this Chebyshev filter with serial resonators.

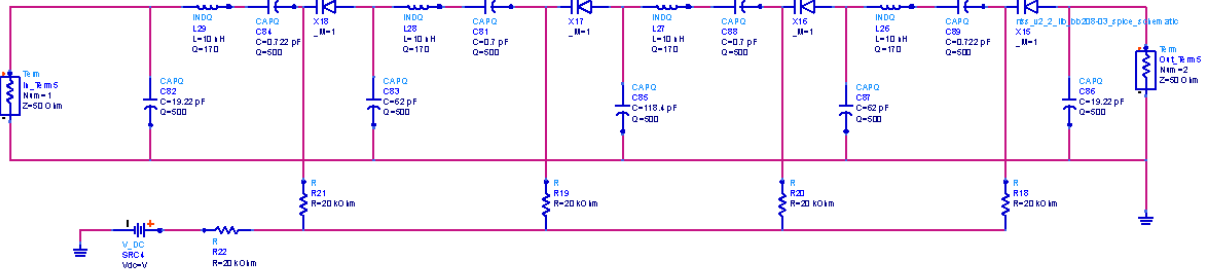


Figure 46. 25MHz Chebyshev Serial Resonator Schematic

The varactor diode is added in series with the resonator capacitor in order to tune the center frequency of the filter. The control voltage is adjusted from 0V to 4.2V to achieve the desired response. In reference to Table 9 above the coupling capacitors are pictured vertically, and the resonator capacitors are pictured horizontally. The numbers refer to the schematic from left to right. Figure 47 shows the response of the Chebyshev serial resonator filter.

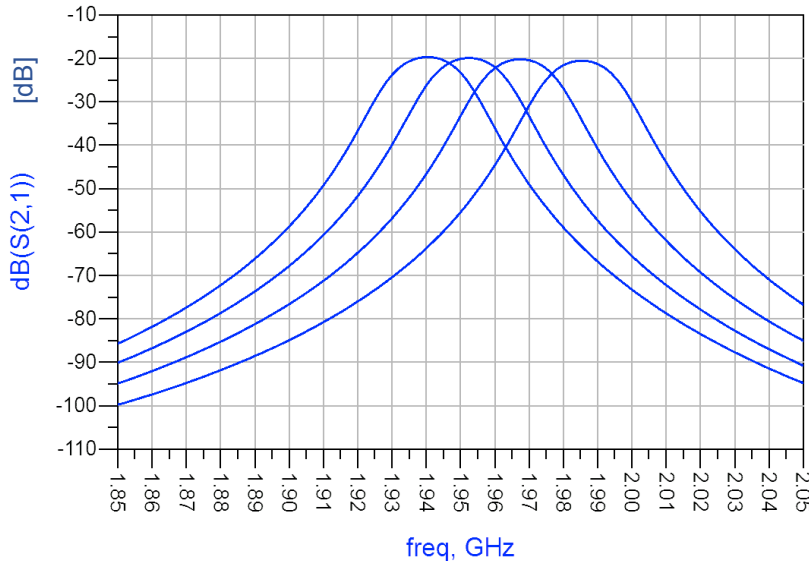


Figure 47. Frequency response (in dB) of 25 MHz Chebyshev Serial Resonator

In Figure 47, the isolation is much better with the same order (60dB), however the in-band response is not nearly as flat. Therefore, we looked to modify the circuit to achieve a flatter in-band response.

5.1.3 Modified Chebyshev 4th Order, 20 MHz, Serial Resonator

In attempting to achieve a flatter in-band response of the Chebyshev filter, we took the values calculated from the previous section and used the non-ideal properties of the components to our advantage. Since our non-ideal response is curved concave down, if we make the change that causes a concave up curve it will turn the overall response to flatten. Therefore, this motivates us to look at the weakly coupled serial resonators. This filter topology is the same as the one discussed above except that the coupling coefficients between the resonators are smaller. If the circuit is weakly coupled the typical simulated response is as shown in Figure 48.

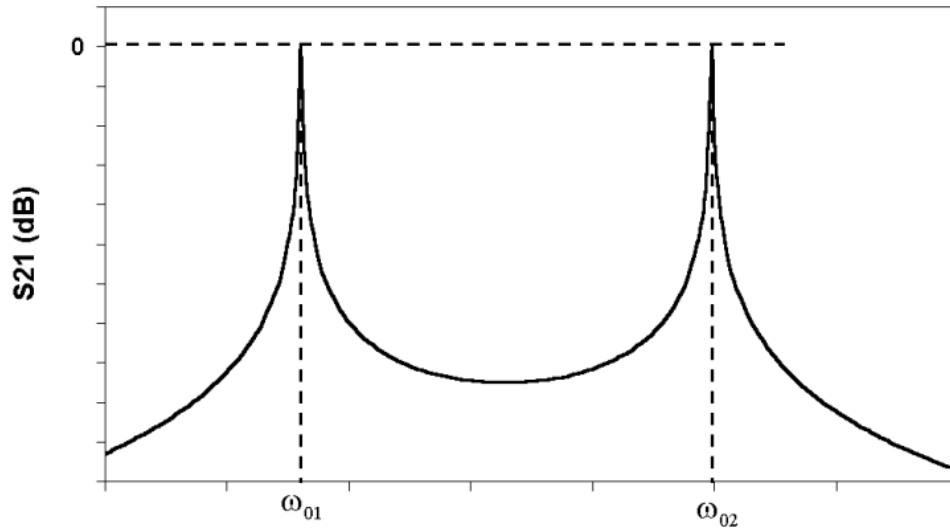


Figure 48. Typical response of a weakly coupled resonator has a concave up passband which can compensate for the undesired downward concavity of the passband due to non-ideal components [34].

Since the coupling coefficients are proportional to the coupling capacitances, we can control the concavity of the response by changing those coupling capacitances. Particularly, the two capacitors 2 and 4 are modified in order to get a flatter response in the non-ideal case. Using the tuning feature of ADS, we experimented with the weakly coupled capacitor concept and found it to be a proper modification to our design.

Because of the undesired decrease in the bandwidth due to non-ideal components, we used the specified bandwidth of 20 MHz to recalculate and modify the component values. The resonator capacitors were unchanged and this did not have an effect of the isolation. The values that were used are tabulated in Table 10. It should be noted that the original calculated value for coupling capacitor 2 and 4 are 105pF. These capacitors are modified to be 64 pF in order to achieve a better response.

Table 10. Modified Component Values for 20MHz Chebyshev Filter

Coupling Capacitor 1/5	19.22 pF
Resonator Capacitor 1/4	0.722 pF
Coupling Capacitor 2/4	64 pF
Resonator Capacitor 2/3	0.700 pF
Coupling Capacitor 3	118.4 pF

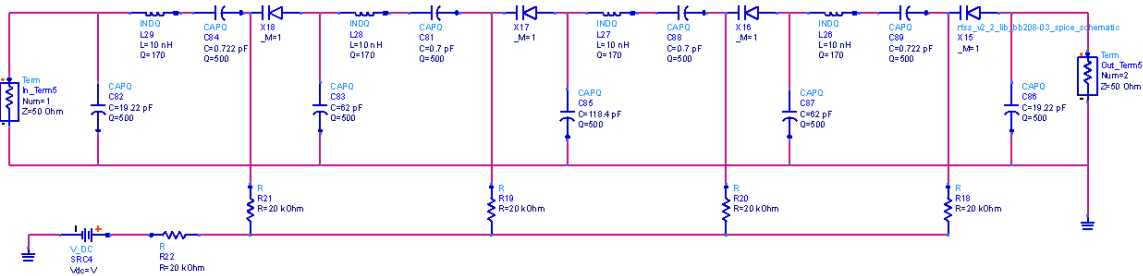


Figure 49. 25MHz Modified Chebyshev Serial Resonator Schematic.

The schematic shown in Figure 49 demonstrates our modified 20MHz Chebyshev filter with serial resonators. The varactor diode is added in series with the resonator capacitor in order to tune the center frequency of the filter. The control voltage is adjusted from 0V to 4.2V to achieve the desired response. In reference to Table 10, the coupling capacitors are pictured vertically, and the resonator capacitors are pictured horizontally. The numbers refer to the schematic from left to right.

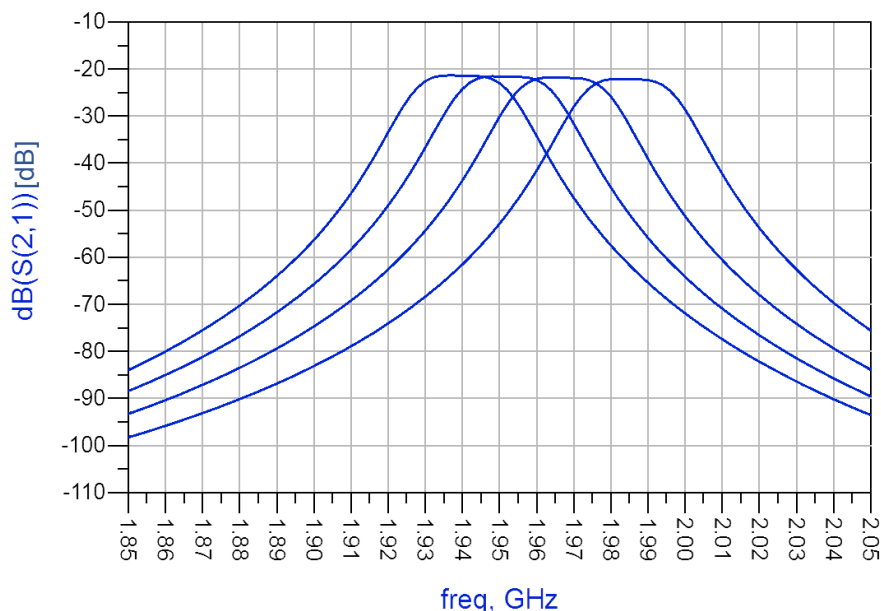


Figure 50. Frequency response (in dB) of 25 MHz Chebyshev Serial Resonator

Figure 50 shows the response of the chebyshev serial resonator filter that has been modified to flatten the in-band response. The shape of the curve is desirable due to its flat in-band response and high isolation (60dB at 80 MHz). However, the problem of loss is still evident which we aim to address in the next section.

5.2 Filter Augmentation

In order to account for the signal loss of greater than 20dB in the lumped element components and varactor diode, we investigated the potential of adding a low noise amplifier (LNA) to the input of the filter.

5.2.1 Adding an Ideal LNA

To determine the effect of adding an active element to the filter, we began using the ideal LNA component in ADS. This component has the ability for the user to manually enter the S-parameters of the amplifier. In order to compensate for the loss, we calculated that 21 dB of amplification was needed. Therefore we set the S21 parameter to be (21,0)dBpolar, the S11 parameter to be (0,0)polar for the ideal case, S12 to be (0)polar and S22 to be (0,180)polar. The circuit diagram for this active filter is shown in Figure 51.

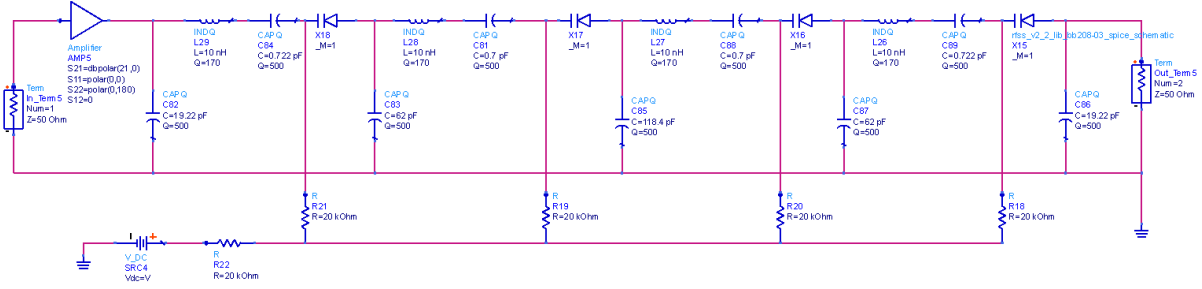


Figure 51. Schematic of the modified Chebyshev C-coupled serial resonator with an ideal LNA

After running the simulation, we observed the following frequency response for the magnitude of S21 shown in Figure 52. Additionally, we added a zoomed in plot to convey the loss within the passband.

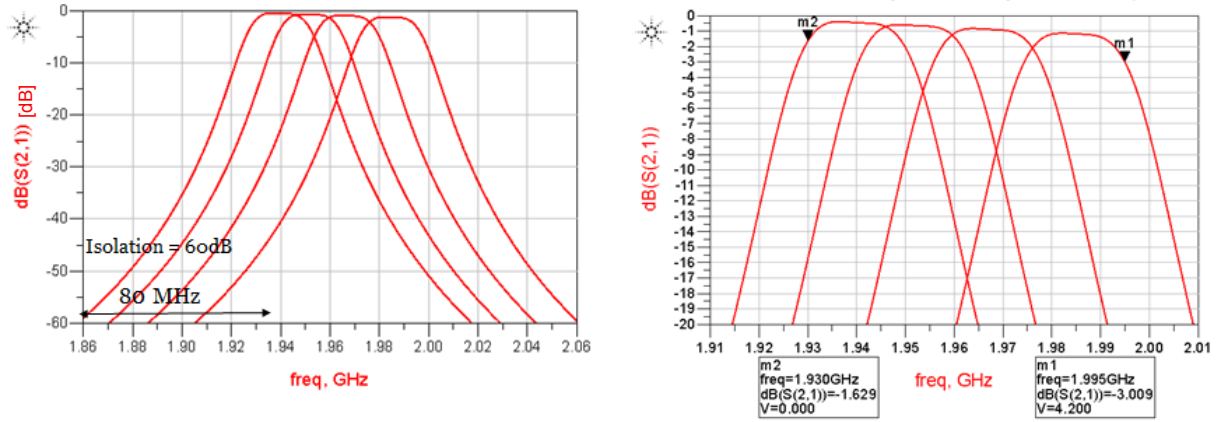


Figure 52. Frequency response (in dB) of the modified Chebyshev with ideal LNA

In Figure 52, we observed that the loss in the passband increases with frequency; however, it does not exceed 3dB at any required frequency. In addition, the isolation remains within our specification of -60dB at 80MHz.

In order to investigate the phase behavior of the final designed topology shown in Figure 51, we simulated the circuit and plotted the phase of S21 parameter. Figure 53 shows the phase response of the topology with an ideal LNA at two center frequencies of the upper and lower frequency limit of band 25.

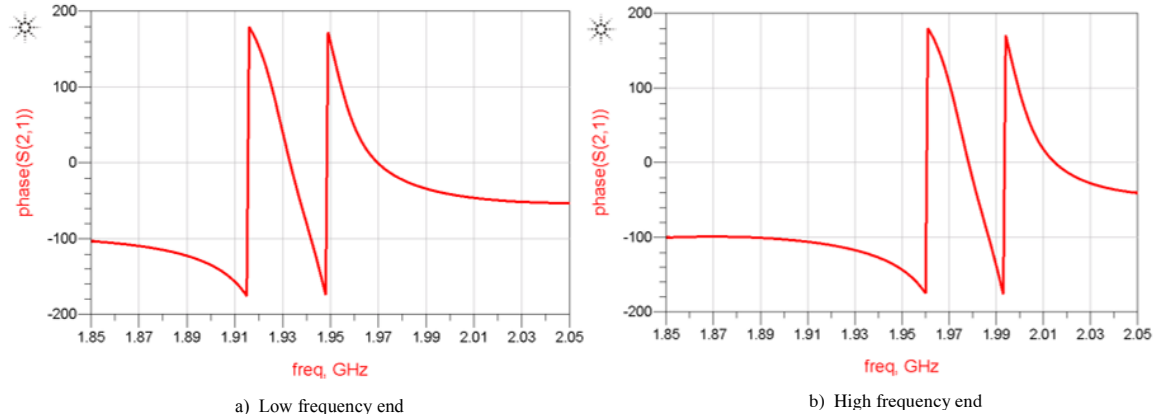


Figure 53. Phase response (in degrees) of the modified Chebyshev filter with ideal LNA at center frequencies of 1.935GHz (a) and 1.98GHz (b). The filter experiences linear phase behavior at the pass-band.

As Figure 53 shows, the phase response starts at about -100 degree, decreases linearly in the pass-band after remaining constant at the high frequency stop band. Since the phase could only be plotted from -180 degree to 180 degree, the graph exhibits wraps when the phase exceeds these two limits.

5.2.2 Adding a Real LNA Model

Due to the ideal LNA compensating for the losses induced by the filtering elements, we investigated the potential of adding a real model of an LNA to our design. We selected and simulated many LNA models from Hittite Microwave and NXP Semiconductor. Each model was contained in a 2 port S-parameter file, which allowed us to replace the ideal LNA from the schematic shown in Figure 51. These models all preserved the shape of the frequency response. The difficulty was in finding a model that had the appropriate amount of gain to compensate for the losses without driving the gain above 0dB. To show an example, the frequency response of our filter design from Section 5.2.1 with a Hittite Microwave HMC548LP3 LNA added is shown in Figure 54.

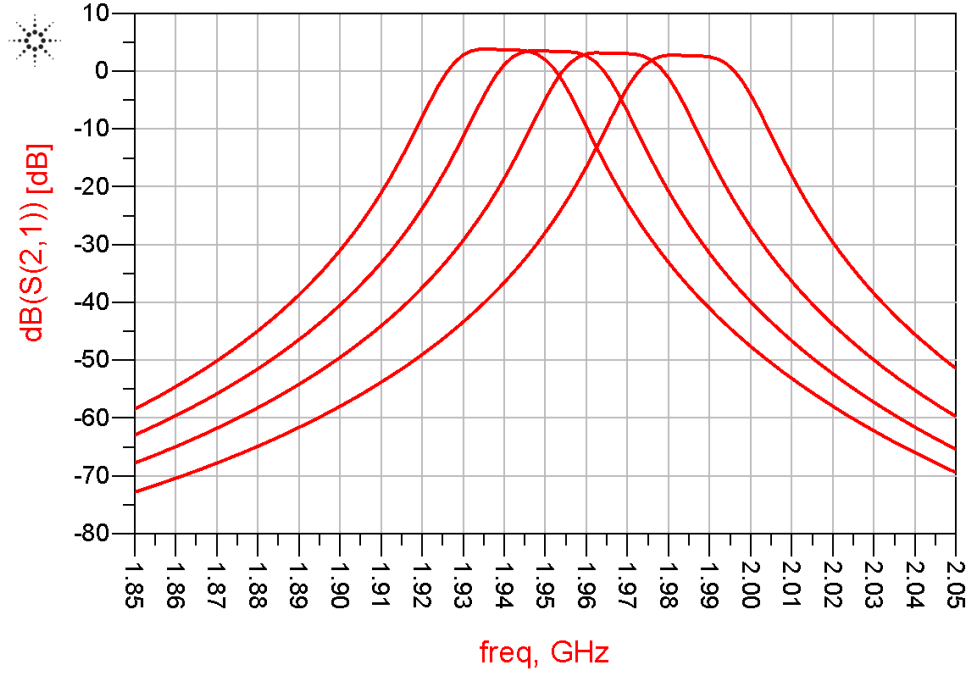


Figure 54. Frequency response (in dB) of design from Figure 51 with real LNA model (HMC548LP3)

As can be seen in Figure 53, although this LNA component preserves the desired response, the highest level of signal is approximately +5dB. The phase response of the filter was investigated and captured in Figure 55.

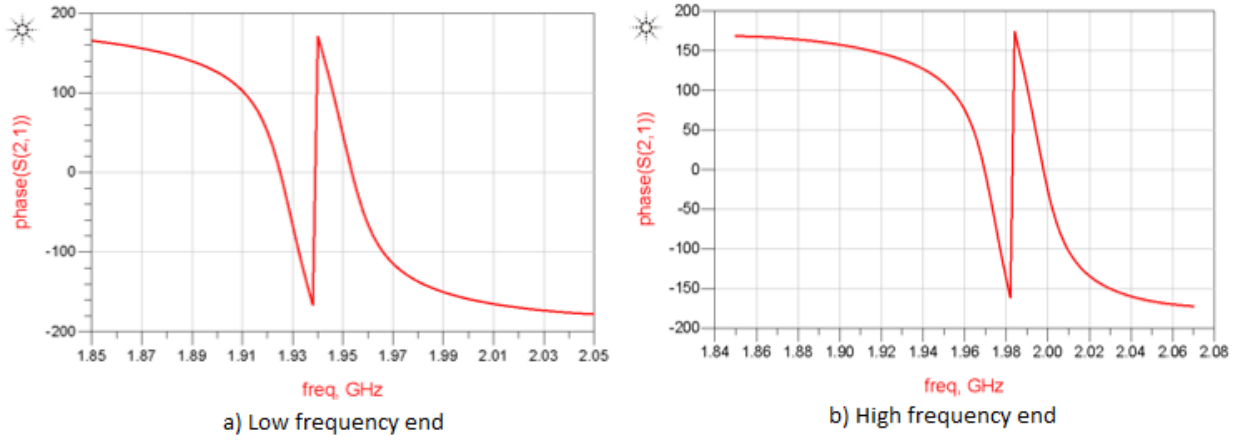


Figure 55. Phase response (in degrees) of the modified Chebyshev filter with ideal LNA at center frequencies of 1.935GHz (a) and 1.98GHz (b). The filter experiences linear phase behavior at the passband.

As the simulations show, similar to the topology using the ideal LNA, the one using the real LNA also exhibits linear phase performances at the passband excluding the wraps at $\pm 180^\circ$. Therefore, a relatively constant group delay can be achieved using the modified Chebyshev topology, which results in the elimination of signal distortion due to time delay within the passband.

CHAPTER 6: DISCUSSION

This chapter examines the various aspects of feasibility when considering the practical implementation of our design. We begin discussing the pros and cons of the design approach, and then compare it to the currently used acoustic filter technology. Finally, we discuss the cost and size implications of the design using currently available components.

6.1 General Observations

The filter design that we propose to accomplish the goal of this project involves first the use of lumped element components (capacitors and inductors). Using lumped elements provides for a simple method of tuning the center frequency of the filter. However, from our background research into prior art, we found that these components are not commonly used at the high frequencies we are working with (1.8GHz-2.1GHz) due to the high amount of signal loss compared to other non-tunable technologies. Additionally, in traditional filter topologies at these frequencies, the values of the capacitors are too small to be realizable in manufacturing. Through investigating alternative filter designs we found that removing the inductor from the coupling circuitry and using a purely capacitive coupling approach, the same response can be achieved with more reasonable values. In Appendix D, we discuss using models of capacitors that are currently commercially available and simulated them in our design. We found that the values determined from our analysis and simulation must be very close to exactly the real value of the component. When we chose the closest value from the libraries downloaded, the response was not up to specification. Therefore it is likely that custom components will need to be manufactured for the design to operate properly.

From researching components and discussing with Skyworks, we determined that an obtainable high quality capacitor could have a quality factor of 500 and an obtainable high quality inductor could have a quality factor of 170. Using these quality factors in models of capacitors and inductors built in ADS, we still experience about 15dB of insertion loss in our design. To account for the loss, we determined that a potential solution was to add a low noise amplifier. Using active filtering technology in addition to determining the feasibility of using this type of filter in mobile handsets were not in the original scope of this project. However, the research has proved that using an active filter with lumped elements is the best approach to achieving the desired goal and should be further investigated. In order to achieve a filter structure with a tunable center frequency, we deployed a varactor diode in series with the resonator capacitor. When controlled by a variable DC source from 0V-3V, the filter is able to be tuned through the required frequency range of 75MHz. We chose the varactor diode because it is a simple method of changing the capacitance of the resonators, without adding switching arms. These elements do, however, introduce some additional loss into the circuit. After investigating multiple libraries of these components to determine which had the least amount of loss, we found that the NXP BB802 was superior to the rest. As a result of using four of these varactor diodes, our design suffered 5dB of signal loss. Through background research we found that there are many theoretical tunable capacitor designs that have higher quality factors and lower loss, such as MEMS capacitors. However, we were unable to find a model of this type of component to be used in simulation.

6.2 Performance comparison

Currently, the smartphone industry generally employs the BAW and SAW acoustic technology to perform bandpass filtering for each device radio and antenna. These filters have generally been widely accepted; however, their major drawback is that they are not tunable due to their complex mechanical nature. An example of the magnitude response of a SAW filter is given in Figure 56. As shown in the figure, the passband of the filter spans approximately 1.92GHz to 2.02GHz. The maximum loss measured at the passband is -3dB. Additionally, the roll-off is extremely steep compared to traditional lumped element filter technology. These characteristics make this filter technology highly attractive in the smartphone industry.

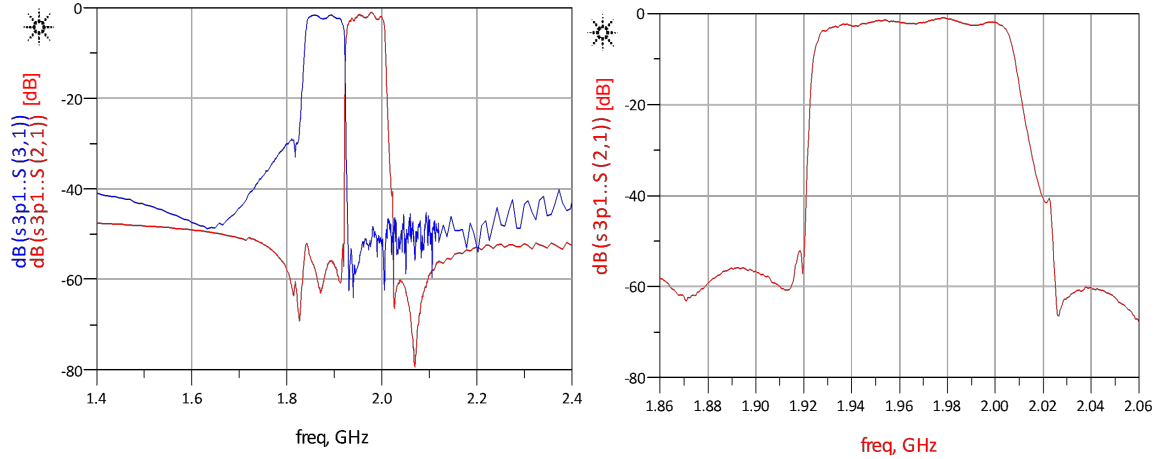


Figure 56. Frequency response (in dB) of the SAW filter (current technology)

When compared to the magnitude response of our proposed filter design (Figure 57), it is evident that our filter implementation with an ideal LNA achieves a slightly improved passband loss (the maximum loss of the SAW filter is 3dB, whereas the maximum drop of the proposed design is 1dB). Both successfully cover the desired frequency range. However, the roll-off of our tunable bandpass filter is not nearly as steep, although still within the specifications.

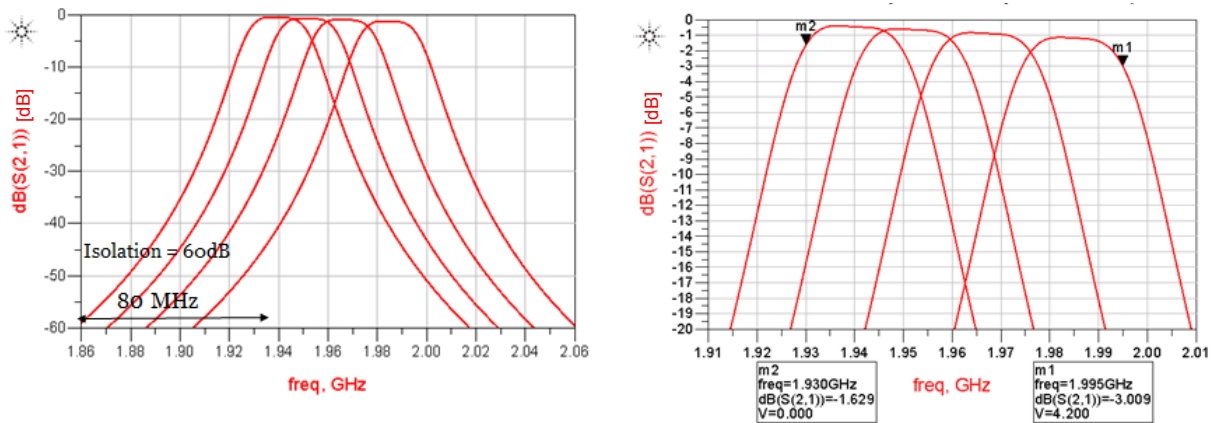


Figure 57. Frequency response (in dB) of proposed filter design

Therefore, this comparison allows us to systematize a set of tradeoffs between the two filter implementations. Both filters achieve relatively small passband loss. However, while the SAW filter has an incomparably sharp out-of-band roll-off, the design we propose achieves tunability for the desired

band 25 frequency range with a roll-off that is still within the spec. The only major issue is that the addition of the LNA to the design will increase the power consumption of the circuitry, which is not desirable in the battery driven smartphone industry.

6.3 Cost and Board Size Analysis

In order to provide cost and board size analysis, we performed extensive market research that focused on locating components that will satisfy several requirements. Although minimizing cost and size were the two prevalent requirements for all of the design components, some components needed to be investigated further. Specifically, high quality factors were desired for the capacitors and inductors, as well as low value tolerances. DigiKey was the main resource for this market research, with the set of prospective design components reported in Table 11.

Table 11. Cost and Board Size Analysis

Ideal component	Quantity	Real component	Price	Size	Q
L = 10nH	4	Wurth Electronics Inc (10nH, 5% tolerance) http://www.digikey.com/product-detail/en/744762110A/732-1808-1-ND/1994388	1 unit = \$0.6200 1000 units = \$206.00	0.102" L x 0.083" W (2.60mm x 2.10mm) AREA = 5.46mm ²	50 @ 1GHz
		Murata http://www.digikey.com/product-detail/en/LQW2BAS10NJ00L/490-5648-1-ND/2625469	1 unit = \$0.48 1000 units = \$222.87	0.082" L x 0.060" W (2.09mm x 1.53mm) AREA = 3.2mm ²	60 @ 500MHz
C = 0.722pF	2	AVX Corporation (0.7pF, +/- 0.05pF) http://www.digikey.com/product-detail/en/ML03510R7AAT2A/478-6729-1-ND/2694243	1 unit = \$0.900 1000 units = \$288.00	0.063" L x 0.033" W (1.60mm x 0.84mm) AREA = 1.344mm ²	
C = 0.699pF	2	Same as above.	1 unit = \$0.900 1000 units = \$288.00	0.063" L x 0.033" W (1.60mm x 0.84mm) AREA = 1.344mm ²	
C = 17.18pF	2	Kemet (18pF, +/- 1%) http://www.digikey.com/product-detail/en/CBR02C180F3GAC/399-8608-6-ND/3479270	1 unit = \$0.370 1000 units = \$90.71	0.024" L x 0.012" W (0.60mm x 0.30mm) AREA = 0.18mm ²	
C = 84.2pF	2	Murata (82pF, +/- 2%) http://www.digikey.com/product-detail/en/GQM1875C2E820GB12D/490-7178-1-ND/3900440	1 unit = \$1.060 1000 units = \$386.02	0.063" L x 0.031" W (1.60mm x 0.80mm) AREA =	

				1.28mm ²	
C = 94.7pF	1	American Technical Ceramics (91pF, +/- 1%) http://www.digikey.com/product-detail/en/600S910FT/1284-1251-1-ND/3905560	1 unit = \$2.270 1000 units = \$1,052.60	0.063" L x 0.032" W (1.60mm x 0.81mm) AREA = 1.296mm ²	
R = 20kOhms	5	Stackpole Electronics (20kOhm, +/- 0.01%) http://www.digikey.com/product-detail/en/RNCF0805TKT20K0/RNCF0805TKT20K0CT-ND/2687088	1 unit = \$1.440 1000 units = \$840.0	0.079" L x 0.049" W (2.00mm x 1.25mm) AREA = 2.5mm ²	
Varactor diode	4	NXP BB208 http://www.digikey.com/product-detail/en/BB208-03,115/568-1955-1-ND/807551	1 unit = \$0.640 1000 units = \$227.50	(1.25mm x 0.85mm) AREA = 1.0625mm ²	
LNA	1				
		TOTAL	1 unit = \$20.97	1 unit = 48.2 mm²	

As shown in Table 11, the approximate price for the entire tunable filter is \$21. This price could potentially be reduced depending on the amount of components ordered as well as the potential for in-house component usage. Additionally, a rough estimation of the board size was calculated using the given component sizes and was determined to be 48.2 mm². Note that this is an estimate for the board size and accounts for neither the design layout nor the wiring and that would most likely increase the board size by a certain percentage.

CHAPTER 7: CONCLUSION

The primary goal of this project was to research, design, and simulate a tunable filter topology capable of operating within cellular band 25. We have conducted extensive background research into cellular standards, tunable components, and general design issues with current smartphone filter technology. Our work had to comply with the project goals and objectives based on the specifications from Skyworks.

After investigating the theoretical fundamentals of several types of filter topologies and verifying the responses against our specifications, we realized a new design approach using capacitive coupled resonators was required. We developed a mathematical model capable of calculating component values for this approach, and subsequently developed a MATLAB program to automate the process. We then added a varactor diode to the filter structure to achieve a tunable frequency response by changing a control voltage. The design was optimized and modified to best suit the specifications of the project. However, due to losses in the non-ideal capacitors, inductors, and varactor diodes, we added a Low Noise Amplifier (LNA) in order to compensate for the insertion loss.

Our final design recommendation is detailed in Section 5.2; it includes a 20 MHz Chebyshev filter topology with two modified coupling capacitor values to achieve a flatter passband. Furthermore, varactor diodes in series with the resonator capacitors were deployed to implement the tunable frequency response. Finally, an LNA compensates for the losses introduced by the non-idealities.

Although we succeeded in implementing the desired response, there are several areas where more research is warranted. One future improvement that should be pursued involves exploring additional technologies to replace the varactor diodes as tunable elements. Also, the ability of manufacturing the individual capacitors and inductors to the quality and accuracy required will need to be investigated. Moreover, research should be directed toward the feasibility of implementing the control circuitry for the varactor diodes, or other tunable elements within mobile handsets. The requirements of using an LNA in a mobile device should be investigated in terms of added power, noise, and size. Specifically, using tunable elements and an LNA to create an active filter may require significant power, which is a concern in battery powered devices. Finally, the ability to increase the frequency range of the filter to accommodate other cellular bands, Wi-Fi, Bluetooth, and GPS should be investigated. Our research addressed the design of a lumped element tunable filter for cellular band 25. However, other standards may require extra design considerations.

CHAPTER 8: DELIVERABLES

Our research has generated a range of filter topologies and design procedures, both theoretical and numerical, of interest to our sponsor. We plan to deliver the following items to Skyworks:

- A detailed report which includes
 - Background research of current designs
 - Current state of the art and cellular standards
 - General RF filter classifications and designs
 - Tunable filter solutions
 - Our filter design approaches that will meet the objectives specified in Chapter 3
 - A detailed schematic and analysis of each design approach
 - Our results based on ADS simulations of the proposed filter designs
 - Best recommendations for filter topology and tunable elements
- ADS simulation files used to achieve the simulation results
- MATLAB programs used to theoretically determine the component values

APPENDIX A: Derivation of the inverter networks at two ends of C-coupled filters

The admittance and impedance inverters can be realized using so-called Pi and T capacitive ladders as shown in Figure 30. However, since the negative capacitance cannot be combined by both generator and load ends to yield positive values, another equivalent circuit must be investigated. In fact, we can realize an inverter by using only two capacitors as shown in Figure 58.

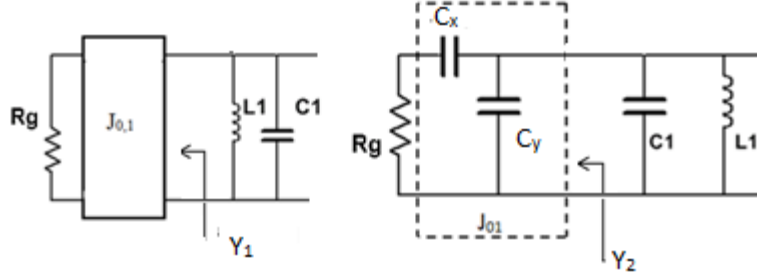


Figure 58. Realization of admittance inverters at the ends of C-coupled filters

If the generators in the two circuits are matched to the characteristic impedance of Z_0 we can calculate the two admittances Y_1 and Y_2 as follows:

$$\begin{aligned}
 Y_1 &= \frac{J_{01}^2}{Y_g} = J_{01}^2 Z_0 & Y_2 &= j\omega_0 C_y + \frac{1}{\frac{1}{j\omega_0 C_x} + Z_0} \\
 & & &= j\omega_0 C_y + \frac{j\omega_0 C_x}{1 + jZ_0\omega_0 C_x} \\
 & & &= j\omega_0 C_y + \frac{j\omega_0 C_x + Z_0(\omega_0 C_x)^2}{1 + (Z_0\omega_0 C_x)^2} \\
 & & &= \frac{Z_0(\omega_0 C_x)^2}{1 + (Z_0\omega_0 C_x)^2} + j(\omega_0 C_y + \frac{\omega_0 C_x}{1 + (Z_0\omega_0 C_x)^2})
 \end{aligned}$$

In order for the two circuits to be equivalent, Y_1 has to be equal to Y_2 for every frequency. By equating the real and imaginary parts of Y_1 and Y_2 , we obtain the results for C_x and C_y :

$$C_x = \frac{J_{01}}{\omega_0 \sqrt{1 - (J_{01} Z_0)^2}} \quad (16)$$

$$C_y = -\frac{C_x}{1 + (Z_0 \omega_0 C_x)^2} \quad (17)$$

It should be noted that if $\omega_0 C_x \ll 1$ the shunt capacitor C_y has approximately the same amplitude as the serial capacitor C_x but with opposite sign.

Similar to the admittance inverter, the impedance inverters at two ends of the serial topology are realized using the equivalent circuit show in Figure 59.

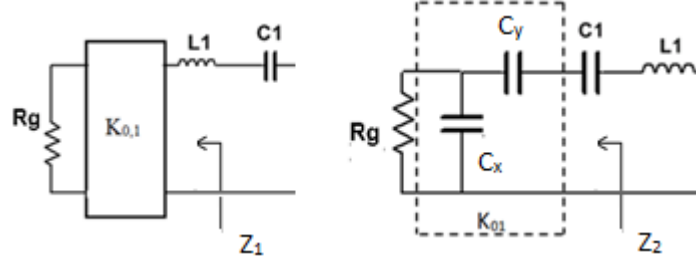


Figure 59. Realization of impedance inverters at the ends of C-coupled filters

Using the same method as demonstrated above, if the generator impedance is Z_0 we can calculate the two impedances looking into the inverters as:

$$\begin{aligned}
 Z_1 &= \frac{K_{01}^2}{Z_0} \\
 Z_2 &= \frac{1}{j\omega_0 C_y} + \frac{1}{j\omega_0 C_x + \frac{1}{Z_0}} \\
 &= \frac{-j}{\omega_0 C_y} + \frac{Z_0}{1 + jZ_0\omega_0 C_x} \\
 &= \frac{-j}{\omega_0 C_y} + \frac{Z_0 - jZ_0^2\omega_0 C_x}{1 + (Z_0\omega_0 C_x)^2} \\
 &= \frac{Z_0}{1 + (Z_0\omega_0 C_x)^2} - j\left(\frac{1}{\omega_0 C_y} + \frac{Z_0^2\omega_0 C_x}{1 + (Z_0\omega_0 C_x)^2}\right)
 \end{aligned}$$

By equating the real parts of Z_1 and Z_2 and setting the imaginary part of Z_2 to be 0, we can calculate the capacitors C_x and C_y as:

$$C_x = \frac{\sqrt{1 - \left(\frac{K}{Z_0}\right)^2}}{K_{01}\omega_0} \quad (16)$$

$$C_y = -C_x - \frac{1}{(Z_0\omega_0)^2 C_x} \quad (17)$$

Unlike the admittance inverters, for impedance inverters it usually turns out that $(Z_0\omega_0)^2 C_x \gg 1$. Therefore, serial capacitors have approximately the same amplitude as the shunt ones but with a negative sign.

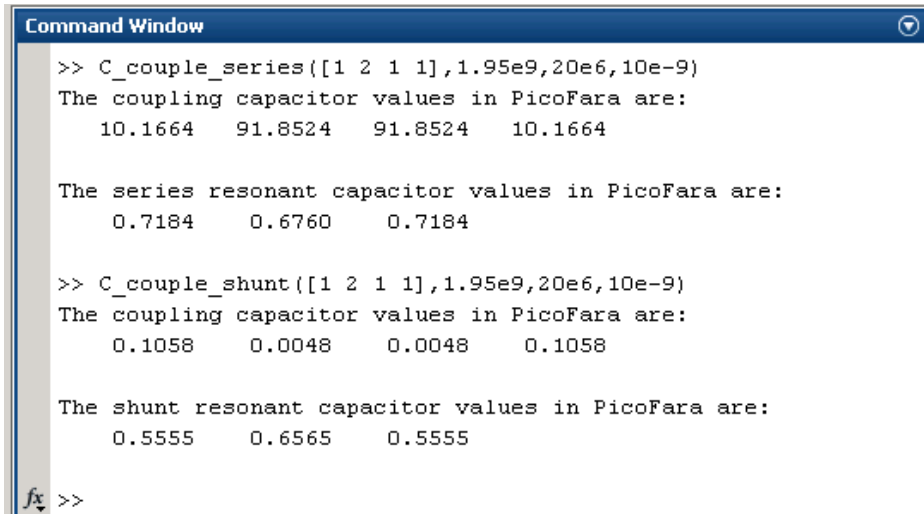
APPENDIX B: MATLAB Code

We investigated the C-coupled filter theoretically and discussed the derivations of the component values in Section 4.4. Based on those derivations, we created two MATLAB functions that can calculate the capacitor values when given the g coefficients of the filter topology, the center frequency, the bandwidth and the specified inductor. The two function prototypes are:

```
function y = C_couple_shunt(g,f0,BW,L)
```

```
function y = C_couple_series(g,f0,BW,L)
```

In the prototypes above, g is the array of the filter coefficients as captured in the tables in Appendix F; f_0 is the center frequency in Hertz, BW is the bandwidth in Hertz, and L is the inductor value in Henries. Figure 60 below shows sample executions of the two functions to calculate the capacitor values of a third order Butterworth C-coupled bandpass filter topologies. From Table 12, the g coefficients for the third order maximally flat Butterworth filter are 1, 2, 1 and 1. The center frequency is 1.95GHz; bandwidth is 20MHz and the inductor is 10 nH.



```
Command Window
>> C_couple_series([1 2 1 1],1.95e9,20e6,10e-9)
The coupling capacitor values in PicoFara are:
    10.1664    91.8524    91.8524    10.1664

The series resonant capacitor values in PicoFara are:
     0.7184     0.6760     0.7184

>> C_couple_shunt([1 2 1 1],1.95e9,20e6,10e-9)
The coupling capacitor values in PicoFara are:
     0.1058     0.0048     0.0048     0.1058

The shunt resonant capacitor values in PicoFara are:
     0.5555     0.6565     0.5555

fx >>
```

Figure 60: Sample executions of the two MATLAB functions and results

As Figure 60 demonstrates, the functions can calculate both the coupling capacitor and the resonant capacitor values in picofarads. The next subsections provide the detailed code for these two functions.

C-coupled Shunt Resonator

```
function y = C_couple_shunt(g,f0,BW,L)
%Filter order, impedance
    n = length(g);          %order = n-1
    Z0 = 50;

%Calculate critical frequencies
    w0 = 2*pi*f0;           %Center freq
    w1 = w0 - 2*pi*BW/2;    %Lower cut-off
    w2 = w0 + 2*pi*BW/2;    %Higher cut-off
    delta = BW/f0;          %Inverse of Loaded quality factor

%Capcitor of the shunt resonator
    C = 1/(L*w0^2);
    display(C);

%Calculate coupling coefficents based on Equation 10a,b,c
```

```

J=zeros(size(g));
J(1)= sqrt(w0*C*delta/(Z0*1*g(1)));
J(n)= sqrt(w0*C*delta/(Z0*g(n-1)*g(n)));
for i = 2:1:n-1
    J(i) = w0*C*delta/(sqrt(g(i-1)*g(i)));
end

%Calculate coupling capacitor values based on Equation 12a,b,c
C_coupled = J/w0;
C_coupled(1) = J(1)/w0/sqrt(1-(J(1)*Z0)^2);
C_coupled(n) = J(n)/w0/sqrt(1-(J(n)*Z0)^2);

%Calculate coupling capacitor values based on Equation 14
C_resonator = zeros(1,n-1);
for i=1:n-1
    C_resonator(i)=C-C_coupled(i)-C_coupled(i+1);
end
%Display result
disp('The coupling capacitor values in PicoFara are: ');
disp(C_coupled*10^12);
disp('The shunt resonant capacitor values in PicoFara are: ');
disp(C_resonator*10^12);
end

```

C-coupled Serial Resonator

```

function y = C_couple_series(g,f0,BW,L)
%Filter order, impedance
n = length(g);          %order = n-1
Z0 = 50;

%Calculate critical frequencies
w0 = 2*pi*f0;           %Center freq
w1 = w0 - 2*pi*BW/2;    %Lower cut-off
w2 = w0 + 2*pi*BW/2;    %Higher cut-off
delta = BW/f0;          %Inverse of Loaded quality factor

%Capcitor of the shunt resonator
C = 1/(L*w0^2);
display(C);

%Calculate coupling coefficients based on Equation 11a,b,c
K=zeros(size(g));
K(1)= sqrt(w0*L*delta*Z0/(1*g(1)));
K(n)= sqrt(w0*L*delta*Z0/(g(n-1)*g(n)));
for i = 2:1:n-1
    K(i) = w0*L*delta/(sqrt(g(i-1)*g(i)));
end

%Calculate coupling capacitor values based on Equation 13a,b,c
C_coupled = 1./(K*w0);
C_coupled(1) = sqrt(Z0^2-K(1)^2)/K(1)/w0/Z0;
C_coupled(n) = sqrt(Z0^2-K(n)^2)/K(n)/w0/Z0;

%Calculate coupling capacitor values based on Equation 15
C_resonator = zeros(1,n-1);
for i=1:n-1
    C_resonator(i)=1/(1/C-1/C_coupled(i)-1/C_coupled(i+1));
end

```

```
    end
%Display result
    disp('The coupling capacitor values in PicoFara are: ');
    disp(C_coupled*10^12);
    disp('The series resonant capacitor values in PicoFara are: ');
    disp(C_resonator*10^12);
end
```

APPENDIX C: NXP BB208 Varactor Diode Datasheet

BB208-02; BB208-03

Low voltage variable capacitance diode

Rev. 2 — 8 September 2011

Product data sheet

1. Product profile

1.1 General description

The BB208-02 is a planar technology variable capacitance diode in a SOD523 (SC-79) ultra small SMD plastic package.

The BB208-03 is a planar technology variable capacitance diode in a SOD323 (SC-76) very small SMD plastic package.

1.2 Features and benefits



- Very small SMD plastic packages
- Very low series resistance
- Excellent CV linearity
- $C_d(1V)$: 21.5 pF; $C_d(7.5V)$: 4.9 pF
- High ratio.

1.3 Applications

- Voltage Controlled Oscillators (VCO)
- Voltage Controlled Crystal Oscillators/Temperature Controlled Crystal Oscillators (VCXO/TCXO).



2. Pinning information

Table 1. Discrete pinning: SOD523

Pin	Description	Simplified outline	Symbol
1	cathode		
2	anode		

sym008

Table 2. Discrete pinning: SOD323

Pin	Description	Simplified outline	Symbol
1	cathode		
2	anode		

sym008



3. Ordering information

Table 3. Ordering information

Type number	Package		Version
	Name	Description	
BB208-02	-	plastic surface mounted package; 2 leads	SOD523
BB208-03	-	plastic surface mounted package; 2 leads	SOD323

4. Marking

Table 4. Marking

Type number	Marking code
BB208-02	A1
BB208-03	A2

5. Limiting values

Table 5. Limiting values

In accordance with the Absolute Maximum Rating System (IEC 60134).

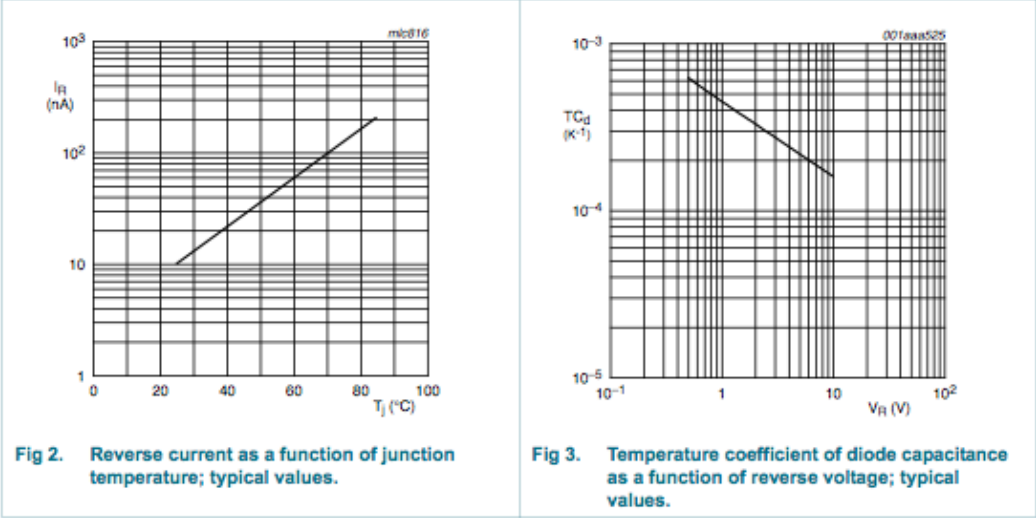
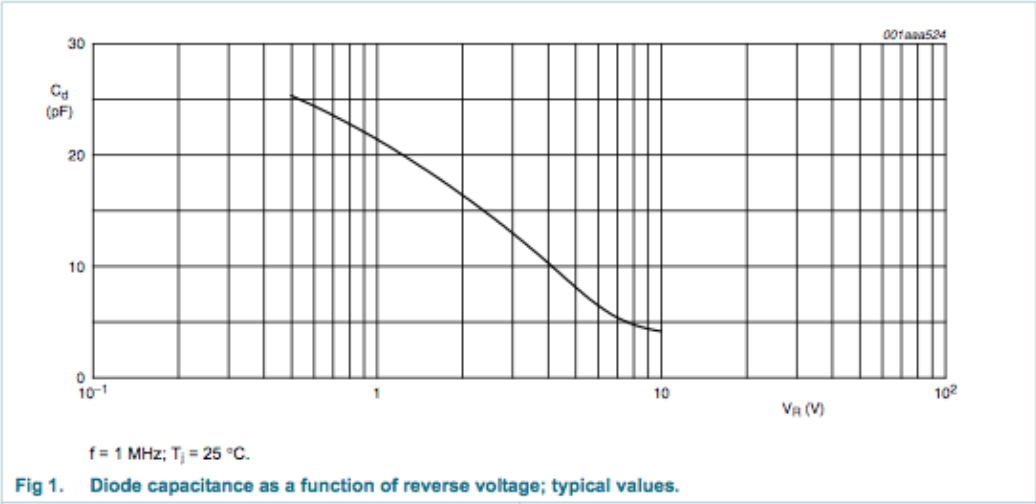
Symbol	Parameter	Conditions	Min	Max	Unit
V_R	continuous reverse voltage		-	10	V
I_F	continuous forward current		-	20	mA
T_{stg}	storage temperature		-55	+150	°C
T_j	operating junction temperature		-55	+125	°C

6. Characteristics

Table 6. Electrical characteristics

$T_j = 25\text{ °C}$ unless otherwise specified.

Symbol	Parameter	Conditions	Min	Typ	Max	Unit
I_R	reverse current	$V_R = 10\text{ V}$; see Figure 2	-	-	10	nA
		$V_R = 10\text{ V}$; $T_j = 85\text{ °C}$; see Figure 2	-	-	200	nA
r_s	diode series resistance	$f = 100\text{ MHz}$; $V_R = 3\text{ V}$	-	0.35	0.5	Ω
C_d	diode capacitance	$f = 1\text{ MHz}$; see Figure 1 and Figure 3				
		$V_R = 1\text{ V}$	19.9	-	23.2	pF
		$V_R = 4\text{ V}$	-	10.1	-	pF
		$V_R = 7.5\text{ V}$	4.5	-	5.4	pF
$\frac{C_d(1V)}{C_d(4V)}$	capacitance ratio	$f = 1\text{ MHz}$	2.0	-	-	
$\frac{C_d(1V)}{C_d(7.5V)}$	capacitance ratio	$f = 1\text{ MHz}$	3.7	-	5.2	



7. Package outline

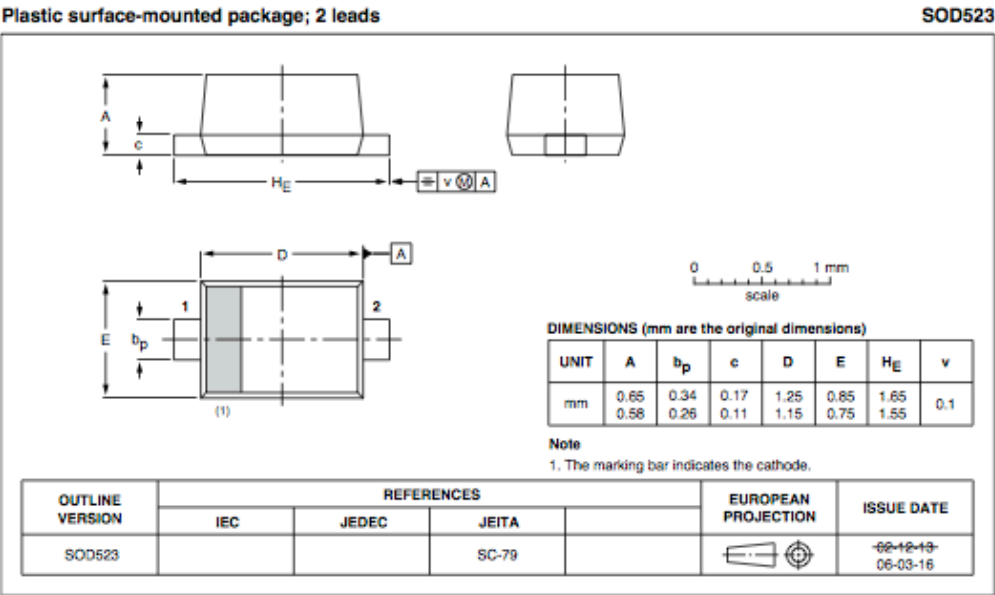


Fig 4. Package outline (BB208-02).

Plastic surface-mounted package; 2 leads

SOD323

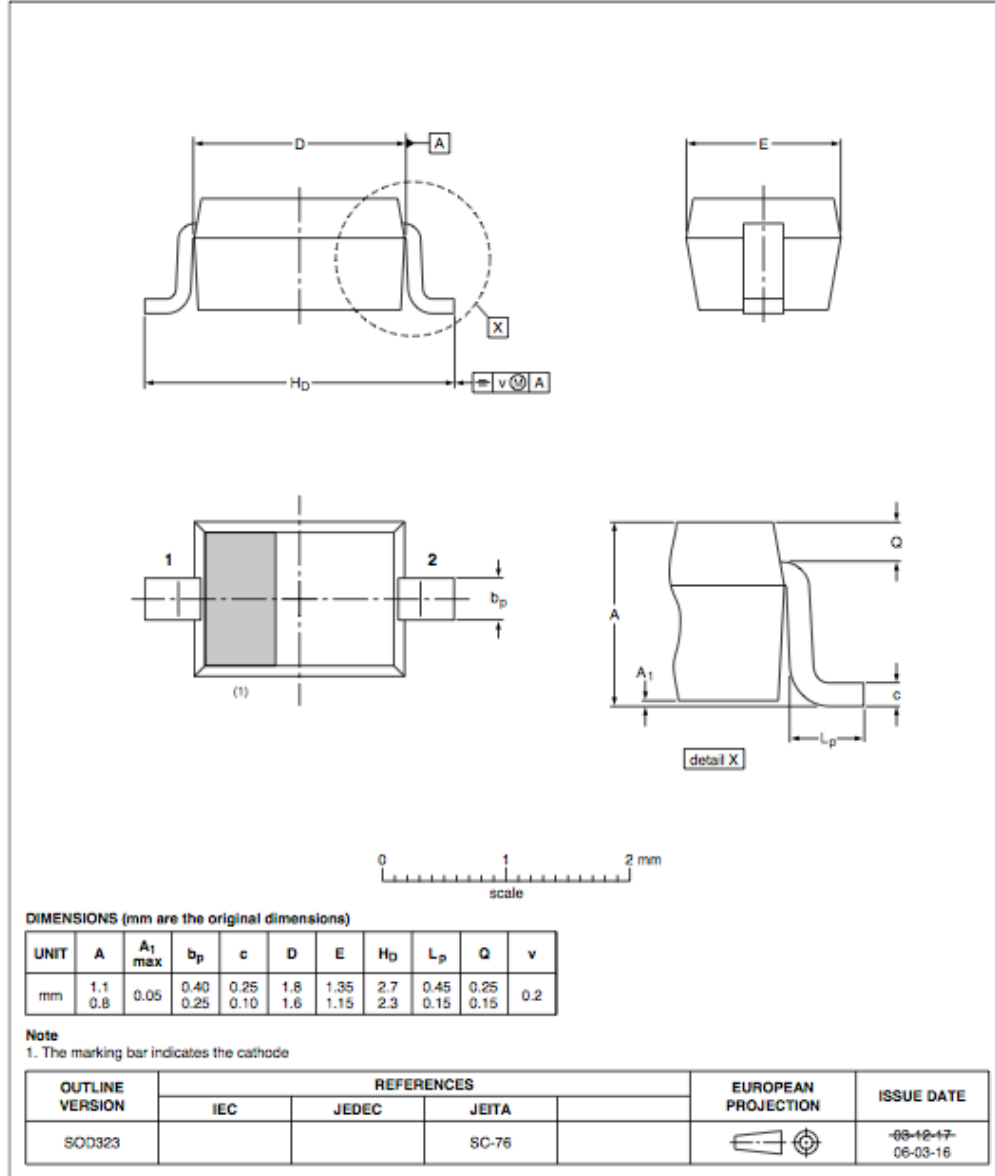


Fig 5. Package outline (BB208-03).

8. Revision history

Table 7. Revision history

Document ID	Release date	Data sheet status	Change notice	Supersedes
BB208-02_BB208-03 v.2	20110908	Product data sheet	-	BB208-02_BB208-03 v.1
Modifications:	<ul style="list-style-type: none">• The format of this data sheet has been redesigned to comply with the new identity guidelines of NXP Semiconductors.• Legal texts have been adapted to the new company name where appropriate.• Package outline drawings have been updated to the latest version.			
BB208-02_BB208-03 v.1 (9397 750 12696)	20040407	Product data	-	-

9. Legal information

9.1 Data sheet status

Document status ^{[1][2]}	Product status ^[3]	Definition
Objective [short] data sheet	Development	This document contains data from the objective specification for product development.
Preliminary [short] data sheet	Qualification	This document contains data from the preliminary specification.
Product [short] data sheet	Production	This document contains the product specification.

[1] Please consult the most recently issued document before initiating or completing a design.

[2] The term 'short data sheet' is explained in section "Definitions".

[3] The product status of device(s) described in this document may have changed since this document was published and may differ in case of multiple devices. The latest product status information is available on the Internet at URL <http://www.nxp.com>.

9.2 Definitions

Draft — The document is a draft version only. The content is still under internal review and subject to formal approval, which may result in modifications or additions. NXP Semiconductors does not give any representations or warranties as to the accuracy or completeness of information included herein and shall have no liability for the consequences of use of such information.

Short data sheet — A short data sheet is an extract from a full data sheet with the same product type number(s) and title. A short data sheet is intended for quick reference only and should not be relied upon to contain detailed and full information. For detailed and full information see the relevant full data sheet, which is available on request via the local NXP Semiconductors sales office. In case of any inconsistency or conflict with the short data sheet, the full data sheet shall prevail.

Product specification — The information and data provided in a Product data sheet shall define the specification of the product as agreed between NXP Semiconductors and its customer, unless NXP Semiconductors and customer have explicitly agreed otherwise in writing. In no event however, shall an agreement be valid in which the NXP Semiconductors product is deemed to offer functions and qualities beyond those described in the Product data sheet.

9.3 Disclaimers

Limited warranty and liability — Information in this document is believed to be accurate and reliable. However, NXP Semiconductors does not give any representations or warranties, expressed or implied, as to the accuracy or completeness of such information and shall have no liability for the consequences of use of such information.

In no event shall NXP Semiconductors be liable for any indirect, incidental, punitive, special or consequential damages (including - without limitation - lost profits, lost savings, business interruption, costs related to the removal or replacement of any products or rework charges) whether or not such damages are based on tort (including negligence), warranty, breach of contract or any other legal theory.

Notwithstanding any damages that customer might incur for any reason whatsoever, NXP Semiconductors' aggregate and cumulative liability towards customer for the products described herein shall be limited in accordance with the Terms and conditions of commercial sale of NXP Semiconductors.

Right to make changes — NXP Semiconductors reserves the right to make changes to information published in this document, including without limitation specifications and product descriptions, at any time and without notice. This document supersedes and replaces all information supplied prior to the publication hereof.

Suitability for use — NXP Semiconductors products are not designed, authorized or warranted to be suitable for use in life support, life-critical or safety-critical systems or equipment, nor in applications where failure or

malfunction of an NXP Semiconductors product can reasonably be expected to result in personal injury, death or severe property or environmental damage. NXP Semiconductors accepts no liability for inclusion and/or use of NXP Semiconductors products in such equipment or applications and therefore such inclusion and/or use is at the customer's own risk.

Applications — Applications that are described herein for any of these products are for illustrative purposes only. NXP Semiconductors makes no representation or warranty that such applications will be suitable for the specified use without further testing or modification.

Customers are responsible for the design and operation of their applications and products using NXP Semiconductors products, and NXP Semiconductors accepts no liability for any assistance with applications or customer product design. It is customer's sole responsibility to determine whether the NXP Semiconductors product is suitable and fit for the customer's applications and products planned, as well as for the planned application and use of customer's third party customer(s). Customers should provide appropriate design and operating safeguards to minimize the risks associated with their applications and products.

NXP Semiconductors does not accept any liability related to any default, damage, costs or problem which is based on any weakness or default in the customer's applications or products, or the application or use by customer's third party customer(s). Customer is responsible for doing all necessary testing for the customer's applications and products using NXP Semiconductors products in order to avoid a default of the applications and the products or of the application or use by customer's third party customer(s). NXP does not accept any liability in this respect.

Limiting values — Stress above one or more limiting values (as defined in the Absolute Maximum Ratings System of IEC 60134) will cause permanent damage to the device. Limiting values are stress ratings only and (proper) operation of the device at these or any other conditions above those given in the Recommended operating conditions section (if present) or the Characteristics sections of this document is not warranted. Constant or repeated exposure to limiting values will permanently and irreversibly affect the quality and reliability of the device.

Terms and conditions of commercial sale — NXP Semiconductors products are sold subject to the general terms and conditions of commercial sale, as published at <http://www.nxp.com/profile/terms>, unless otherwise agreed in a valid written individual agreement. In case an individual agreement is concluded only the terms and conditions of the respective agreement shall apply. NXP Semiconductors hereby expressly objects to applying the customer's general terms and conditions with regard to the purchase of NXP Semiconductors products by customer.

No offer to sell or license — Nothing in this document may be interpreted or construed as an offer to sell products that is open for acceptance or the grant, conveyance or implication of any license under any copyrights, patents or other industrial or intellectual property rights.

Export control — This document as well as the item(s) described herein may be subject to export control regulations. Export might require a prior authorization from national authorities.

Non-automotive qualified products — Unless this data sheet expressly states that this specific NXP Semiconductors product is automotive qualified, the product is not suitable for automotive use. It is neither qualified nor tested in accordance with automotive testing or application requirements. NXP Semiconductors accepts no liability for inclusion and/or use of non-automotive qualified products in automotive equipment or applications.

In the event that customer uses the product for design-in and use in automotive applications to automotive specifications and standards, customer (a) shall use the product without NXP Semiconductors' warranty of the product for such automotive applications, use and specifications, and (b) whenever customer uses the product for automotive applications beyond

NXP Semiconductors' specifications such use shall be solely at customer's own risk, and (c) customer fully indemnifies NXP Semiconductors for any liability, damages or failed product claims resulting from customer design and use of the product for automotive applications beyond NXP Semiconductors' standard warranty and NXP Semiconductors' product specifications.

9.4 Trademarks

Notice: All referenced brands, product names, service names and trademarks are the property of their respective owners.

10. Contact information

For more information, please visit: <http://www.nxp.com>

For sales office addresses, please send an email to: salesaddresses@nxp.com

APPENDIX D: Using realistic currently available high-quality lumped element models

In order to check the validity of our design, we decided to implement the realistic component models into the 3rd order tunable C-coupled serial resonator. Specifically, we downloaded the component libraries from Murata and Coilcraft and investigated which model would be most suitable for our predicted values. The serial resonator design requires very precise capacitor values as can be seen in Figure 61 ($C = 0.7340\text{pF}$, 0.6901pF , 10.2718pF , 92.8043pF), which turns out to be a challenge for both industrial models.

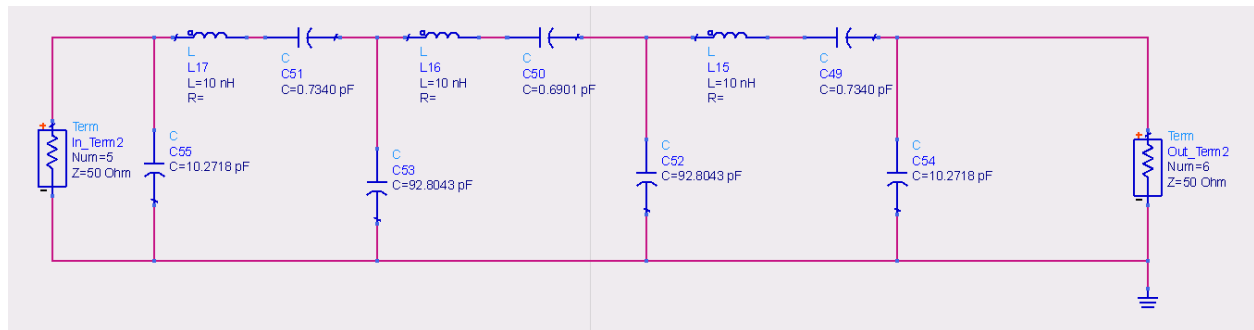


Figure 61. Using real currently available high quality lumped element models

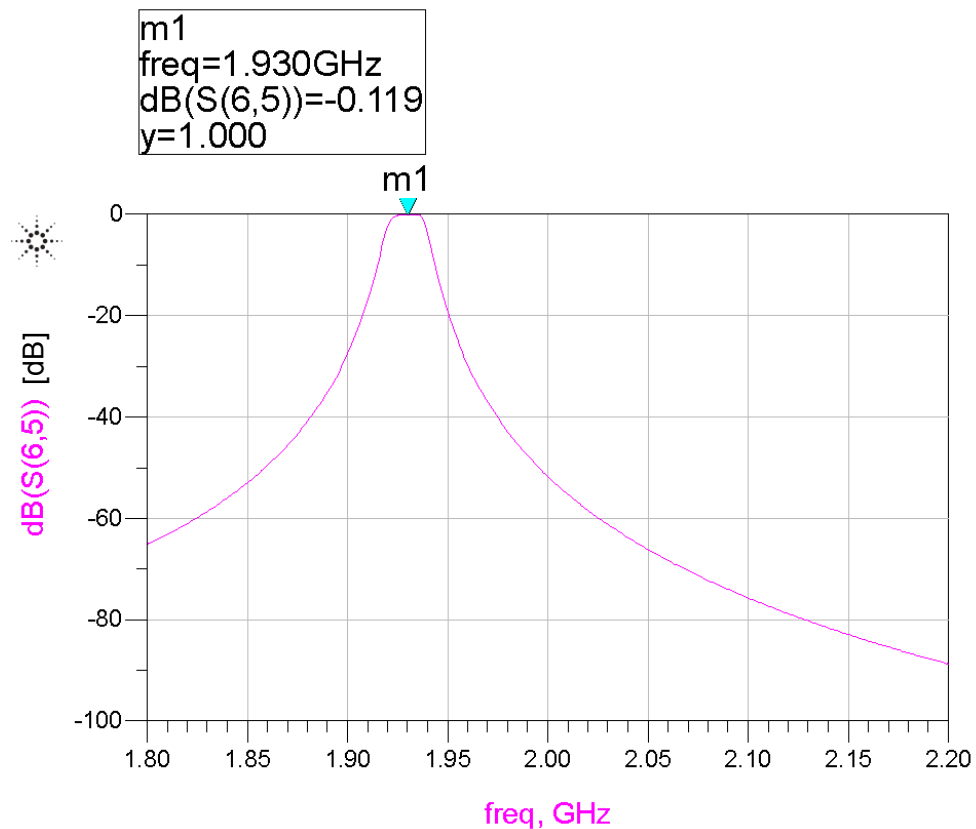


Figure 62. Frequency response (in dB) of the 3rd order C-coupled serial resonator

Checking in the Murata catalog¹, we discovered two types of high frequency HiQ capacitors differing in size and capacitance value. Both were the chip monolithic ceramic capacitors; they are shown in Figure 63.

High Frequency HiQ Type (0402 Size Max.)												
 GJM												
Series	LxW (mm) <Size Code (Inch)>	Rated Voltage (Vdc)	Capacitance Range (F)									
			0.1 p	1 p	10 p	100 p	1000 p	10000 p	0.1 μ	1 μ	10 μ	100 μ
GJM02	0.4X0.2 <01005>	16	0.2pF			22pF						
GJM03	0.6X0.3 <0201>	25	0.2pF			20pF						
		6.3				22pF						
GJM15	1.0X0.5 <0402>	50	0.1pF			47pF						

High Frequency HiQ Type (0603 Size Min.)												
 GQM												
Series	LxW (mm) <Size Code (Inch)>	Rated Voltage (Vdc)	Capacitance Range (F)									
			0.1 p	1 p	10 p	100 p	1000 p	10000 p	0.1 μ	1 μ	10 μ	100 μ
GQM18	1.6X0.8 <0603>	250		1.0pF		47pF						
		100		1.0pF		68pF						
		50			7.0pF	100pF						
GQM21	2.0X1.25 <0805>	250		1.0pF		100pF						
		100		1.0pF		18pF						
		50			20pF	100pF						
GQM22	2.8X2.8 <1111>	500		1.0pF		100pF						

Figure 63. Murata High Frequency HiQ ceramic capacitors

The range of values also matched our design requirements (GJM: 0.10pF – 47pF, GQM: 1pF – 100pF). We proceeded to investigate the exact Q values that these capacitors will exhibit at high frequencies. The information was found in the datasheet that was specific to this set of Murata capacitors.²

¹ Murata Products Line Up, <http://www.murata.com/products/catalog/pdf/k70e.pdf>

² Chip Monolithic Ceramic Capacitors, <http://www.murata.com/products/catalog/pdf/c02e.pdf>

High Frequency High Q Type 1005(in mm)/0402(in inch) Size Max.

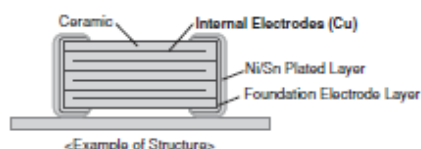
GJM Series **HIQ**

This product improves the high frequency characteristics and contributes to a reduction of power consumption by the High Q and low ESR.

Features

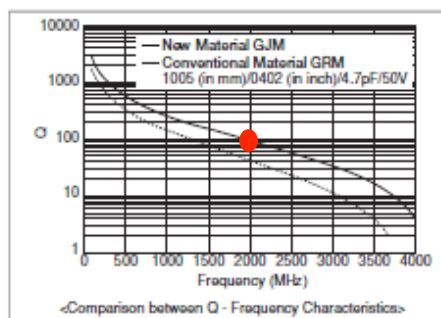
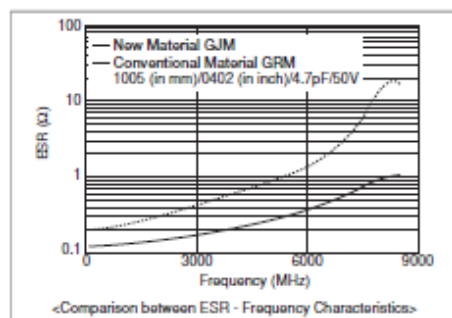
① Mainly ideal for mobile communication devices and temperature compensation of related modules.

This product is ideal for temperature compensation of high frequency circuits, such as resonant circuits, tuning circuits, and impedance matching circuits where the operating characteristics of the device are greatly affected by the capacitance fluctuation.



② High Q and low ESR in VHF, UHF and microwave frequency bands.

High Q and low ESR were achieved at a high frequency by adopting ceramic material as the dielectric material which enables an extremely low loss at high frequency, and base metal electrodes as the internal electrodes.



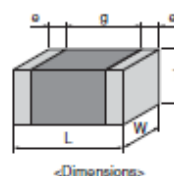
③ Can be used for tight tolerance.

In addition to standard tolerance, the allowable range of this product is also suitable for the following tight tolerance.

Capacitance Range	Standard Capacitance Tolerance (Capacitance Tolerance Symbol)	Narrow Capacitance Tolerance (Capacitance Tolerance Symbol)
<~0.9pF	±0.1pF (B)	±0.05pF (W)
1.0 to 5.0pF	±0.25pF (C)	±0.05pF (W), ±0.1pF (B)
5.1 to 9.9pF	±0.5pF (D)	±0.05pF (W), ±0.1pF (B), ±0.25pF (C)
>~10pF	±5% (J)	±2% (G)

Specifications

Size	0.4×0.2mm to 1.0×0.5mm
Rated Voltage	DC6.3V to 50V
Capacitance	0.1pF to 47pF
Main Applications	Small communication devices, such as mobile phones and high frequency communication modules



This catalog contains only a portion of the product lineup.
Please refer to the capacitor search tool on the Murata Web site for details.



For GJM Series, the Q factor at 2GHz is approximately 100, which is unfortunately on the lower end for our application which needs a range of 100 - 500.

High Frequency High Q Type 1608(in mm)/0603(in inch) Size Min.

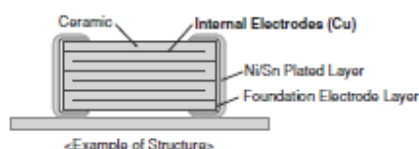
GQM Series **HIQ**

High Frequency Capacitor Ideal for PA Design of Base Stations

Features

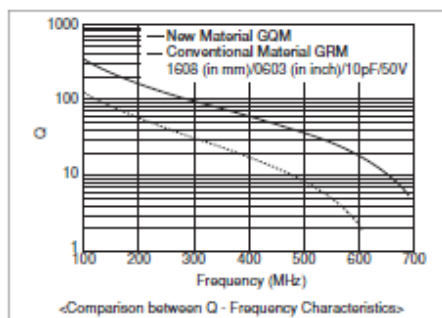
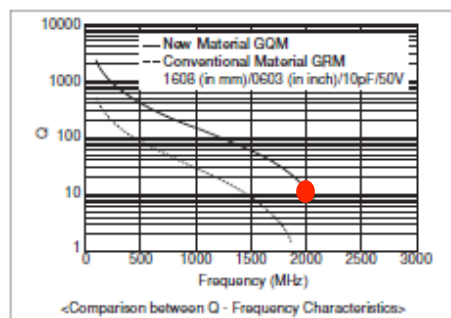
- ① **Mainly ideal for base stations of mobile communication devices and temperature compensation of related modules.**

This product is ideal for temperature compensation of high frequency circuits, such as resonant circuits, tuning circuits, and impedance matching circuits where the operating characteristics of the device are greatly affected by the capacitance fluctuation.



- ② **High Q and low ESR in VHF, UHF and microwave frequency bands.**

High Q and low ESR were achieved at a high frequency by adopting ceramic material as the dielectric material which enables an extremely low loss at high frequency, and base metal electrodes as the internal electrodes.



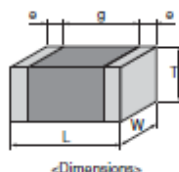
- ③ **Can be used for tight tolerance.**

In addition to standard tolerance, the allowable range of this product is also suitable for the following narrow tolerance.

Capacitance Range	Standard Capacitance Tolerance (Capacitance Tolerance Symbol)	Narrow Capacitance Tolerance (Capacitance Tolerance Symbol)
<~0.9pF	±0.1pF (B)	±0.05pF (W)
1.0 to 5.0pF	±0.25pF (C)	±0.05pF (W), ±0.1pF (B)
5.1 to 9.9pF	±0.5pF (D)	±0.05pF (W), ±0.1pF (B), ±0.25pF (C)
>~10pF	±5% (J)	±2% (G)

Specifications

Size	1.6×0.8mm to 2.8×2.8mm
Rated Voltage	DC50V to 500V
Capacitance	0.1pF to 510pF
Main Applications	Mobile phone base stations



This catalog contains only a portion of the product lineup.
Please refer to the capacitor search tool on the Murata Web site for details.

For the GQM Series, the Q factor at 2GHz is approximately 13, which is too low for our application (need a range of 100 - 500). However, in order to obtain the capacitance values that are necessary for our design we cannot only pursue the GJM series that has a relatively better Q factor. Hence, for our experimental purposes we implemented both GJM and GQM series capacitors in our design as seen in Figure 64.

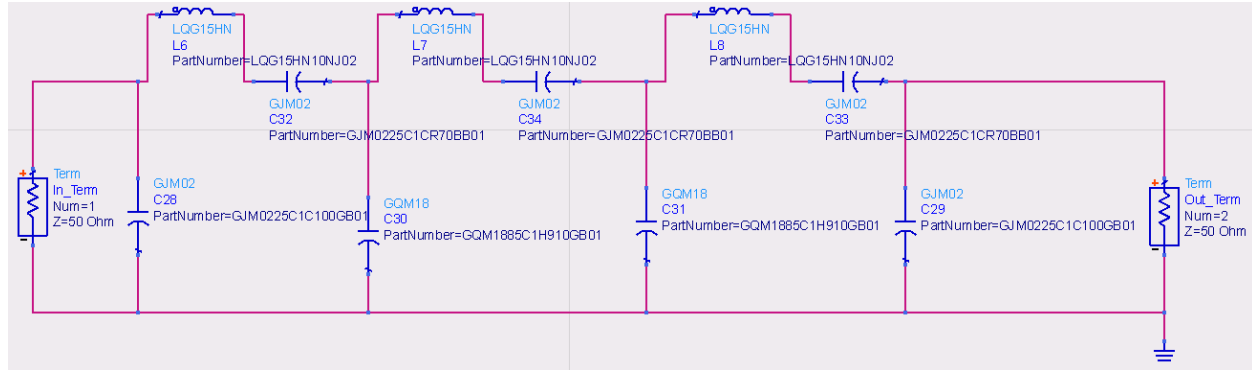


Figure 64. Implementing Murata component models in the serial resonator design

In addition, Murata offers a range of inductors (Figure 65) that we also employed in our design for this testing purpose.

RF Inductors															
	Series	Structure	Size Code inch (mm)	Inductance Range (H)								Rated Current (A)			
				1n	10n	100n	1μ	10μ	100μ	1m	10m	10m	100m	1	10
RF Inductors	LQG15HN_02	Multilayer Type (Non-Magnetic Core)	0402 (1005)		120nH									150mA	300mA
	LQG15HS_02		0402 (1005)		270nH									110mA	300mA
	LQG18HN_00		0603 (1608)		100nH									300mA	500mA
	LQP02TN_02	Film Type (Non-Magnetic Core)	01005 (0402)		0.2nH to 39nH									90mA	320mA
	LQP02TQ_02		01005 (0402)		0.4nH to 10nH									170mA	900mA
	LQP03TG_02		0201 (0603)		0.6nH to 120nH									80mA	850mA
	LQP03TN_02		0201 (0603)		0.6nH to 270nH									60mA	850mA
	LQP15MN_02		0402 (1005)		33nH									60mA	400mA
	LQP18MN_02		0603 (1608)		100nH									50mA	300mA
	LQW03AW_00	Wire Wound Type (Non-Magnetic Core)	-		13nH									280mA	450mA
	LQW04AN_00		03015 (0804)		33nH									140mA	900mA
	LQW15AN_00		0402 (1005)		120nH									110mA	1.0A
	LQW15AN_10		0402 (1005)		5.6nH									800mA	1.2A
	LQW15AN_80		0402 (1005)		75nH									320mA	3.15A
	LQW18AN_00		0603 (1608)		470nH									75mA	850mA
	LQW18AN_10		0603 (1608)		33nH									550mA	1.4A
	LQW18AN_80		0603 (1608)		390nH									190mA	3.2A
	LQW2BAS_00		0805 (2015)		820nH									180mA	300mA
	LQW2BHN_03		0805 (2015)		470nH									160mA	1.32A
	LQW2BHN_13		0805 (2015)		27nH									900mA	1.9A
	LQW2UAS_00		1008 (2520)		4.7μH									260mA	1.0A
	LQW31HN_03		1206 (3216)		100nH									230mA	750mA
	LQW21HN_00	Wire Wound Type (Ferrite Core)	0805 (2012)		2.2μH								75mA	160mA	
	LQH31HN_03		1206 (3216)		880nH								180mA	920mA	

Figure 65. Murata RF Inductors

The only one in the list that was designed for high Q applications is the LQP02TQ_02. However the ADS model for this inductor type does not support the inductance value of 10nH. Hence, we had to utilize a different type, LQG15HN. As can be seen from Figure 66, the Q value of this type of inductor is in the 30s.

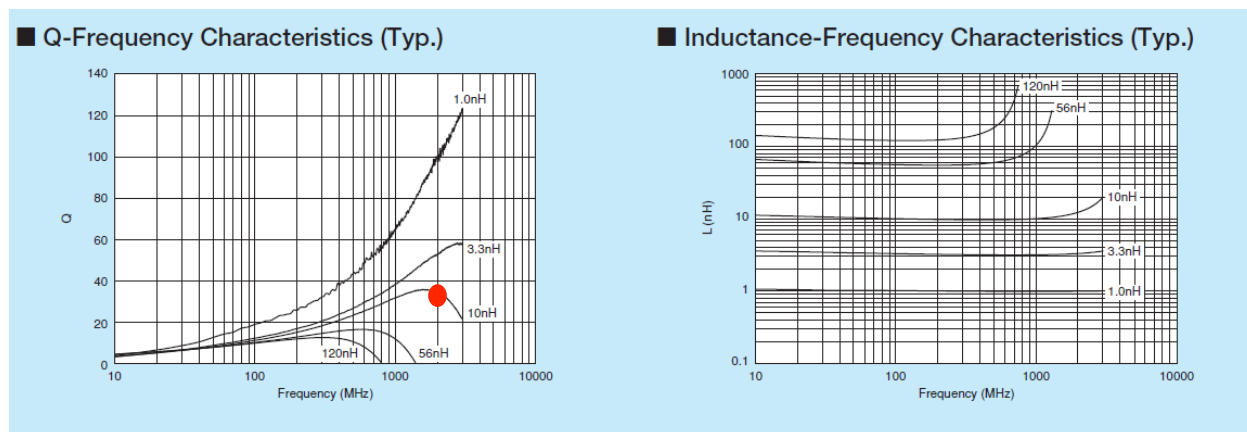


Figure 66. LGQ15HN Murata Inductor behavior

The response of our design with the implemented Murata models can be observed in Figure 67. The ideal response is also shown as a reference.

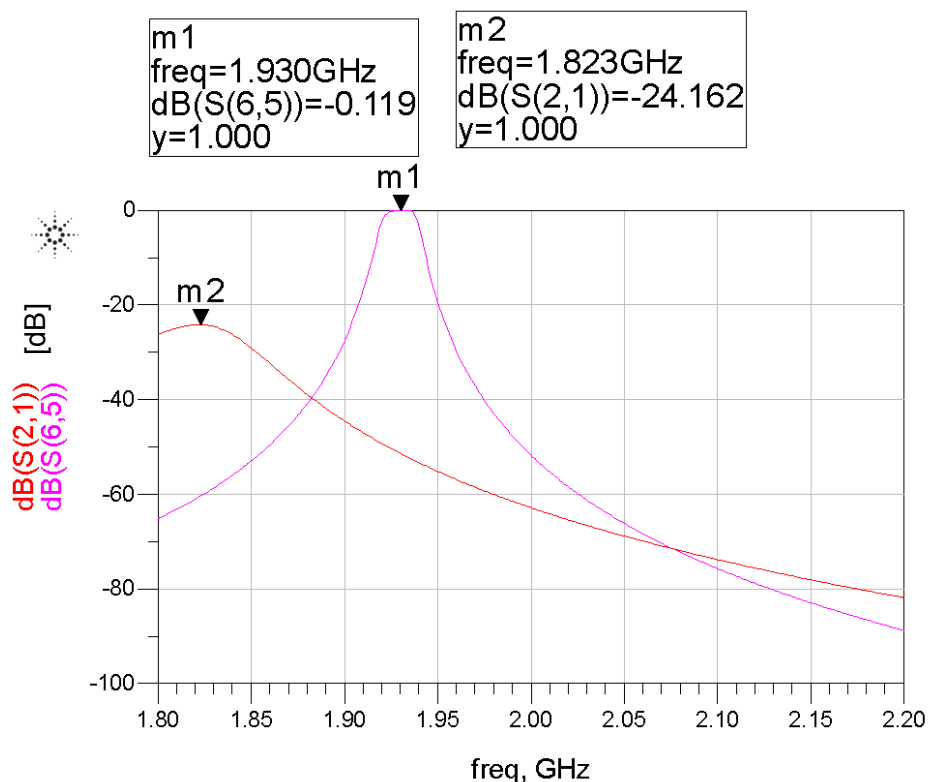
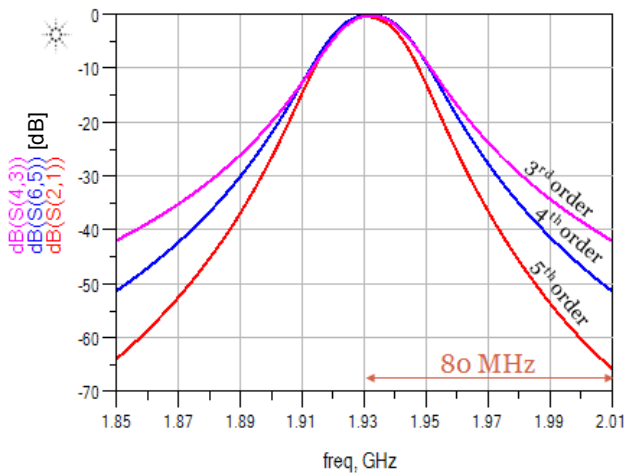


Figure 67. Frequency response (in dB) of the 3rd order C-coupled serial resonator (ideal vs. model)

APPENDIX E: Butterworth Filter Bandwidth/Roll-off

Non-ideal Butterworth Order Investigation



Butterworth Filter Order comparison

	Third order	Fourth order	Fifth order
Isolation	42dB	51dB	64dB
Amplification	12.5 dB	13.5 dB	16.5 dB

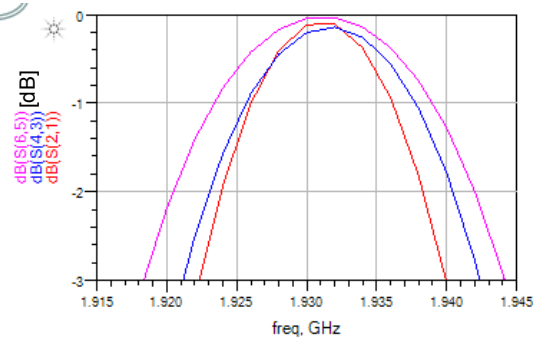
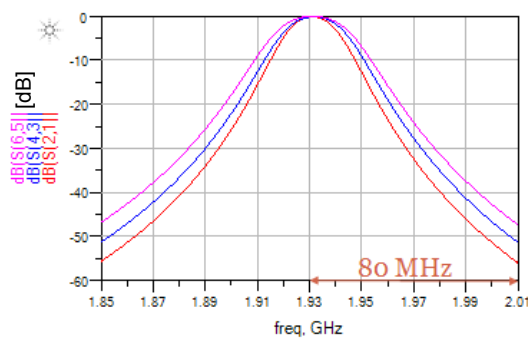
$f_c = 1.93\text{GHz}$

Required specs:

$\pm 80\text{MHz}$ (i.e. 1.85GHz & 2.01GHz) – a roll off of 50dB

- Fourth order provides desired isolation

Non-ideal Butterworth Bandwidth Investigation



Ideal BW	20 MHz	25 MHz	30 MHz
Real BW	18 MHz	21 MHz	26 MHz
Isolation	56 dB	51 dB	48 dB

Does not guarantee
desired bandwidth due to
non-ideal components

Provides desired
bandwidth and isolation for
non-ideal case

Does not guarantee
desired isolation

APPENDIX F: Coefficients of different filter configurations

Table 12. Coefficients for maximally flat Butterworth low-pass filter (N=1 to 10) [9]

N	g_1	g_2	g_3	g_4	g_5	g_6	g_7	g_8	g_9	g_{10}	g_{11}
1	2.0000	1.0000									
2	1.4142	1.4142	1.0000								
3	1.0000	2.0000	1.0000	1.0000							
4	0.7654	1.8478	1.8478	0.7654	1.0000						
5	0.6180	1.6180	2.0000	1.6180	0.6180	1.0000					
6	0.5176	1.4142	1.9318	1.9318	1.4142	0.5176	1.0000				
7	0.4450	1.2470	1.8019	2.0000	1.8019	1.2470	0.4450	1.0000			
8	0.3902	1.1111	1.6629	1.9615	1.9615	1.6629	1.1111	0.3902	1.0000		
9	0.3473	1.0000	1.5321	1.8794	2.0000	1.8794	1.5321	1.0000	0.3473	1.0000	
10	0.3129	0.9080	1.4142	1.7820	1.9754	1.9754	1.7820	1.4142	0.9080	0.3129	1.0000

Table 13: Coefficients for linear phase Butterworth low-pass filter (N=1 to 10) [9]

N	g_1	g_2	g_3	g_4	g_5	g_6	g_7	g_8	g_9	g_{10}	g_{11}
1	2.0000	1.0000									
2	1.5774	0.4226	1.0000								
3	1.2550	0.5528	0.1922	1.0000							
4	1.0598	0.5116	0.3181	0.1104	1.0000						
5	0.9303	0.4577	0.3312	0.2090	0.0718	1.0000					
6	0.8377	0.4116	0.3158	0.2364	0.1480	0.0505	1.0000				
7	0.7677	0.3744	0.2944	0.2378	0.1778	0.1104	0.0375	1.0000			
8	0.7125	0.3446	0.2735	0.2297	0.1867	0.1387	0.0855	0.0289	1.0000		
9	0.6678	0.3203	0.2547	0.2184	0.1859	0.1506	0.1111	0.0682	0.0230	1.0000	
10	0.6305	0.3002	0.2384	0.2066	0.1808	0.1539	0.1240	0.0911	0.0557	0.0187	1.0000

Table 14: Coefficients for 3dB Chebyshev low-pass filter (N=1 to 10) [9]

N	g_1	g_2	g_3	g_4	g_5	g_6	g_7	g_8	g_9	g_{10}	g_{11}
1	1.9953	1.0000									
2	3.1013	0.5339	5.8095								
3	3.3487	0.7117	3.3487	1.0000							
4	3.4389	0.7483	4.3471	0.5920	5.8095						
5	3.4817	0.7618	4.5381	0.7618	3.4817	1.0000					
6	3.5045	0.7685	4.6061	0.7929	4.4641	0.6033	5.8095				
7	3.5182	0.7723	4.6386	0.8039	4.6386	0.7723	3.5182	1.0000			
8	3.5277	0.7745	4.6575	0.8089	4.6990	0.8018	4.4990	0.6073	5.8095		
9	3.5340	0.7760	4.6692	0.8118	4.7272	0.8118	4.6692	0.7760	3.5340	1.0000	
10	3.5384	0.7771	4.6768	0.8136	4.7425	0.8164	4.7260	0.8051	4.5142	0.6091	5.8095

Table 15: Coefficients for 0.5dB Chebyshev low-pass filter (N=1 to 10) [9]

N	g_1	g_2	g_3	g_4	g_5	g_6	g_7	g_8	g_9	g_{10}	g_{11}
1	0.6986	1.0000									
2	1.4029	0.7071	1.9841								
3	1.5963	1.0967	1.5963	1.0000							
4	1.6703	1.1926	2.3661	0.8419	1.9841						
5	1.7058	1.2296	2.5408	1.2296	1.7058	1.0000					
6	1.7254	1.2479	2.6064	1.3137	2.4758	0.8696	1.9841				
7	1.7372	1.2583	2.6381	1.3444	2.6381	1.2583	1.7372	1.0000			
8	1.7451	1.2647	2.6564	1.3590	2.6964	1.3389	2.5093	0.8796	1.9841		
9	1.7504	1.2690	2.6678	1.3673	2.7939	1.3673	2.6678	1.2690	1.7504	1.0000	
10	1.7543	1.2721	2.6754	1.3725	2.7392	1.3806	2.7231	1.3485	2.5239	0.8842	1.9841

References

- [1] Ian Poole. 2013, Oct 5. *LTE Frequency Bands and Spectrum Allocation* [Online]. Available: <http://www.radio-electronics.com/info/cellulartelecomms/lte-long-term-evolution/lte-frequency-spectrum.php>
- [2] Ian Poole. 2013, Oct 11. *RF Filter Basics Tutorial* [Online]. Available: <http://www.radio-electronics.com/info/rf-technology-design/rf-filters/rf-filter-basics-tutorial.php>
- [3] Reinhold Ludwig, Gene Bogdanov. *RF Circuit Design: Theory and Applications*. Saddle River, NJ: Prentice-Hall, 2009.
- [4] Robert Aigner. 2013, October 12. *SAW, BAW and the future of wireless* [Online]. Available: <http://www.edn.com/design/wireless-networking/4413442/SAW-BAW-and-the-future-of-wireless>
- [5] Tomasz Trzcinski, 2008, October 29, *Surface Acoustic Wave (SAW) filter technology* [Online]. Available: <http://areeweb.polito.it/didattica/corsiddc/01NVD/Studmat/SAW08/SAWfilterReport-TomaszTrzcinski.pdf>
- [6] Christopher Rice and Harry Worstell, "Filter having tunable center frequency and/or tunable bandwidth," U.S. Patent 5 917 387, Apr 1, 1998.
- [7] Michael Koechlin, "Wideband analog bandpass filter," U.S. Patent 2011 0 187 448, Jan 23, 2013.
- [8] Yang, X.; Wu, J.; Lou, J.; Xing, X.; Oate, D.E.; Dionne, G.F.; Sun, N.X., "Compact tunable bandpass filter on YIG substrate," *Electronics Letters*, vol.48, no.17, pp.1070,1071, August 16 2012
- [9] Carter, Philip S., "Magnetically-Tunable Microwave Filters Using Single-Crystal Yttrium-Iron-Garnet Resonators," *Microwave Theory and Techniques*, IRE Transactions on, vol.9, no.3, pp.252,260, May 1961
- [10] Peng Wong; Hunter, I., "Electronically Tunable Filters," *Microwave Magazine*, IEEE, vol.10, no.6, pp.46,54, Oct. 2009
- [11] Manavalan, Sriraj G., "Structural and electrical properties of barium strontium titanate thin films for tunable microwave applications" (2005). Graduate School Theses and Dissertations. <http://scholarcommons.usf.edu/etd/756>
- [12] Sanderson, G.; Cardona, Albert H.; Watson, T.C.; Chase, D.; Roy, M.; Paricka, J.M.; York, R.A., "Tunable IF Filter using Thin-Film BST Varactors," *Microwave Symposium*, 2007. IEEE/MTT-S International, vol., no., pp.679,682, 3-8 June 2007
- [13] Peregrine Semiconductor, "DTC Theory of Operation", Application Note AN29, http://www.psemi.com/pdf/app_notes/an29.pdf
- [14] K. Jeganathan, "Design of a Simple Tunable/Switchable Bandpass Filter," *Applied Microwave and Wireless*, pp. 32-40.
- [15] Hussaini, A.S.; Abd-Alhameed, R.; Rodriguez, J., "Tunable RF filters: Survey and beyond," *Electronics, Circuits and Systems (ICECS)*, 2011 18th IEEE International Conference on, vol., no., pp.512,515, 11-14 Dec. 2011

- [16] Qizheng Gu; De Luis, J.R., "RF MEMS tunable capacitor applications in mobile phones," Solid-State and Integrated Circuit Technology (ICSICT), 2010 10th IEEE International Conference on, vol., no., pp.635,638, 1-4 Nov. 2010
- [17] Dufek, I., "Concept of the tunable filter unit for agile mobile handsets," Antennas and Propagation Conference (LAPC), 2012 Loughborough, vol., no., pp.1,4, 12-13 Nov. 2012
- [18] Radio Electronics, "Varactor Diode Specifications", <http://www.radio-electronics.com/info/data/semicond/varactor-varicap-diodes/specifications-parameters.php>
- [19] J. B. Calvert, "Varactors", University of Denver, Feb. 2002, <http://mysite.du.edu/~etuttle/electron/elect40.htm>
- [20] Skyworks Inc., "Application Note Varactor Diodes" <http://www.skyworksinc.com/uploads/documents/200824A.pdf>
- [21] Zahirul Alam, A.H.M.; Islam, M.R.; Khan, S.; Farhana, S.; Nik Mohd.Salleh, N.N.A.B.; Aziz, N., "RF bandpass tunable filter using RF MEMS," Computer and Communication Engineering, 2008. ICCCE 2008. International Conference on, vol., no., pp.609,612, 13-15 May 2008
- [22] HASHIMOTO, KEN-YA; Tanaka, S.; Esashi, M., "Tunable RF SAW/BAW filters: Dream or reality?," Frequency Control and the European Frequency and Time Forum (FCS), 2011 Joint Conference of the IEEE International , vol., no., pp.1,8, 2-5 May 2011
- [23] Jens Berkmann, et al., "On 3G LTE Terminal Implementation – Standard Algorithms, Complexities and Challenges," Wireless Communications and Mobile Computing Conference 2008, Crete Island, pp.970-975.
- [24] Magdalena Nohrborg. (2013, November 11). *LTE*. [Online]. Available: <http://www.3gpp.org/LTE>
- [25] 3rd Generation Partnership Project; Technical Specification Group Radio Access Network; Evolved Universal Terrestrial Radio Access (E-UTRA); Physical layer procedures (Release 11), 3GPP TS 36.213 V11.4.0 (2013-09)
- [26] Unknown. (2013, November 11). *OFDM/OFDMA: Orthogonal Frequency Division Multiplexing/ Orthogonal Frequency Division Multiple Access*. [Online] Available: <http://www.4gamerica.org/index.cfm?fuseaction=page§ionid=253>
- [27] David Whitefield, "Skyworks-WPI MQP 2013-2014," unpublished.
- [28] Jack Browne. (2011, July 11). *Digital Capacitors are Super Agile*. [Online]. Available: <http://mwrf.com/digital-semiconductors/digital-capacitors-are-frequency-agile>
- [29] Xiaoguang Liu; Katehi, L. P B; Chappell, W.J.; Peroulis, D., "High- Q Tunable Microwave Cavity Resonators and Filters Using SOI-Based RF MEMS Tuners," Microelectromechanical Systems, Journal of , vol.19, no.4, pp.774,784, Aug. 2010
- [30] Teledyne Microwave, "YIG Filters, the complete microwave solution", [Online]. Available: http://www.teledynewireless.com/pdf_YIG/Teledyne%20Microwave%20YIG%20Filter%20Products%200507.pdf
- [31] Petri Possi. (2013, November 11). *CDMA Overview*. [Online]. Available: <http://www.umtsworld.com/technology/cdmabasics.htm>

- [32] MathWorks, Classic IIR Filter Design, <http://www.mathworks.com/help/dsp/examples/classic-iir-filter-design.html>, last accessed on 02/24/2014
- [33] Cohn, Seymour B., "Direct-Coupled-Resonator Filters," *Proceedings of the IRE* , vol.45, no.2, pp.187,196, Feb. 1957,
URL: <http://ieeexplore.ieee.org/stamp/stamp.jsp?tp=&arnumber=4056485&isnumber=4056472>
- [34] Jiafeng Zhou (2010). Microwave Filters, Microwave and Millimeter Wave Technologies from Photonic Bandgap Devices to Antenna and Applications, Igor Minin (Ed.), Available from: <http://www.intechopen.com/books/microwave-and-millimeter-wave-technologies-from-photonic-bandgap-devices-to-antenna-and-applications/microwave-filters>
- [35] Tzong-Lin Wu (2013). "Filter", EMC Laboratory, Department of Electrical Engineering, National Taiwan University. Available from: <http://ntuemc.tw/upload/file/201102212235523ca26.pdf>
- [36] George L. Matthaei, Leo Young, E. M. T. Jones. *Microwave Filters Impedance Matching Networks and Coupling Structures*. New York, NY: McGraw Hill, 1964.